DYNAMICS OF NON-ABELIAN AHARONOV-BOHM SYSTEMS

Thesis by

Patrick McGraw

In Partial Fulfillment of the Requirements
for the Degree of
Doctor of Philosophy

California Institute of Technology
Pasadena, California

1996
(Submitted May 31, 1996)

Acknowledgments

I wish to thank my advisor, Prof. John Preskill, for several years of expert advice and guidance in approaching the questions studied here, and for many helpful comments during the course of the work, as well as assistance with the practical side of beginning a career. I have also benefitted greatly from discussions with other colleagues, including especially Hoi-Kwong Lo, Robert Navin and David Politzer. They helped me not only by discussing ideas and offering comments, but by providing encouragement. Conversations with Anton Kapustin were helpful in the writing of Chapter 2.

I also would like to thank my family and friends for the love and support which they provided even while living hundreds of miles away or on different continents. Finally, I thank the members of Dabney House for making my stay at Caltech more enjoyable and helping me relax during some of the difficult times.

" Made the scene, week to week
Day to day, hour to hour
The gate is straight, deep and wide
Break on through to the other side
Break on through to the other side."

-The Doors

Abstract

This thesis examines several examples of systems in which non-Abelian magnetic flux and non-Abelian forms of the Aharonov-Bohm effect play a role. We consider the dynamical consequences in these systems of some of the exotic phenomena associated with non-Abelian flux, such as Cheshire charge holonomy interactions and non-Abelian braid statistics. First, we use a mean-field approximation to study a model of $U(2)$ non-Abelian anyons near its free-fermion limit. Some self-consistent states are constructed which show a small $SU(2)$-breaking charge density that vanishes in the fermionic limit. This is contrasted with the bosonic limit where the $SU(2)$ asymmetry of the ground state can be maximal. Second, a global analogue of Chesire charge is described, raising the possibility of observing Cheshire charge in condensed-matter systems. A potential realization in superfluid He-3 is discussed. Finally, we describe in some detail a method for numerically simulating the evolution of a network of non-Abelian (S_3) cosmic strings, keeping careful track of all magnetic fluxes and taking full account of their non-commutative nature. I present some preliminary results from this simulation, which is still in progress. The early results are suggestive of a qualitatively new, non-scaling behavior.

Table of Contents

Chapter 1
Introduction

In 1959, Aharonov and Bohm[1] described how a tube of magnetic flux can cause a shift in the interference pattern of two electron beams when those beams traverse paths on opposite sides of the flux tube, even if the electrons pass exclusively through regions in which the magnetic field and classical magnetic force are zero. This has proved to be a very profound discovery in the history of quantum mechanics. In modern language, the Aharonov-Bohm (A-B) effect can be understood as an essentially topological interaction. The electrons are propagating under the influence of an electromagnetic background gauge connection, but the connection is locally flat in all of the regions where the electrons propagate. The interaction therefore depends on the overall topology of the connection and the particle trajectories and cannot be described in terms of any gauge-invariant local property of the background.

Since this discovery, the Aharonov-Bohm effect, and topological interactions in general, have been shown to play a role in many disparate contexts, including observed systems and hypothetical models. Cosmic strings,[2] for example, are thin, confined tubes of magnetic flux, much like the thin solenoids considered by Aharonov and Bohm. If cosmic strings exist, A-B scattering is presumably one of their most important mechanisms for interacting with ordinary matter.

Topological phases also are important in condensed-matter physics. Anyons,[3] particles in $(2 + 1)$ dimensions with statistics intermediate between bosons and fermions, are thought to play a role in the quantum Hall effect[4] and in high-temperature superconductivity.[5] One particularly useful mathematical description of anyons is through Chern-Simons theory, in which anyons are described as ordinary fermions or bosons interacting with a statistical gauge field described by the Chern-Simons Lagrangian. The Gauss constraint of this theory causes each charged particle to become attached to a unit of magnetic flux, and the statistical phases acquired by particles whose trajectories wind around each other arise in this description from the

Aharonov-Bohm interaction of one particle's charge with another particle's associated flux.

Close analogues of cosmic strings also are abundant in the realm of condensed-matter physics in systems which are (unlike cosmic strings) experimentally accessible, such as superfluids, nematic liquid crystals and type II superconductors.[6,7] This leads to a very productive interaction between condensed matter physicists and cosmologists.[8]

The Aharonov-Bohm effect, properly so called, occurs only in gauge theories. However, it is mathematically akin to many instances of geometric phases. In the presence of global topological defects, a type of frame-dragging may occur even in the absence of gauge connections, and this may lead to an effect that closely mimics A-B scattering.[9] The discovery of this global analogue of the A-B effect raises the possibility of new experimentally realizable applications. Condensed-matter physics offers more examples of broken global symmetries than gauge symmetries.

In the original electromagnetic context, the phase associated with a path enclosing magnetic flux is a single complex number; an element of the group U(1). If the group is non-Abelian and/or discrete, however, an additional range of exotic phenomena may occur. Discrete gauge theories are interesting in that they have no massless gauge fields, but they do have topological interactions. In such a case, gauge charge can be detected at long range *only* through topological interactions and not through classical forces. One of the early motivations for studying discrete gauge theories was the hope that such long-range interactions without massless fields might lead to a way of circumventing the black-hole "no-hair" theorem and partly resolving the information loss puzzle.[10] The cosmic strings associated with discrete symmetry groups differ from U(1)-type strings in that they form branching networks. This can have consequnces for the dynamics of strings after they are formed in a phase transition,[11] as I will discuss below in Chapter 4.

Non-Abelian topological interactions and non-Abelian magnetic fluxes lead to quite a wide range of exotic phenomena which have only been discussed fairly recently.[12–16]

For the most part, these exotic phenomena all are consequences of the fact that non-Abelian magnetic flux is not a gauge-invariant quantity. In two space dimensions, non-Abelian braid statistics may occur. Non-Abelian Chern-Simons particles,[17] a generalization of anyons, are one example. It has been suggested that such particles, called "nonabelions," may occur as quasiparticles in the quantum Hall effect.[18] Another is non-Abelian vortices. A peculiar feature of non-Abelian vortices is that the transport of one vortex around another changes the quantum numbers of the vortices. In vortex-vortex scattering, this so-called holonomy interaction[19] can lead to an exchange contribution to the scattering amplitude even when the vortices have different fluxes (vortices can be "indistinguishable but not the same.")[16] In three spatial dimensions, non-Abelian cosmic strings also exhibit holonomy interactions and tend to form branched networks. An additional consequence of the non-invariance of flux under group transformations is the phenomenon of "Cheshire charge."[15,14] Quantum tunneling between states of different flux within the same conjugacy class allows a loop of string (or, in two dimensions, a pair of vortices) to exist in states that have no definite flux but rather are irreducible representations of the symmetry group. They carry a charge which has no local source on or near the string, but is a global topological property. Aharonov-Bohm interactions with charged particles can lead to a transfer of charge from the particle to the string loop.

With the basic facts of non-Abelian topological interactions now fairly well understood, it is interesting to ask the following two types of questions: 1) How do non-Abelian A-B interactions affect the dynamics and many-body physics of systems in which they occur? 2) In what contexts might the non-Abelian A-B effect be phenomenologically relevant? The goal of this thesis is to address a few of these questions. The remainder is organized as follows:

In Chapter 2, I discuss a model of non-relativistic matter coupled to a $U(2)$ Chern-Simons (statistical) gauge field.[20] The model with bosonic matter has previously been studied by Cappelli and Valtancoli using the Boguliubov approximation based on a mean-field ground state.[21] Those authors showed that the $SU(2)$ symmetry is spontaneously broken in the ground state for certain values of the coupling constants. In Chapter 2, I consider the same model with a fermionic matter field. I describe a set

of self-consistent mean-field states with a small $SU(2)$ "isospin" asymmetry for certain values of the Chern-Simons coupling constants. The SU(2)-breaking charge density vanishes, however, as the limit of free fermions is approached. This is contrasted with the free-boson limit of the boson-based theory, where the the asymmetry is large.

The discovery of a global analogue of the Aharonov-Bohm effect raised interesting possibilities for its observation in condensed-matter systems. Chapter 3 shows how a counterpart of the "Alice" string[22] can occur in a model with no gauge symmetries, leading to a global analogue of Cheshire charge.[23] A possible realization in superfluid helium-3 is pointed out. The presence of Cheshire charge on a pair of vortices can create a repulsion between them which may balance their logarithmically confining attraction. The amount of charge necessary to stabilize the pair against collapse is calculated in an appendix to chapter 3.

In Chapter 4, I describe a numerical simulation whose aim is to learn how the peculiar interactions of non-Abelian cosmic strings affect their dynamics.[24] A network of S_3 strings is chosen as a representative example of a non-Abelian string system. The method of the simulation is described in some detail, as the simulation of non-Abelian fluxes poses many subtle problems. Finally, the end of the chapter describes some preliminary results from the simulation, which is still in progress. These are suggestive of qualitatively new behavior for this network.

REFERENCES

1. Y. Aharonov and D. Bohm, Phys. Rev. **119** 485 (1959)

2. T.W.B. Kibble, Phys. Rep. **67**, 183 (1980); J. Preskill, "Vortices and Monopoles," in Architecture of the Fundamental Interactions at Short Distances, ed. P. Ramond and R. Stora (North-Holland, Amsterdam 1987).

3. M. Leinaas, D. Myrheim, Nouvo Cimento B 37, 1 (1971); G.A. Goldin, R. Menikoff,D.H. Sharp, J. Math. Phys. **22**, 1664 (1981); F. Wilczek, Phys. Rev. Lett. **48**, 1144 (1982); **49**, 957 (1982).

4. B. Halperin, Phys. Rev. Lett. **62**, 86 (1989), D.P. Arovas, J.R. Schrieffer, F. Wilczek, Phys. Rev. Lett **53**, 722 (1984).

5. F. Wilczek, ed., Fractional Statistics and Anyon Superconductivity (World Scientific, Singapore, 1990); Y. H. Chen, F. Wilczek, E. Witten, B. Halperin, Int. J. Mod. Phys. **B 3**, 1001 (1989).

6. N. D. Mermin, Rev. Mod. Phys. **51**, 591 (1979).

7. M. M. Salomaa, G. E. Volovik, Rev. Mod. Phys. **59**, 533 (1987).

8. See, for example: I. Chuang, R. Durrer, N. Turok, B. Yurke, Science **251**, 1336 (1991).

9. J. March-Russell, J. Preskill, and F. Wilczek, Phys. Rev. Lett **68**, 2567 (1992); R. L. Navin, Caltech Preprint CALT-68-1896; M.V. Khazan, JETP Lett. **41**, 486 (1985).

10. L. Krauss, F. Wilczek, Phys. Rev. Lett. **62**, 1221 (1989); B. Coleman, J. Preskill, F. Wilczek, Nuc. Phys. **B 378**, 175 (1992); J. Preskill, L. Krauss, Nucl. Phys. **B 341**, 50 (1990).

11. T. Vachaspati, A. Vilenkin, Phys. Rev. **D 35**, 1131 (1986).

12. M. Alford, K. M. Lee, J. March-Russell, J. Preskill, Nucl. Phys. **B 384**, 241 (1992).

13. H. K. Lo, Phys. Rev. **D 52**, 7247 (1995).

14. M. Bucher, H. K. Lo, J. Preskill, Nucl. Phys. **B 386**, 3 (1992).

15. M. Alford, K. Benson, S. Coleman, J. March-Russell, F. Wilczek. Phys. Rev. Lett. **64** (1990), 1632; J. Preskill, L. Krauss. Nuc Phys **B 341** (1990), 50; M. Bucher, K. M. Lee, J. Preskill, Nucl. Phys. **B 386**, 27 (1992).

16. H.K. Lo, J. Preskill, Phys. Rev. **D 48**, 4821 (1993).

17. T. Lee, P. Oh, Ann. Phys. **235**, 413 (1994); Phys. Lett. **B 319**, 497 (1993); Phys. Rev. Lett. **72**, 1141 (1994); M. H. Kim, P. Oh, J. Math. Phys. **35**, 3959 (1994).

18. X.G. Wen, Phys. Rev. Lett. **66**, 802 (1991); G. Moore, N. Read, Nucl. Phys. **B 360**, 382 (1991).

19. F.A. Bais, Nucl. Phys. **B 170**, 32 (1980).

20. P. McGraw, Caltech Preprint CALT-68-2058.

21. A. Cappelli, P. Valtancoli, Nucl. Phys. **B 453**, 727 (1995).

22. A.S. Schwarz, Nucl. Phys. **B 208**, 141 (1982).

23. P. McGraw, Phys. Rev. **D 50**, 952 (1994).

24. P. McGraw, Caltech Preprint CALT-68-2044 (hep-th/9603153), submitted to Phys. Rev. **D**.

Chapter 2

Mean Field Theory for Fermion-Based U(2) Anyons

In this chapter, we consider a $2+1$ dimensional model with a non-relativistic matter field Ψ minimally coupled to an $SU(2) \times U(1) = U(2)$ "statistical" or Chern-Simons gauge field. The matter will be taken to carry a unit of $U(1)$ charge and a fundamental representation of $SU(2)$ "isospin." The Lagrangian is given by:

$$\mathcal{L} = i\Psi^\dagger(D_0\Psi) - \frac{1}{2m}(D_i\Psi)^\dagger(D_i\Psi) + \frac{\tilde{\kappa}}{2}\epsilon^{\alpha\beta\gamma}(A^a_\alpha \partial_\beta A^a_\gamma - \frac{1}{3}\epsilon_{abc}A^a_\alpha A^b_\beta A^c_\gamma) + \frac{\kappa}{2}\epsilon^{\alpha\beta\gamma}A_\alpha \partial_\beta A_\gamma, \tag{1}$$

where A_μ and A^a_μ are the $U(1)$ and $SU(2)$ gauge fields, with Chern-Simons coupling constants κ and $\tilde{\kappa}$ respectively, and the covariant derivative is

$$D_\mu = \partial_\mu + iA_\mu + iA^a_\mu \frac{\sigma^a}{2}. \tag{2}$$

We will consider cases of either bosonic or fermionic matter fields, so that Ψ may obey either canonical commutation or anticommutation relations. The Hamiltonian corresponding to (1) is given by

$$H = \int d^2\mathbf{x} \frac{1}{2m}(D_i\Psi)^\dagger(D_i\Psi) \tag{3}$$

while the gauge fields are subject to constraints which relate them to the matter fields:

$$B \equiv -F_{12} = \epsilon_{ij}\partial_i A_j = -\frac{1}{\kappa}\rho,$$

$$B^a \equiv -F^a_{12} = \epsilon_{ij}(\partial_i A^a_j + \frac{1}{2}\epsilon^{abc}A^b_i A^c_j) = -\frac{1}{\tilde{\kappa}}\rho^a, \tag{4}$$

and

$$F_{0i} = -\frac{1}{\kappa}\epsilon ij J_j,$$

$$F^a_{0i} = -\frac{1}{\tilde{\kappa}}\epsilon_{ij}J^a_j, \tag{5}$$

where the densities and currents are defined by:

$$\rho = \Psi^\dagger\Psi, \rho^a = \Psi^\dagger\frac{\sigma^a}{2}\Psi,$$

$$J_i = \frac{1}{2im}(\Psi^\dagger D_i\Psi - (D_i\Psi)^\dagger\Psi), J^a_i = \frac{1}{2im}(\Psi^\dagger\frac{\sigma^a}{2}D_i\Psi - (D_i\Psi)^\dagger\frac{\sigma^a}{2}\Psi). \tag{6}$$

Since there is no Maxwell term, the gauge fields are non-dynamical and are completely determined (up to gauge transformation) by (4) and (5).

As usual, the theory is gauge invariant only when $\tilde{\kappa}$ is an integer multiple of $1/4\pi$. The Gauss constraints ensure that any electrically charged particle also carries magnetic flux, so the particles experience mutual Aharonov-Bohm interactions resulting in exotic statistics. In this case, the braiding of two particles leads not only to an overall phase change of the wave function but also a non-Abelian rotation acting on the isospin indices of the two particles. A two-particle wave function $\psi(x_1, x_2)$ is acted on by the braiding operator

$$\exp[i(\theta + \tilde{\Theta})] \equiv \exp[\frac{-i}{2\kappa} + \frac{i\sigma_{(1)}\cdot\sigma_{(2)}}{\tilde{\kappa}}], \tag{7}$$

where $\tilde{\Theta}$ can be thought of as a matrix-valued $SU(2)$ "phase". The eigenstates of this two-particle braiding operator are states of definite total isospin, i.e., pure iso-singlet or triplet states.

This model of "non-Abelian anyons" was studied in reference [1] using a mean field approximation. In this mean field technique one first quantizes the matter field in the presence of a classical background magnetic field. One searches for a self-consistent ground state having a uniform expectation value of the matter and isospin densities consistent with the Gauss constraints. Then, using the densities and currents as fundamental variables, one can study the effect of fluctuations about this approximate ground state, using the Bogoliubov approximation in which the commutators of fluctuation operators are replaced by their expectation values in the zeroth-order ground state.[2]

In reference [1], it was shown that with bosonic matter the mean field ground state energy behaves differently depending on the values of the two Chern-Simons couplings. In particular, there was a phase in which the energy was minimized in the mean field approximation by the generation of a non-zero isospin density, and thus the $SU(2)$ symmetry was spontaneously broken. This paper will investigate the consequences of coupling fermions instead of bosons to the $U(2)$ Chern-Simons field. We will show that for spinless (or polarized) fermions, the resulting mean field theory differs from the bosonic case in two ways: (1) The form of the mean field energy density as a function of matter and charge densities is independent of the Chern-Simons coupling constants and (2) For a given particle density, the lowest energy always occurs when the $SU(2)$ charge density is zero. Thus the mean field picture does not show any breaking of the $SU(2)$ symmetry. In the case of spin-1/2 fermions, however, there is a hint of spontaneous symmetry breaking which vanishes smoothly as the theory approaches that of pure fermions.

1 Mean field approximation for fermion-based U(2) anyons

For a theory where the matter field Ψ is fermionic, we now search, much as in reference [1], for a self-consistent ground state $|\Omega\rangle$ with uniform matter and isospin densities:

$$\langle\rho\rangle = \rho_0, \langle J_i\rangle = 0,$$

$$\langle\rho^a\rangle = \rho_0^a, \langle J_i^a\rangle = 0. \tag{8}$$

According to the Gauss constraints, these nonzero densities will imply uniform magnetic fields. We will consider matter in the background of these fields, and then demand that the number of particles per unit area be consistent with the Gauss constraints. We can take the isospin density to be along the σ_3 direction, $\langle\rho^a\rangle = \delta_3^a\tilde{\rho}_0$. Then we have $U(1)$ and $SU(2)$ magnetic fields given by

$$\langle B\rangle = B_0 = -\frac{1}{\kappa}\rho_0, \langle B^a\rangle = \delta_3^a\tilde{B}_0 = -\frac{1}{\tilde{\kappa}}\delta_3^a\tilde{\rho}_0. \tag{9}$$

In the symmetric (or isotropic) gauge[3] $A_i = (B/2)\epsilon_{ij}x^j$, the gauge field can be

written as

$$A_i = \epsilon_{ij}\frac{x^j}{2}(\frac{\rho_0}{\kappa} + \frac{\tilde{\rho}_0}{2\tilde{\kappa}}\sigma_3). \tag{10}$$

The single-particle orbitals are split into two sets according to the eigenvalue of σ_3. Particles in states of up or down isospin feel different effective magnetic fields, $B_+ = (B_0 + \tilde{B}_0/2)$ and $B_- = (B_0 - \tilde{B}_0/2)$, respectively. The single-particle energy levels thus fall into two sets of Landau levels. The kth energy levels of the isospin up and down systems have energies given by

$$\epsilon_k^{\pm} = \frac{B_{\pm}}{m}(k + \frac{1}{2}), \tag{11}$$

and have degeneracy per unit area $N_{\pm}/A = |B_{\pm}|/2\pi$.

Uniformity of the density requires that all orbitals of any given Landau level be filled with the same number of particles.[4] In the case of spinless (or spin-polarized) fermions, this means either 0 or 1 per orbital. For spin-1/2 fermions, the possible occupancies are 0,1, and 2. Let us first consider spinless fermions. The total energy per unit area for a state with the lowest n levels filled is given by:

$$\frac{E}{A} = \frac{B}{2\pi}\sum_{k=0}^{n-1}\epsilon_k = \frac{B^2n^2}{4\pi m}. \tag{12}$$

(The factor $B/2\pi$ in front of the sum represents the degeneracy.) In our system, if the lowest n_+ and n_- of the isospin up and down levels, respectively, are uniformly filled with one particle per orbital, then the combined energy is given by

$$\frac{E}{A} = \frac{n_+^2}{4\pi m}(B_0 + \frac{\tilde{B}_0}{2})^2 + \frac{n_-^2}{4\pi m}(B_0 - \frac{\tilde{B}_0}{2})^2. \tag{13}$$

The density of isospin-up particles is given by the number of filled Landau levels times the degeneracy, $\rho_+ = n_+N_+/A$, and similarly for the down particles it is $\rho_- = n_-N_-/A$. The matter density ρ is the sum of the up and down densities, while the

isospin density for isospin-1/2 particles is given by half the difference[1]:

$$\rho_0 = \rho_+ + \rho_- = \frac{n_+ N_+}{A} + \frac{n_- N_-}{A} = n_+ \frac{|B_0 + \tilde{B}_0/2|}{2\pi} + n_- \frac{|B_0 - \tilde{B}_0/2|}{2\pi},$$

$$\tilde{\rho}_0 = \frac{1}{2}(\rho_+ - \rho_-) = \frac{1}{2}(n_+ \frac{|B_0 + \tilde{B}_0/2|}{2\pi} - n_- \frac{|B_0 - \tilde{B}_0/2|}{2\pi}). \tag{14}$$

These equations may be rewritten in the form

$$\frac{n_+|B_0 + \tilde{B}_0/2|}{2\pi} = \frac{\rho_0}{2} + \tilde{\rho}_0, \frac{n_-|B_0 - \tilde{B}_0/2|}{2\pi} = \frac{\rho_0}{2} - \tilde{\rho}_0. \tag{15}$$

The expression (13) for the energy then becomes:

$$\frac{E}{A} = \frac{\pi}{m}[(\frac{\rho_0}{2} + \tilde{\rho}_0)^2 + (\frac{\rho_0}{2} - \tilde{\rho}_0)^2] = \frac{2\pi}{m}(\frac{\rho_0^2}{4} + \tilde{\rho}_0^2). \tag{16}$$

For comparison, the result in the bosonic case of [1] was found to be:

$$\frac{E}{A} = \frac{1}{2m}\left[|\frac{\rho_0}{\kappa} + \frac{\tilde{\rho}_0}{2\tilde{\kappa}}|(\frac{\rho_0}{2} + \tilde{\rho}_0) + |\frac{\rho_0}{\kappa} - \frac{\tilde{\rho}_0}{2\tilde{\kappa}}|(\frac{\rho_0}{2} - \tilde{\rho}_0)\right]. \tag{17}$$

The latter expression is different because in the bosonic case, only the lowest of each of the two sets of Landau levels is occupied in the ground state, whereas in the fermionic system, the exclusion principle requires that higher levels be occupied. The two expressions (16) and (17) are plotted in figure 1 for representative values of the coupling constants.

We note the following features of the fermionic result which differ from those of the bosonic result: (1) The expression is completely independent of the Chern-Simons coupling constants κ and $\tilde{\kappa}$, and was derived without any reference to the Gauss constraints $-\kappa B_0 = \rho_0$ and $-\tilde{\kappa}\tilde{B}_0 = \tilde{\rho}_0$. (2) For a given matter density ρ_0, the energy is always minimized by $\tilde{\rho}_0 = 0$. Thus it appears that the assumptions (14) for the ground state are not self-consistent unless $\tilde{\rho}_0 = 0$, and there is, in this approximation, no spontaneous breaking of the $SU(2)$ symmetry.

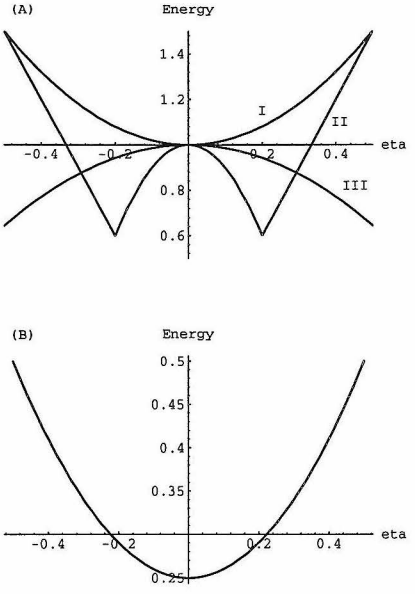

Figure 1: Upper plot (A) (adapted from reference [1]) : energy of bosonic mean-field theory plotted against the ratio $\tilde{\rho}_0/\rho_0$ for three values of the coupling constants. Curve I is for $\tilde{\kappa}/\kappa = 0.5$, and is typical of the region $\kappa\tilde{\kappa} > 0$. curve II, with $\tilde{\kappa}/\kappa = -0.1$, is typical for $\kappa\tilde{\kappa} < 0$ and $|\tilde{\kappa}|/|\kappa| < .25$. Curve III, with $\tilde{\kappa}/\kappa = -0.7$, is representative of $\kappa\tilde{\kappa} < 0$, $|\tilde{\kappa}|/|\kappa| > 0.25$ On the x-axis is the ratio $\tilde{\rho}_0/\rho_0$, on the y-axis is energy in units of $1/2m\kappa$. In case I, The minimum occurs at $\rho_0 = 0$. In case III there is a self-consistent mean-field ground state with maximal isospin density, $\tilde{\rho}_0 = \rho_0/2$ In case II, the mean-field approximation is not self-consistent: The minimum energy occurs in a limit where one of the effective magnetic fields B_+ or B_- goes to zero and the Landau level picture breaks down. The lower graph (B) shows the much simpler form of the energy expression for spinless fermions: it is independent of κ and $\tilde{\kappa}$, and is always a minimum when $\tilde{\rho}_0 = 0$. The energy scale for the lower plot is $\pi/2m$.

The first of the above observations is not entirely surprising in view of the results for the Abelian model (which should correspond to the limit $1/|\tilde{\kappa}| \ll 1/|\kappa|$). When $\tilde{\rho}_0 = 0$, (16)reduces to the result for fermion-based Abelian anyons. This result is similarly independent of the Chern-Simons coupling, and is equal to the energy of a degenerate Fermi gas in $2+1$ dimensions. Corrections to this fermi energy are found only when one includes the effects of fluctuations to quadratic order. The second property, the absence of a spontaneous non-Abelian charge density, is less obvious. In the boson-based case, it was found that the phase with $\tilde{\rho}_0 = \pm\rho_0/2$ was stable in the regime $1/|\tilde{\kappa}| < 4/|\kappa|$ with $\tilde{\kappa}$ and κ having opposite signs. Fermions can in principle be generated from bosons by setting the Abelian Chern-Simons coupling to $\kappa = -1/2\pi$, resulting in a statistical angle of π. If we were to continue naively from the behavior near the bosonic point ($\kappa \to \infty$) to $\kappa = -1/2\pi$, we might expect symmetry breaking at the fermionic end when $|\tilde{\kappa}| > \frac{1}{8\pi}$. It might be argued, in view of the spin-statistics connection, that it is not natural to expect a theory of spinless bosons to be be connected continuously to one of *spinless* fermions. The properties of the pure Abelian theory obtained in refs. [1] and [2] interpolate smoothly between the bosonic theory and a theory of unpolarized spin-1/2 fermions. Therefore, in the next section, we will consider a spin-1/2 matter field.

Qualitatively, the comparatively greater susceptibility of the bosonic model to the development of a spontaneous asymmetry between the isospin-up and down Landau levels may be explained in terms of the particles' exclusion properties. An isospin asymmetry generally raises the energies of one set of Landau levels while lowering those of the other. Since any number of bosons may occupy the lowest Landau level, it can become energetically favorable to lower the energy of, say, the isospin-up Landau level and place all of the particles into this lowered level, while leaving the raised level unoccupied. The fermionic system, on the other hand, can be regarded to a first approximation as two fermi fluids, one filling the isospin-up levels and one filling the down levels. The development of an isospin asymmetry requires that more particles be added to one of the two fluids. Even if energy of the kth Landau level is lowered by the asymmetry, the levels must be filled up to a higher value of k, which offsets the energetic advantage.

2 SPIN-1/2 FERMIONS

We now ask whether the result of the previous section is changed if we consider spin-1/2 fermions instead of spinless ones. For spin-1/2 fermions, there are two states per orbital, and so it is possible to fill a Landau level with either 1 or 2 particles per orbital. (We are supposing that the statistical gauge field does not couple to the spin, so that this double occupation is the only effect.) Let $n = 2p + \sigma, \sigma = 0, 1$, and consider a state in which the lowest $n/2$ of a set of Landau levels are filled. If n is odd ($\sigma = 1$), we mean by this that the lowest p levels are doubly filled, and the $p+1$ level is filled with one particle per orbital. The total energy per unit area of such a configuration is[1]

$$\frac{E}{A} = \frac{B}{2\pi}[2\sum_{k=0}^{p-1}\frac{B}{m}(k+\frac{1}{2}) + \sigma\frac{B}{m}(p+\frac{1}{2})] = \frac{B^2}{8\pi m}(n^2+\sigma). \tag{18}$$

For our system with two sets of Landau levels, the total energy becomes

$$\frac{E}{A} = \frac{(n_+^2+\sigma_+)}{8\pi m}(B_0+\frac{\tilde{B}_0}{2})^2 + \frac{(n_-^2+\sigma_-)}{8\pi m}(B_0-\frac{\tilde{B}_0}{2})^2. \tag{19}$$

As before, the $+$ and $-$ subscripts refer to the isospin states. Whereas the corresponding equation (13) for the spinless case only involved the products $n_\pm|B_0 \pm \frac{\tilde{B}_0}{2}|$ and thus could be expressed in terms of the densities without reference to the Gauss constraints, that is not the case here. Using the Gauss constraints, we write

$$B_0 \pm \frac{\tilde{B}_0}{2} = -\frac{\rho_0}{\kappa} \mp \frac{\tilde{\rho}_0}{2\tilde{\kappa}},$$

and thus

$$\frac{E}{A} = \frac{\pi}{m}[(\frac{\rho_0^2}{4}+\tilde{\rho}_0^2) + \frac{\sigma_+}{8\pi^2}(\frac{\rho_0}{\kappa}+\frac{\tilde{\rho}_0}{2\tilde{\kappa}})^2 + \frac{\sigma_-}{8\pi^2}(\frac{\rho_0}{\kappa}-\frac{\tilde{\rho}_0}{2\tilde{\kappa}})^2]. \tag{20}$$

Since the second and third terms are non-negative, we see that, at the mean-field level, the lowest energy state for a given ρ_0 is still one with $\sigma_+ = \sigma_- = 0$ and $\tilde{\rho}_0 = 0$.

However, if σ_+ or σ_- is restricted to be 1, then a minimum of the energy does in fact appear at

$$\tilde{\rho}_0 = \pm\frac{2\tilde{\kappa}}{\kappa}(\frac{1}{32\pi^2\tilde{\kappa}^2+1})\rho_0 \approx \frac{\pm\rho_0}{16\pi^2\kappa\tilde{\kappa}}. \tag{21}$$

(See figure 2.) This expectation value of $\tilde{\rho}$ vanishes in the limit of free fermions ($1/\kappa \to 0, 1/\tilde{\kappa} \to 0$). The corresponding energy, in the limit where both $1/\kappa$ and $1/\tilde{\kappa}$ are small, is given by

$$\frac{E}{A} = \frac{\pi}{m}[\frac{\rho_0^2}{4} + \frac{\rho_0^2}{8\pi^2\kappa^2} + \mathcal{O}(\frac{1}{\kappa^4})]. \tag{22}$$

It is worth noting that in the Abelian case, states with the top level half-filled are also energetically unfavorable at the mean-field level, but that fluctuations introduce σ- dependent corrections of the same approximate size ($\mathcal{O}(1/\kappa^2)$) and *opposite sign.* Thus it is concievable that in our model, the $\sigma_\pm = 1$ ground states might be stabilized by quadratic corrections. Also, in the Abelian model, the half-filled ground states are the only consistent ones at odd values of the coupling constant.

3 Consistency of mean-field theories

The assumption of a uniform matter density in a uniform magnetic field requires that all orbitals within a Landau level be filled equally. This means that the only degree of freedom for the ground-state distribution of particles in a set of Landau levels is the filling factor, which must be an integer. In the case of a bosonic ground state, this integer represents the occupation number of all orbitals in the lowest Landau level, while in a fermionic ground state it represents the number of levels which are filled. Combined with the Gauss constraints, this condition will in general pick out a discrete set of values of the Chern-Simons coupling constants at which the mean-field ground state is well-defined. In the case of Abelian anyons (either boson- or fermion-based) there is only one set of Landau levels which may be filled with an integer factor. The matter density is given by the filling factor times the Landau level degeneracy per unit area. The degeneracy is related to the magnetic field, which

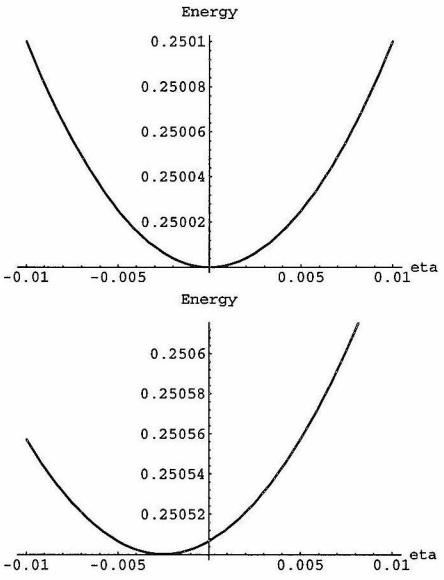

Figure 2 A: Energy of fermion- based anyons for $\sigma_+ = \sigma_- = 0$ (top) and for $\sigma_+ = 1, \sigma_- = 0$ (bottom).

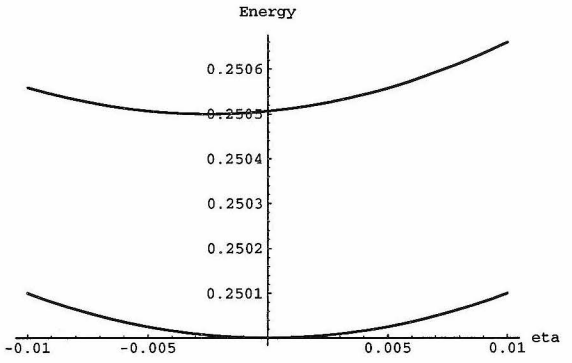

Figure 2 B: The two curves of figure 2 A, shown on the same axes.

is in turn related to the density by the Gauss constraint:

$$\rho_0 = \frac{n|B_0|}{2\pi} = \frac{n}{2\pi}|\frac{\rho_0}{\kappa}|. \tag{23}$$

ρ_0 may be divided out from both sides, leading to the familiar series of allowed values of the coupling constant: $\kappa = n/2\pi$, corresponding to the series of statistical angles $2\pi/n$ and $1 - 2\pi/n$ based on bosons and fermions, respectively.

Similar constraints occur in the non-Abelian model we are considering, but the consistency conditions are more complicated because two sets of Landau levels are involved. This issue was not addressed in reference [1], so we consider here both the bosonic and fermionic systems. The basic equations are those of (14), which relate the isospin and matter densities to the filling factors and magnetic fields. When the Gauss constraints (4) are applied to substitute for the magnetic fields in (14), these equations become:

$$\rho_0 = \frac{n_+}{2\pi}|\frac{\rho_0}{\kappa} + \frac{\tilde{\rho}_0}{2\tilde{\kappa}}| + \frac{n_-}{2\pi}|\frac{\rho_0}{\kappa} - \frac{\tilde{\rho}_0}{2\tilde{\kappa}}|,$$

$$\tilde{\rho}_0 = \frac{n_+}{2\pi}|\frac{\rho_0}{\kappa} + \frac{\tilde{\rho}_0}{2\tilde{\kappa}}| - \frac{n_-}{2\pi}|\frac{\rho_0}{\kappa} - \frac{\tilde{\rho}_0}{2\tilde{\kappa}}|. \tag{24}$$

These basic equations have the same form for fermi and bose-based systems; only the interpretation of the filling factors n_+ and n_- is different.

Now consider a mean-field state with

$$\tilde{\rho}_0 = \frac{\eta}{2}\rho_0,$$

where $-1 < \eta < 1$. In such a state, equations (24) become:

$$1 = \frac{n_+}{2\pi}|\frac{1}{\kappa} + \frac{\eta}{4\tilde{\kappa}}| + \frac{n_-}{2\pi}|\frac{1}{\kappa} - \frac{\eta}{4\tilde{\kappa}}|$$

$$\eta = \frac{n_+}{2\pi}|\frac{1}{\kappa} + \frac{\eta}{4\tilde{\kappa}}| - \frac{n_-}{2\pi}|\frac{1}{\kappa} - \frac{\eta}{4\tilde{\kappa}}|. \tag{25}$$

Because of the quantization of $\tilde{\kappa}$ we may write $\tilde{\kappa} = m/4\pi$, where m is an integer. with this substitution, the equations (25) may be combined into a relation between

n_+ and n_-, and another relation involving only n_+:

$$(1-\eta)\frac{n_+}{2\pi}|\frac{1}{\kappa}+\frac{\eta\pi}{m}| = (1+\eta)\frac{n_-}{2\pi}|\frac{1}{\kappa}-\frac{\eta\pi}{m}|, \tag{26}$$

$$\pi\frac{1+\eta}{n_+} = |\frac{1}{\kappa}+\frac{\eta\pi}{m}|. \tag{27}$$

In the case $\eta = 0$, these reduce to $\kappa = \frac{n_+}{\pi} = \frac{n_-}{\pi}$, reproducing the familiar set of Abelian mean-field theories. The bosonic ground state of maximal isospin alignment described in ref. [1] corresponds to $\eta = 1$. In this case, we have $n_- = 0$ and

$$\frac{1}{\kappa} = \frac{2\pi}{n_+} - \frac{\pi}{m}, \tag{28}$$

and thus find that κ takes values which are rational, but not necessarily integer, multiples of $1/\pi$. κ approaches integer values only in the limit $m \gg n_+$, or $\tilde{\kappa} \gg \kappa$.

We now consider the mean-field energy minimum (21) of the spin-1/2 fermion-based theory, which corresponds to

$$\eta = \frac{-4\tilde{\kappa}}{\kappa}\left(\frac{1}{32\pi^2\tilde{\kappa}^2+1}\right) = \frac{-m}{\pi\kappa}\left(\frac{1}{2m^2+1}\right). \tag{29}$$

The conditions on the coupling constants for a consistent mean-field theory at this value of η turn out to be more complicated. Noting the useful expressions

$$1 \pm \eta = \frac{\pi\kappa(2m^2+1) \mp m}{\pi\kappa(2m^2+1)} \tag{30}$$

and

$$|\frac{1}{\kappa} \pm \frac{\eta}{4\tilde{\kappa}}| = \frac{1}{|\kappa|}\left(\frac{2m^2+1\mp 1}{2m^2+1}\right), \tag{31}$$

we find that equation (26) (which relates n_- and n_+) takes the form

$$n_+[\pi\kappa(2m^2+1)+m]m^2 = n_-[\pi\kappa(2m^2+1)-m](m^2+1). \tag{32}$$

Note that, as usual, $\pi\kappa$ must be rational; we may write $\pi\kappa = p/q$, where p and q are relatively prime integers. By assumption, n_- is even while n_+ is odd. When equation (32)is multiplied by q, the RHS is even, so that $n_+[p(2m^2+1)+qm]m^2$ must likewise be even. This can only be satisfied if either m is even, or p,q, and m are all odd.

If $\kappa > 0$, the other consistency equation (27) becomes, after substitution of the expressions (30) and (31):

$$\pi\kappa(2m^2+1) - m = 2m^2 n_-,$$

or

$$\pi\kappa = \frac{2m^2 n_+ + m}{2m^2+1}. \tag{33}$$

Substitution of the above expression for $\pi\kappa$ in (32) yields:

$$m(mn_+ + 1) = n_-(m^2+1). \tag{34}$$

Letting $n_+ = n_- + D$, with D an odd integer, we find

$$D(m^2+1) + m = n_+. \tag{35}$$

By substituting this into the expression (33) for $\pi\kappa$, we finally obtain a relation between the two coupling constants:

$$\pi\kappa = \frac{2m^2((Dm^2+1)+m)}{2m^2+1}$$

$$\approx Dm^2 = 16\pi^2 D\tilde{\kappa}^2, \tag{36}$$

the latter expression being valid in the limit of small inverse coupling constants $\frac{1}{\kappa}, \frac{1}{\tilde{\kappa}} \to 0$ (near the point of free fermions).

4 Discussion and Conclusions

The relation (36) describing the coupling constants at which ground states with broken $SU(2)$ occur is a rather peculiar one. It is nonlinear, and does not appear to connect continuously to the theory's behavior near the bosonic point. Translated

into the variables $\theta \equiv 1/\pi\kappa$ and $\tilde{\theta} \equiv 1/\pi\tilde{\kappa}$, which represent the sizes of the Abelian and non-Abelian statistical phases, the relation becomes (in the $\theta, \tilde{\theta} \to 0$ limit):

$$\theta = \frac{\tilde{\theta}^2}{16D}. \tag{37}$$

In figure 3, the behavior of the mean field theory is plotted in the $\theta - \tilde{\theta}$ plane between $\theta = 0$ and $\theta = \pi$. The points $(0,0)$ and $(\pi,0)$ mark free bosons and free fermions, respectively, and it is near these two points that one expects the mean-field approximation to be useful. The odd-n fermion-based ground states appear between the line $\theta = \pi$ and a parabola, and are clustered near the $\theta = \pi$ axis. There is no obvious way to continue this behavior to that at the bosonic point.

One might draw one of two conclusions: Either there are phase transitions on the $\theta - \tilde{\theta}$ plot other than the ones shown (i.e., between $\theta = 0$ and $\theta = \pi$), or mean-field theory alone is not sufficient to understand the symmetry-breaking behavior of this theory near the free-fermion point. The fact that the expectation value (21) of the isospin density is second order in inverse coupling constants lends credence to the suspicion that the second conclusion is true: mean-field results typically receive corrections at quadratic order in inverse coupling constants due to fluctuations. The results in this paper, however, suggest that: (1) if there is a spontaneous isospin density near the fermionic point, it vanishes smoothly as that point is approached, and (2) it is worthwhile to study the question using other methods. It has been shown, for example, that the pure $SU(2)$ theory (to which our model reduces in the limit $\kappa/\tilde{\kappa} \to 0$) is susceptible to the formation of Cooper pairs in an isosinglet state.[5] The condensation of isosinglet Cooper pairs would naturally form a ground state with zero isospin density. But it is possible that when the Abelian coupling is also included, isotriplet Cooper pairs might form in some regions of parameter space.

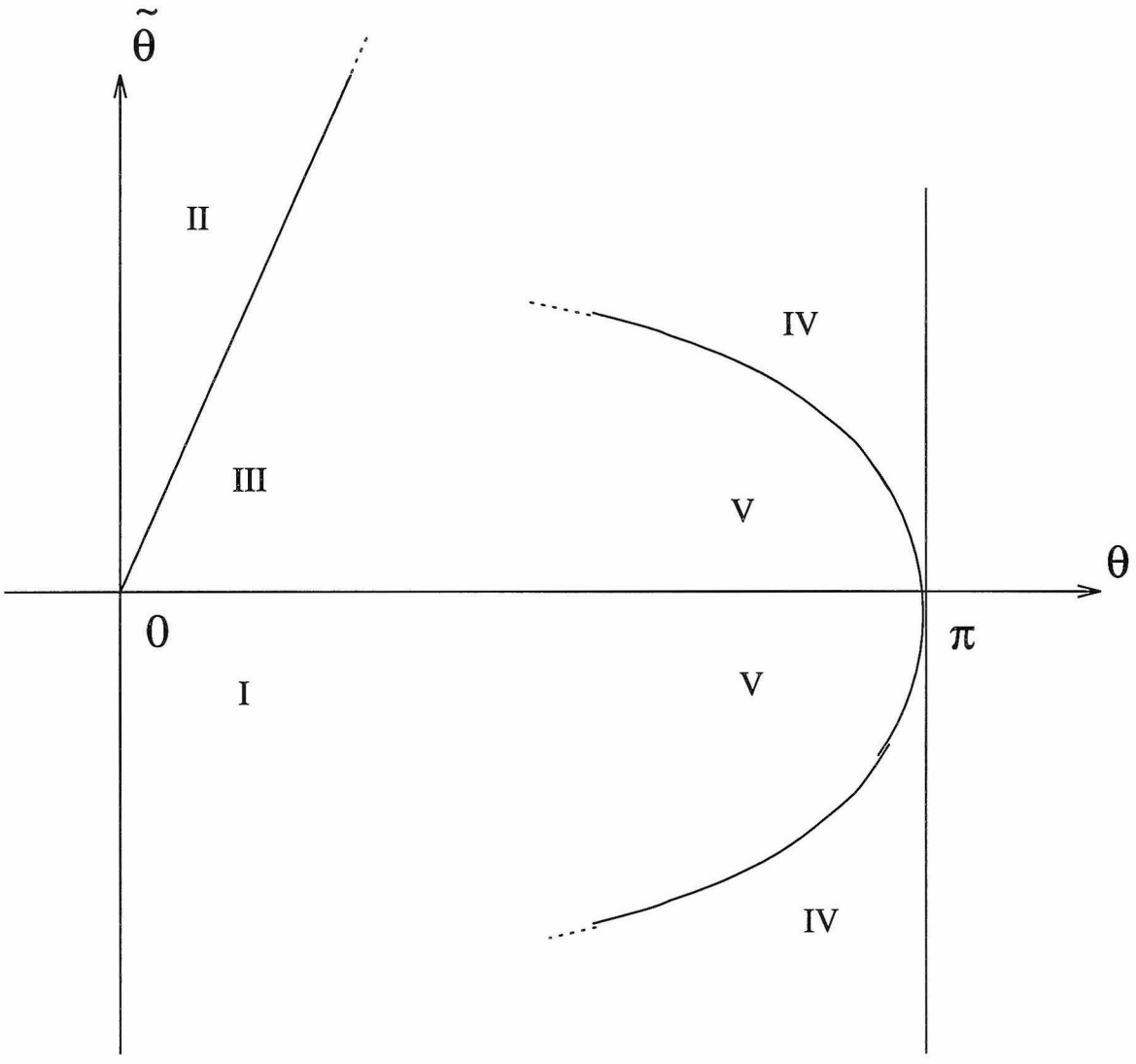

Figure 3: The $\theta - \tilde{\theta}$ plane. The theory's behavior near the points $(0,0)$ (pure bosons) and $(0,\pi)$ (pure fermions) delineates several regions. In region I, there is no spontaneous breaking of $SU(2)$: the energy is minimized by $\tilde{\rho} = 0$, In region III, there is a consistent mean-field ground state with a maximal expectation value of $\langle\tilde{\rho}\rangle = \rho_0/2$. In region II, mean-field theory fails: The ground state energy appears to have a minimum at some $\langle\tilde{\rho}\rangle < \rho_0/2$, but no self-consistent state can be constructed at that minimum. These are the three regions of parameter space corresponding to the curves I, II, and III in figure 1. Near the fermion point $(0,\pi)$ (regions IV and V), there are mean-field ground states with $\langle\tilde{\rho}\rangle = 0$. In region IV, there also exist states differing from the others only at quadratic order, and having a small expectation value of $\tilde{\rho}$. These are the odd filling factor states we have been discussing. It is not clear how these regions might connect to one another in areas far from the fermionic and bosonic points.

REFERENCES

1. A. Cappelli and P. Valtancoli, Nuc. Phys. **B 453**, 727 (1995).

2. C.A. Trugenberger, Phys. Rev. **D 45**, 3807 (1992).

3. See, for example, E. Fradkin, Field Theories of Condensed Matter Systems (Addison-Wesley, New York, 1991).

4. Some subtleties are being hidden within the phrase "all orbitals of any given Landau level." A droplet of finite area, uniform everywhere inside and dropping sharply at the edges, is generated by filling a finite number of degenerate orbitals, and a consideration of the droplet's edges is necessary when fluctuations about the mean-field state are taken into account. See G.V. Dunne, Int. J. Mod. Phys **B 8**, 1625 (1994).

5. A. Kapustin, unpublished calculation.

Chapter 3

A Global Analogue of Cheshire Charge

March-Russell, Preskill, and Wilczek[1] showed that vortices of a theory with a global $U(1)$ symmetry broken to Z_2 can scatter quanta of Z_2 charge with a cross section almost equal to to the maximal Aharonov-Bohm cross-section, due to a frame-dragging of local mass eigenstates. Here we demonstrate the realization of a non-abelian Aharonov-Bohm phenomenon (Cheshire charge) in the context of a global model.

In the first section, we describe a relativistic field theory that supports a global analog of Alice strings[2] and then describe how the process of charge exchange occurs by means of quantum interference. Some differences as well as similarities to the parallel phenomenon of Cheshire charge in gauge theories are mentioned, as well as the manner in which the global phenomenon can be viewed as a limit of the gauge case at very weak gauge coupling.

One of the motivations for studying global vortices and global Aharonov-Bohm scattering is that many more global than local symmetry-breaking transitions are available for manipulation in condensed matter systems. The possibility arises of finding condensed-matter systems which can serve as laboratory analogs of otherwise observationally inaccessible gauge string phenomena. In section 2, we consider the possibility of finding a laboratory analog of Cheshire charge in the superfluid A phase of helium-3. The group-theoretic properties necessary for the existence of Cheshire charge are present in He-3 A, although in practice it may be difficult to devise an experiment to observe it.

1 Cheshire Charge in a Theory With Broken Global Symmetry

The Model

Consider a theory with a global $SO(3)$ symmetry containing a Higgs scalar Φ transforming as the 5-dimensional symmetric tensor representation, which we will write as a 3×3 $SO(3)$ matrix, and another scalar field Ψ transforming as a 3-dimensional vector. Ψ will serve as the test particle that scatters from vortices. The fields transform under $SO(3)$ according to:

$$\Psi \rightarrow \Omega\Psi, \quad \Phi \rightarrow \Omega\Phi\Omega^{-1}, \tag{1}$$

where Ω is 3×3 $SO(3)$ matrix. We will denote the generators of $G = SO(3)$ as:

$$T_1 = \begin{bmatrix} 0 & 0 & 0 \\ 0 & 0 & -i \\ 0 & i & 0 \end{bmatrix}, \; T_2 = \begin{bmatrix} 0 & 0 & i \\ 0 & 0 & 0 \\ -i & 0 & 0 \end{bmatrix}, \; T_3 = \begin{bmatrix} 0 & -i & 0 \\ i & 0 & 0 \\ 0 & 0 & 0 \end{bmatrix}. \tag{2}$$

We also introduce a bilinear coupling of the Ψ fields to the Higgs:

$$\Delta\mathcal{L} = \lambda\Psi^T\Phi\Psi. \tag{3}$$

Now let the Higgs field acquire a vacuum expectation value $\Phi_0 = \nu diag(1, 1, -2)$. This breaks the symmetry group down to $H = U(1) \times_{S.D.} Z_2$. This is the same symmetry breaking pattern previously considered in the case of Alice strings [2] ; the difference is that we are considering a global, rather than a gauge, symmetry. The VEV Φ_0 induces a mass splitting among the the members of the multiplet Ψ, much as in Reference [1]. The first two components of Ψ are degenerate and are mixed by the unbroken $U(1)$ generator T_3, while the third component is an H singlet. From the first two we can form basis eigenstates of opposite $U(1)$ charges:

$$u_+ = (1, i, 0), \; u_- = (1, -i, 0). \tag{4}$$

The VEV in this theory can be thought of as taking values on the surface of a sphere with antipodal points identified. A visual analogy for the symmetry-breaking

pattern is the director field of a nematic liquid crystal (NLC). The order parameter of the NLC, like that of our theory, can be thought of as an undirected line segment at each point in space. The group of transformations which leave this segment invariant include continuous rotations about the director's axis (the $U(1)$ component) as well as a discrete 180° rotation about an axis perpendicular to the segment. This 180° flip generates the Z_2 component. Since the discrete 180° rotation does not commute with continuous rotations about the preferred axis, the full unbroken group is a *semidirect* product. This visual analogy will be useful later in explorations of condensed-matter systems. Our model can be reformulated in terms of a director field $\vec{\mathbf{d}}$, a vector in internal space, rather than a tensor, by defining

$$\Phi_{ab} = d_a d_b - d^2 \delta_{ab} \tag{5}$$

and making the identification $\vec{\mathbf{d}} \equiv -\vec{\mathbf{d}}$.

Construction of Alice Strings and Vortices

The above model can form topologically stable π_1 type defects. For simplicity we consider the model in two spatial dimensions, so that the defects are vortices. All arguments can be generalized straightforwardly to strings in three spatial dimensions. A vortex with core at the origin could have an asymptotic field configuration far from the origin given in polar coordinates by:

$$\Phi(\mathbf{x}) = \exp[\frac{-i\varphi T_1}{2}]\Phi_0 \exp[\frac{i\varphi T_1}{2}]. \tag{6}$$

The Higgs field is single valued, but the mass eigenstates of the Ψ field are not well-defined globally. One can define local (frame-dragged) mass eigenstates ρ_i at any point outside the core by $\rho = \exp[\frac{-i\varphi T_1}{2}]\Psi$.

As in reference [1], these local eigenstates define a frame at each point outside the core, and a state is adiabatically transported if its components in the local basis remain unchanged at each point. Notice that $\rho_2(0) = -\rho_2(2\pi)$. This means that when a state ρ_2 is adiabatically transported through a loop that encloses the vortex

core once, it acquires an Aharonov-Bohm-like phase of -1, whereas ρ_1 acquires no such phase. In terms of the fields of definite U(1) charge, $\rho_+ = \rho_1 + i\rho_2$ and $\rho_- = \rho_1 - i\rho_2$, the boundary condition can be written as $\rho_+(2\pi) = \rho_-(0), \rho_-(2\pi) = \rho_+(0)$. This means that the sign of the global U(1) charge is reversed when a ρ particle is adiabatically transported once around the string. Thus we have a global analog of the Alice string that occurs in the corresponding gauge theory.

In the gauge theory case it is known that a vortex-antivortex pair can acquire a "Cheshire charge" which compensates the charge gained by the particle upon threading the pair, so that the total charge is actually conserved.[3] This charge is a global property of the vortex pair; it cannot gauge-invariantly be localized to either one of the vortices or to any region of space near them. To see how charge conservation is maintained in this global model, consider a vortex-antivortex pair with the two cores separated along the x-axis by a distance D which is large compared to the core radius. Outside the cores, the vortex-antivortex solution to the field equations can be written:

$$\Phi_0(\mathbf{x}) = \exp[\frac{-i\Delta\varphi T_1}{2}]\Phi_0 \exp[\frac{i\Delta\varphi T_1}{2}] \tag{7}$$

where $\Phi_0 = \nu \mathrm{diag}(1, 1, -2)$ and $\Delta\varphi = \varphi_1 - \varphi_2$ as defined in figure 1. (Since the fluxes of the two vortices lie in the same $U(1)$ subgroup, it is easy to show that when the Higgs field is constrained to lie in the vacuum manifold, the static 2-d field equations reduce to Laplace's equation. Thus $\vec{\nabla}\Phi$ is dual to the electric field of two opposite charges in two dimensions, and the solution (7) is obtained.)

At points far away from both cores ($r \gg D$), the Higgs field approaches a single asymptotic value Φ_0. Thus the embedding of the unbroken group H is well-defined on any large circle outside the the two cores: its connected component is the $U(1)$ generated by T_3.

The local mass eigenstates are given by $\rho = \exp[-i\Delta\varphi T_1/2]\Psi$ and are thus unchanged under adiabatic transport along paths that remain far away from the pair where $\Delta\varphi \approx 0$. However, if a Ψ_2 state is transported from $y = -\infty$ to $y = +\infty$ along the y-axis (or along any path that passes between the two cores), the angle $\Delta\varphi$

winds through 2π, and the state Ψ_2 acquires an Aharonov-Bohm phase of -1, whereas Ψ_1 acquires no such phase. None of the triplet components acquires a phase if it is transported from $y = -\infty$ to $y = +\infty$ on a path which does not pass between the two cores. Thus an eigenstate of $U(1)$ charge changes the sign of its charge when it passes through the pair.

In order to understand how charge conservation is maintained, we must realize that there is an infinite family of vortex pair solutions related by $U(1)$ rotations. The solutions

$$\Phi_\alpha(\mathbf{x}) = \exp(i\alpha T_3)\Phi_0(\mathbf{x})\exp(-i\alpha T_3), \tag{8}$$

where $0 < \alpha < 2\pi$ and $\Phi_0(\mathbf{x})$ is given by (7), all have the same energy because they are related by a global symmetry transformation. Since they all have the same asymptotic value of the Higgs field, they can be continuously deformed into each other; thus there is a charge rotor zero mode. Figure 2 shows the action of the symmetry on the field of a vortex-antivortex pair. The order parameter is drawn as an undirected line segment as discussed above. Figure 2a shows one representative of a class of flux eigenstates. Other states degenerate with this one are obtained by rotating each of the directors through arbitrary angle α about the x-axis: Fig. 2b shows the result when $\alpha = \pi/2$. (Note that unlike our model, *physical* NLC's do not in general possess a continuous degeneracy of this type, but only a twofold degeneracy, because the free energy is not invariant under purely internal rotations of the director, but only under rotations of the whole coordinate frame.[4] The broken symmetry in NLC's is not truly an internal one of the type that occurs in relativistic field theories.)

The pair states which transform as irreducible representations of the asymptotically unbroken $U(1)$ group are coherent superpositions of the solutions (8): they are the quantized energy levels of the zero mode. A state with charge n is given by:

$$|n> = \int_0^{2\pi} d\alpha \exp(-in\alpha)|\Phi_\alpha> . \tag{9}$$

The Charge Transfer Process To understand the process of charge transfer by which a test particle reverses its charge and the vortex pair acquires a compensating charge, consider first the case where the vortex pair is originally in the state $|\alpha>$ described above. For each value of α, there is one component of Ψ that acquires a phase upon passing between the vortices, and another which does not. However, these states depend on the value of α. Let $u_{1\alpha}$ be the state which acquires no phase, and $u_{2\alpha}$ be the state which acquires a phase of -1. Then:

$$u_{1\alpha} = (\cos\alpha, -\sin\alpha, 0),\ u_{2\alpha} = (\sin\alpha, \cos\alpha, 0). \tag{10}$$

The $U(1)$ charge eigenstates $u_+ = (1, i, 0)$ and $u_- = (1, -i, 0)$ are expressed in terms of $u_{1\alpha}$ and $u_{2\alpha}$ as:

$$u_+ = \exp(-i\alpha)(u_{1\alpha} + iu_{2\alpha}),\ u_- = \exp(i\alpha)(u_{1\alpha} - iu_{2\alpha}). \tag{11}$$

Thus, when the state u_+ is adiabatically transported along a path that threads the pair, it is turned into the state $\exp(-2i\alpha)u_-$, whereas u_- becomes $\exp(2i\alpha)u_+$. These relations may be expressed simply in terms of a monodromy matrix, written in the charge eigenstate basis as follows:

$$\rho(2\pi) = \mathcal{M}(\alpha)\rho(0),$$

where

$$\mathcal{M}(\alpha) = \begin{bmatrix} 0 & e^{2i\alpha} \\ e^{-2i\alpha} & 0 \end{bmatrix}. \tag{12}$$

Now take an initial state in which the vortex pair is in the charge-zero eigenstate $|0>$ and the test particle is in the state u_+:

$$|u_+> \otimes |0> = \int_0^{2\pi} d\alpha |u_+> \otimes |\Phi_\alpha> . \tag{13}$$

After the particle is dragged through the loop, the final state will be:

$$\int_0^{2\pi} d\alpha \exp(-2i\alpha)|u_- > \otimes|\Phi_\alpha >= |u_- > \otimes|2 > . \tag{14}$$

The state has evolved into one in which the vortex pair has charge +2, because of the different phases acquired by the wavefunction in the different α sectors. The zero mode has been excited by means of a quantum-mechanical interference process, which is the usual means for the transfer of Cheshire charge, except that in this case it has occurred in a model with no gauge symmetry and does not have any topological interpretation[5] in terms of lines of electric flux being trapped between the vortices.

It may be noticed that even though the charged states $|n>$ exist for all integers, only those with n even can be produced by this process from an initially uncharged vortex. This is not necessarily the case in gauge Alice models. We can, in the case of a gauge model, take the initial gauge group G to be $SU(2)$ rather than $SO(3)$, and include matter fields transforming in the spinor representation. After the symmetry is broken to $U(1)\times_{S.D.} Z_2$, the spinor components become two oppositely charged states which interchange under the action of the Z_2 flip. The smallest electric charge in the theory is that carried by these spinor particles, and it is by passing these through a loop of Alice string (or pair of Alice vortices) that the odd-numbered Cheshire charge states are excited. However, the frame-dragging effect considered in Ref. [1] and in the present paper requires a matter field bilinearly coupled to the symmetry-breaking order parameter. Since the Higgs field in our model transforms in the 5-dimensional representation, no singlet can be formed from the Higgs field with only two spinors, and we are forced to consider matter fields Ψ lying in a vector representation. Thus, in comparing our global Alice system to the corresponding gauge model, the states which we have called $\rho_\pm$ should be thought of as doubly charged. The monodromy matrix (12), for example, has the property $\mathcal{M}^2 = 1$, rather than $\mathcal{M}^2 = -1$ as in the case of singly charged objects.[6]

Comparison With Ordinary Gauge Cheshire Charge

It is interesting that, although the existence of Cheshire charge is a consequence

of the symmetry breaking pattern only, and occurs in this global model for the same reason as in a gauge theory, the nature of the charge is rather different. As we see in the following paragraphs, global Cheshire charge actually is localizable and is carried by the scalar fields rather than the vector fields.

In the global theory we are considering, the zero mode is simply a "rigid" $U(1)$ rotation of the entire Higgs field configuration: thus it is a subgroup of the global $SO(3)$ transformations. α is the coordinate of the zero mode, and *classically* the excitations of this mode are states where $d\alpha/dt \neq 0$. Quantum mechanically, $d\alpha/dt$ will be replaced by a canonical momentum with discrete eigenvalues. This is to be contrasted with the case of a gauge model, where a rigid rotation of the Higgs fields alone fails to satisfy the equations of motion. In temporal gauge, the zero mode can be written[7]:

$$\Phi = \Omega\bar{\Phi}\Omega^{-1},\ A_\mu = \Omega\bar{A}_\mu\Omega^{-1} + \delta^i_\mu\partial_i\Omega\Omega^{-1}, \tag{15}$$

where $\bar{\Phi}$ and $\bar{A}_\mu$ are static solutions and $\Omega(x,t)$ is a *spatially varying* $SO(3)$ transformation that tends to an element of the unbroken group H (namely $\exp(i\alpha T_3)$) at infinity. (Notice that if the term $\delta^i_\mu\partial_i\Omega\Omega^{-1}$ were replaced by $\partial_\mu\Omega\Omega^{-1}$ then this would be a physically irrelevant gauge transformation.) By transforming to another gauge, one can view the zero mode as purely an excitation of the gauge fields,

$$\Phi = \bar{\Phi}, A_\mu = \bar{A}_\mu - \delta^0_\mu\partial_0\Omega^{-1}\Omega, \tag{16}$$

whereas in the global case it is purely an excitation of the scalar fields.

In our global case one can see that there is a nonzero charge density (i.e. , 0 component of the global current) which is localized in the region of space surrounding the vortices:

$$J_{0(3)} = 2\mathrm{Tr}\Phi T_3\overleftrightarrow{\partial_0}\Phi = 36\nu\sin^2(\Delta\varphi/2)(d\alpha/dt). \tag{17}$$

This definitely localizable charge carried by the scalar fields contrasts with the usual case, where the charge is carried by the gauge fields and its apparent location can be moved by performing gauge transformations[8]. Since the global charge density is

locally measurable, it must be the case that the charge is gradually transferred as the charged particle moves between the vortex cores. One must suppose that the charge density propagates away from the particle as the particle moves, and spreads itself through the region of space surrounding the cores. The transfer of gauge Cheshire charge, on the other hand, cannot gauge-invariantly be said to happen at a particular time and place, or even incrementally at a well-defined rate.

The relation between charge and energy is also different in the global case compared to the gauge case. This can be demonstrated by quantizing the zero mode. First treat α as a classical coordinate. Assume that the Higgs field configuration is given by

$$\Phi(x,t) = \exp[i\alpha(t)T_3]\Phi_0(x)\exp[-i\alpha(t)T_3] \tag{18}$$

i.e., a time-varying rigid rotation of the angle α. Then $\partial_t\Phi = i\dot{\alpha}[T_3,\Phi_0]$ and the gradient part of the Lagrangian gives

$$L = \int dt d^3x \partial_0\Phi\cdot\partial^0\Phi = -\int dt\int d^3x \mathrm{Tr}([T_3,\Phi_0]\dot{\alpha})^2. \tag{19}$$

(Since the static configurations of different α are degenerate, all other terms in the Lagrangian are independent of α and do not enter in that coordinate's equations of motion.) Letting

$$I = \int d^3x \mathrm{Tr}[T_3,\Phi_0]^2, \tag{20}$$

we can define a momentum Π_α conjugate to α and write a Hamiltonian

$$H = \frac{\Pi_\alpha^2}{2I}. \tag{21}$$

Now the commutator $[T_3,\Phi_0]$ is of order $|\Phi|$ within some volume surrounding the vortex cores. Since there is no domain wall connecting the cores, D is the only relevant length scale, and dimensional analysis then dictates that the "moment of inertia" I scales as D^d, where d is the number of spatial dimensions. Accordingly, the charge rotor Hamiltonian has eigenvalues $E_n = \frac{n^2\hbar^2}{2I} \approx n^2\hbar^2/(|\Phi|^2\times\text{Volume})$, so

the energy splittings among the global charge eigenstates scale as $1/D^d$. One may contrast this with the Coulomb energy (logarithmic in 2 space dimensions, $1/D$ in 3) of the usual gauge Cheshire charge.

The global vortex pair can be considered as a limit of the gauge model where the gauge coupling is so small that the Compton wavelength of the massive vector bosons is much larger than the separation D of the two vortex centers. In this limit, the Higgs field cores (regions where the Higgs leaves the vacuum manifold) can remain small while the gauge field cores (regions of nonzero magnetic flux) of the vortices become much larger than D so that there is actually no winding of the gauge field near the pair. In this case all the fields are defined on a trivial bundle and the Higgs VEV is covariantly non-constant just as in the global model. Presumably the Cheshire charge states will behave as in the global case, with a gauge invariantly localizable charge density carried by the scalars near the string.

Scattering From a Global Alice String

It is worth noting briefly that a single global Alice string of the type we have constructed will scatter incoming quanta of the Ψ fields. In fact, if we limit our attention to the ρ_2 and ρ_3 components, the calculation of the scattering amplitude proceeds precisely as in reference [1]. ρ_1, on the other hand, does not scatter at all (except perhaps off the vortex core itself). In other words, ρ_1 and ρ_2 are the monodromy eigenstates, and ρ_1 has eigenvalue unity. The result is that, if an incoming plane wave consists of either of the charge eigenstates ρ_+ and ρ_-, the scattered wave will be pure ρ_2, which is a superposition $-i(\rho_+ - \rho_-)/2$ of the two charge eigenstates. Consider the scattering of a ρ_+ incident at momentum below the threshold for ρ_3 production. We expect the ρ_1 and ρ_2 to behave asymptotically as an incoming and a scattered wave. We may write this asymptotic behavior as follows:

$$\begin{pmatrix} \rho_1 \\ \rho_2 \end{pmatrix} = \begin{pmatrix} 1 & 0 \\ 0 & e^{i\varphi/2} \end{pmatrix} \left\{ \begin{pmatrix} 1 \\ i \end{pmatrix} e^{-ikx} + \begin{pmatrix} 1 \\ i \end{pmatrix} f_+(\varphi) \frac{e^{ikr}}{r^{1/2}} + \begin{pmatrix} 1 \\ -i \end{pmatrix} f_-(\varphi) \frac{e^{ikr}}{r^{1/2}} \right\}. \tag{22}$$

f_+ and f_- are the charge-preserving and charge-reversing amplitudes for the scattered particle. The diagonal matrix in front enforces the boundary conditions on the frame-

dragged states. For simplicity we are considering a vortex in the flux eigenstate with $\alpha = 0$. Proceeding by analogy with [1], the equations of motion for the second component lead to

$$f_+(\varphi) - f_-(\varphi) = \frac{e^{-i\varphi/2}}{(2\pi ik)^{1/2}} \left(\frac{1}{\cos(\varphi/2)} + 2\sum_{n=0}^{\infty}(-1)^n(e^{i\Delta_n} - 1)\cos\left[(n+\frac{1}{2})\varphi\right] \right),$$

$$\Delta_n = \pi\left(n + \frac{1}{2} - \sqrt{(n+\frac{1}{2})^2 + \frac{1}{4}}\right). \qquad (23).$$

Since the first component does not scatter, we also have $f_+(\varphi) + f_-(\varphi) = 0$ and the amplitudes are uniquely determined. The differential cross-sections for charge-preserving and charge-flipped scattering, $d\sigma_+/d\theta$ and $d\sigma_-/d\theta$, are identical to each other and equal to one fourth the scattering cross-section derived in reference [1] for an Abelian global vortex:

$$\frac{d\sigma_+}{d\theta} = \frac{d\sigma_-}{d\theta} = \frac{1}{8\pi k}\frac{1}{\sin^2(\theta/2)}(1 + C(\theta)) \qquad (24)$$

where $\theta = \pi - \varphi$ is the scattering angle and $C(\theta)$, which vanishes at $\theta = 0$, is a function obtained by summing (and squaring) the series in (23). The inclusive cross section $d\sigma_+/d\theta + \sigma_-/d\theta$ is half that of the Abelian case considered in [1], because the ρ_1 state is, so to speak, "filtered out" of the scattered wave, just as a linear polarizer halves the intensity of a circularly polarized light beam.

Setting $C(\theta) = 0$ in (24) would give the cross section for doubly charged projectiles scattering from a gauge Alice string. $C(\theta)$, a correction present only in the global analog, results from diagonal $1/r^2$ potential terms appearing in the equations of motion for the ρ fields.* Evidently, these corrections modify the inclusive cross section but they do not affect the ratio σ_+/σ_-, which depends on the monodromy properties of the scattered particles and not on the local or global nature of the vortices.

---

* This cross-section was derived by neglecting off-diagonal terms that cause mixing of ρ_2 and ρ_3 near the vortex. Navin's analysis[9] suggests that the corrections to the standard Aharonov-Bohm cross section may disappear when the scattering problem is solved exactly.

2 A Condensed-Matter Example

Cheshire charge is a generic phenomenon that occurs when a theory has vortices whose winding fails to commute with a generator of the unbroken symmetry group of the vacuum. The results of the previous section show that Cheshire charge also arises if the theory has only global and not gauge symmetries. The essential group-theoretic concept is the same although the mechanism is different.

In this section, we discuss a physical system which exhibits the type of symmetry-breaking necessary for the existence of Cheshire charge: one which allows mixing of flux eigenstates within a conjugacy class. The system is the superfluid A-phase of liquid helium-3. While the right symmetry-breaking pattern is present, it may be difficult to observe Cheshire charge phenomena experimentally. There are many complications in dealing with a real condensed-matter system rather than a relativistic field theory. Some of these difficulties will be pointed out.

The Order Parameter in Superfluid He-3 A

He-3 atoms are fermions. A condensation of Cooper pairs of atoms is thought to be responsible for superfluidity in this system. Unlike the electrons in BCS superconductors, however, the helium atoms tend to pair in p-wave, rather than s-wave states, so they have a net orbital angular momentum of 1. In order for the two-atom wavefunction to be symmetric, therefore, members of the pair must also have their *spins* aligned in a triplet state with total spin 1. In addition to the overall phase of the condensate wavefunction, there are thus two separate angular momentum vectors which can a priori rotate independently. The full internal symmetry group of the pair wavefunction is[10][11]

$$SO(3)^{(L)} \times SO(3)^{(S)} \times U(1)^{\phi}.$$

This richness in degrees of freedom leads to a wealth of interesting phenomena associated with He-3 superfluidity. Let us denote the generators of these three factors by $\hat{\vec{L}}, \hat{\vec{S}}$, and $\hat{I}$, respectively. The symmetry of the superfluid ground state depends on temperature and pressure: there are at least two phases which are stable in bulk,

unmagnetized fluid, characterized by different ground state configurations. The A phase is described by a spin state $|10>$ along some preferred direction, and an orbital state $|11>$ along some other axis. The object corresponding to the Higgs field is a 3×3 complex matrix of two-particle correlation functions, A_{ai}, with each entry representing a particular spin state and orbital harmonic. Rotations in spin space act on the first index, a, and rotations in ordinary space act on the second index: A_{ai} transforms as a vector under each of the two $SO(3)$ factors of the symmetry group. The $U(1)$ factor acts on the overall phase of the matrix. In the A-phase, the matrix takes a value of the form:

$$A_{ai} = \Delta_A(T) d_a (e_{1i} + i e_{2i}) e^{i\phi}. \tag{25}$$

Here $\Delta_A(T)$, a temperature-dependent gap parameter, can be thought of as the magnitude of the superfluid wave function, much like the magnitude of the Higgs vev in a field theory. The vector $\vec{\mathbf{d}}$ is the axis along which the projection of the spin angular momentum is zero. $\vec{e_1}$ and $\vec{e_2}$, together with the vector $\vec{\ell} = \vec{e_1} \times \vec{e_2}$, define a local orthonormal frame such that the projection of the pair's mutual *orbital* angular momentum onto $\vec{\ell}$ is $+1$. The phase ϕ represents the overall phase of the pair wavefunction.

In order to see what the pattern of symmetry-breaking is, consider what transformations leave the order parameter invariant. Continuous rotations in spin space about the axis $\vec{\mathbf{d}}$ leave A_{ai} unchanged. These form an unbroken $U(1)$ subgroup with generator $\hat{S}_z$. (The state $|10>$ is invariant under rotations about the z axis.) Rotations in orbital space about $\vec{l}$ result in a phase (corresponding to the phase gained in rotations of the state $|11>$ about the z axis.) However, this can be compensated by a change in ϕ. Thus the $\hat{L}_z - \hat{I}$ generates another unbroken U(1) subgroup. These are the only two elements of the Lie algebra which annihilate A_{ai}, but the discrete transformation $\vec{\mathbf{d}} \to -\vec{\mathbf{d}}$, $\phi \to \phi + \pi$ leaves the matrix invariant. The $\vec{\mathbf{d}}$ vector can be flipped 180 degrees if the phase ϕ is simultaneously shifted by π. This makes the unbroken group $H = U(1) \times U(1) \times_{S.D.} Z_2$.

Because of the presence of this discrete 180° rotation in the little group, the spin quantization axis $\vec{\mathbf{d}}$ acts like the director field in a NLC: there are configurations in

which $\vec{\mathbf{d}}$ can be rotated continuously through 180° along a closed path which winds once around the core of a vortex. Such a configuration is the "half-quantum vortex," so called because the phase ϕ winds only halfway around the unit circle and the vortex carries only half of the conventional quantum of circulation. Half-quantum vortices are analogous to the Alice vortices of the previous section. A similar zero mode should in principle exist. In the next section, configurations with such a zero mode are described.

Half-quantum Vortices in He-3 A

Static configurations of the superfluid order parameter are extrema of the Landau-Ginzburg free energy functional[10], which takes the place of the field Hamiltonian. The free energy density includes a gradient energy term:

$$F_G = \gamma_1 \partial_i A_{\alpha j} \partial_i A^*_{\alpha j} + \gamma_2 \partial_i A_{\alpha i} \partial_j A^*_{\alpha j} + \gamma_3 \partial_i A_{\alpha j} \partial_j A^*_{\alpha i} \tag{26}$$

where γ_i are constants. For general values of γ_i, this term is not invariant under rotations of the orbital frame $(\vec{e_1}, \vec{e_2}, \vec{\ell})$ unless the external coordinates are simultaneously rotated. However, since the spin indices α are never contracted with any of the differentiation indices, the gradient energy is invariant under all global rotations of $\vec{\mathbf{d}}$, regardless of the values of γ_i. $SO(3)_{Spin}$ is truly an internal symmetry if only the gradient energy is included.

Only the spin-orbit, or dipole, interaction couples spin with orbital indices. This term has no analog in the model of section 2:

$$F_D = g_D(A_{ii}A^*_{kk} + A_{ik}A^*_{kl}) = -2g_D\Delta_A^2(\vec{\mathbf{d}} \cdot \vec{\ell})^2. \tag{27}$$

The dipole force is weak compared to the other interactions, but it has the consequence that in the bulk fluid, $\vec{\mathbf{d}}$ tends to line up parallel to $\vec{\ell}$. This is known as dipole locking.

In the presence of a pair of HQV's, the dipole energy must depart from minimum over some region between the cores (dipole unlocking). This is because $\vec{\ell}$, unlike $\vec{\mathbf{d}}$, cannot wind by odd multiples of π, so $\vec{\ell}$ will tend instead to remain constant. When

the cores are widely separated, the consequence is that the winding of the $\vec{\mathbf{d}}$ vector occurs within a domain wall, or soliton, whose width is of order

$$\xi_D \sim \sqrt{\frac{\gamma_i}{g_D}}. \tag{28}$$

ξ_D, known as the dipole length, is the scale at which the dipole energy becomes comparable to the gradient energy. The presence of a domain wall causes the half-quantum vortices to be confined linearly rather than merely logarithmically in two dimensions. Figure 3 shows $\vec{\ell}$ and $\vec{\mathbf{d}}$ for such a configuration. Since the dipole energy depends only on the angle between $\vec{\ell}$ and $\vec{\mathbf{d}}$ a global rotation of all the d vectors in figure 3 about the x axis will still leave the Landau-Ginzburg free energy invariant. This is the zero mode which gives rise to Cheshire charge in this case: a global rotation which belongs to the subgroup unbroken at infinity.

The Observability of Cheshire Charge

In the case of He-3 vortices, the "charge" that can be transferred is a form of angular momentum. The momentum conjugate to $\vec{\mathbf{d}}$ is the spin density, or net nuclear magnetization, $\vec{S}$. In the A-phase equilibrium, the spin density has expectation value zero. Dynamics slower than the gap frequency characterizing the symmetry-breaking scale but faster than $\sim 1Hz$ is governed by an effective Hamiltonian

$$\mathcal{H} = \frac{1}{2}\gamma^2 S_\alpha (\chi^{-1})_{\alpha\beta} S_\beta - \vec{H}\cdot\vec{S} + F_G + F_D, \tag{29}$$

where $\vec{H}$ is an externally applied magnetic field and γ is the gyromagnetic ratio of the atomic spins. Unless otherwise stated, we will assume no external field. χ, the magnetic susceptibility, is a symmetric tensor with two distinct eigenvalues $\chi_{\|}$ and $\chi_{\perp}$ reflecting the greater polarizability of the fluid in directions perpendicular to d:

$$\chi_{ij} = \chi_{\|} d_i d_j + \chi_{\perp}(\delta_{ij} - d_i d_j). \tag{30}$$

In spite of the coupling of $\vec{\ell}$ and $\vec{\mathbf{d}}$ through the dipole interaction, (29) ignores the dynamics of the orbital axis $\vec{\ell}$ is because the motion of $\vec{\ell}$ is so strongly damped that

all but very slow motions of $\vec{\mathbf{d}}$ can be treated as occurring on a background of fixed $\vec{\ell}$. 11The Hamiltonian (29), together with the commutation relations $\{S_i, d_j\} = \epsilon_{ijk} d_k$, $\{S_i, S_j\} = \epsilon_{ijk} S_k$, leads to the Leggett[12] equations of motion. $\vec{\mathbf{d}}$ precesses about $\vec{S}$ according to

$$\partial \vec{\mathbf{d}}/\partial t = \gamma \vec{\mathbf{d}} \times (-\frac{\gamma \vec{S}}{\chi_\perp}). \tag{31}$$

Thus the first term of (29) plays the role of a kinetic term for motions of $\vec{\mathbf{d}}$, with $\vec{S}$ being the momentum. In particular, for the pair configuration shown in Figure 3, the x component of $\vec{S}$ will be nonzero when the charge rotor is excited, and the quantized zero mode will have excitations where the total angular momentum $\int d^d x S_x = n\hbar$. These excitations will carry an energy of order

$$E_{ZM} \sim \frac{\gamma^2 n^2 \hbar^2}{\chi_\perp V_{\text{Soliton}}}, \tag{32}$$

where V_{Soliton} is the volume of the dipole-unlocked region near the cores. For large n, one can identify a classical precession frequency $\omega = (1/\hbar) dE/dn$, and the kinetic energy is given by:

$$E_{ZM} \sim \frac{\omega^2 V_{\text{Sol}} \chi_\perp}{\gamma^2}. \tag{33}$$

As in the model of Section 2, this energy has, for fixed n, an inverse dependence on the soliton volume, and thus on the separation of the cores. In a two-dimensional geometry where string tension does not operate, it is possible that a sufficiently excited pair could be stabilized against the attractive force due to the dipole interaction, provided the "Cheshire charge" cannot be radiated away rapidly. This would occur if the energy stored in the zero mode was comparable to the dipole energy of the the soliton connecting the two cores:

$$E_D \sim g_D \Delta_A^2 V_{\text{Sol.}} \sim E_{ZM} \sim \gamma^2 \frac{n^2 \hbar^2}{V_{\text{Sol}} \chi_\perp}. \tag{34}$$

Using formulas and numbers that can be found in Reference[10], one can estimate the

volume at which this occurs (more details of this estimate are found in the Appendix):

$$V \sim n \times (1 - T/T_c)^{-1/2} \times 10^{-16} cm^3. \tag{35}$$

The classical precession frequency of $\vec{\mathbf{d}}$ corresponding to this energy level is approximately $10^4 s^{-1}$. By comparison, the gap frequency below T_c is typically $\sim\ kT_C/\hbar \sim 10^7\ s^{-1}$.

The stability of a charged excited state of a vortex loop or pair is also uncertain. It may depend on details of the spin relaxation behavior of the fluid and such factors as coupling between the superfluid and the normal fluid component[13]. However, since the precession frequency found above to be sufficient to cancel the attractive force is lower than the gap frequency, one would imagine that at least the radiation of "Higgs" modes would be suppressed. Also, since the "Cheshire charge" consists of a nonzero spin density in the direction of $\vec{\ell}$ (assuming that $\vec{\ell}$ maintains a uniform value everywhere which is parallel to the asymptotic value of $\vec{\mathbf{d}}$), no torque should be exerted on this component of $\vec{S}$ by the dipole force. This renders one of the usual means[11] for relaxation of $\vec{S}$ ineffective: namely its damping by coupling to $\vec{\ell}$.

A Charge Exchange Process

The spin wave excitations of the He-3 A order parameter carry quantum numbers which allow the possibility of an Aharonov-Bohm interaction with half-quantum vortices. In general, spin waves consist of a coupled oscillation of $\vec{\mathbf{d}}$ and $\vec{S}$. Consider the form

$$\vec{\mathbf{d}} = \vec{\mathbf{d}}_0(\vec{r}) + \vec{\psi}(\vec{r}, t).$$

Oscillations of ψ parallel to $\vec{\mathbf{d}}_0$ have a gap characterized by the symmetry-breaking scale. On the other hand, oscillations of ψ perpendicular to $\vec{\mathbf{d}}_0$ only have a frequency shift Ω_A proportional to the dipole energy. In particular, the two propagating low-frequency modes obey a wave equation of the form

$$-\frac{\partial^2 \psi}{\partial t^2} = \Omega_A^2 \psi + \Omega_A^2 (U\psi + D\psi), \tag{36}$$

where

$$\Omega_A^2 = \frac{\gamma^2 2\Delta_A^2 g_D}{\chi_\perp}, \tag{37}$$

U is a potential which is zero in the bulk fluid, and D is a kinetic operator:

$$D\psi = -\xi_d^2[\Delta\psi + \frac{\rho_{sp}^{\parallel} - \rho_{sp}^{\perp}}{\rho_{sp}^{\parallel}}\vec{\nabla}\cdot(\vec{\ell}(\vec{\ell}\cdot\vec{\nabla})\psi)]. \tag{38}$$

$\rho_{sp}^{\perp} \propto (2\gamma_1 + \gamma_2 + \gamma_3)$ and $\rho_{sp}^{\parallel} \propto 2\gamma_1$ are the spin rigidity coefficients describing the energy of gradients in $\vec{\mathbf{d}}$. The lower cutoff frequency Ω_A arises because an oscillation of $\vec{\mathbf{d}}$ about $\vec{\ell}$ is an oscillation in the potential well formed by the dipole coupling $g_D(\vec{\ell}\cdot\vec{\mathbf{d}})^2$. (As mentioned previously, $\vec{\ell}$ can effectively be regarded as fixed on the time scales of these oscillations. The fluctuations of $\vec{\ell}$ are diffusive or overdamped.) The potential U becomes nonzero when $\vec{\ell}$ is not parallel to $\vec{\mathbf{d}}$ (as inside domain walls) or when nonuniform textures of the order parameter are present. These oscillations of ψ perpendicular to $\vec{\mathbf{d}}_0$ would be Goldstone modes if the dipole energy were neglected, and they are degenerate with each other as long as $\vec{\mathbf{d}}_0 \parallel \vec{\ell}$.[14] There are thus three modes which have the pattern of splitting analogous to the splitting of the Ψ modes in section 2.

Figure 4 demonstrates the "frame dragging" of the spin wave modes. We assume a frequency lower than the gap frequency, which corresponds to the assumption in Section 2 or in reference [1] that scattering experiments are done at an energy such that only the light components of the split multiplet Ψ are excited. Then the two propagating oscillations (corresponding to Ψ_1 and Ψ_2) are the two different polarizations of ψ perpendicular to $\vec{\mathbf{d}}_0$. In accordance with eqn. (31), the fluctuation of $\vec{\mathbf{d}}$ is accompanied by a fluctuation of $\vec{S}$ in the $\vec{\psi}\times\vec{\mathbf{d}}_0$ direction. In the region far from the vortex cores, $\vec{\ell}$ and $\vec{\mathbf{d}}$ are taken to lie along the x-axis, so that one of the propagating modes, labeled 1, involves ψ_y and S_z, while mode 2 involves ψ_z and S_y. As one follows a path around one of the vortices, however, mode 2 experiences a frame-dragging which causes it to mix with S_z, acquiring an Aharonov-Bohm minus sign when transported around a loop. Mode 1 remains unaffected. It is therefore conceivable that a

similar charge exchange process could occur in the scattering of spin waves off pairs of half-quantum vortices. A circularly polarized spin wave (an eigenstate of the unbroken subgroup of rotations) could scatter from the pair of vortices, changing to the opposite circular polarization and depositing angular momentum (Cheshire charge) in the vicinity of the vortices.

The theoretical possibility of an Aharonov-Bohm type scattering from HQV's using collective excitations of the fluid as the projectiles has been mentioned previously by Khazan and others[15,10]. However, the context studied by these authors was that of NMR experiments in which either spin waves or an orbital "Higgs" excitation called the clapping mode are excited by means of a fluctuating magnetic field. The high *steady-state* magnetic field which is used in NMR breaks the degeneracy between the two "light" spin wave modes, leaving us with an Abelian situation like that of reference [1]. Situations in which the non-Abelian Aharonov-Bohm effect might be seen were not discussed.

It may in practice be difficult to devise a Cheshire charge experiment without having the $SO(3)$ symmetry destroyed by an external field. An additional difficulty arises from the potentials U in equation (36). In addition to the Aharonov-Bohm effect, one expects spin waves to be scattered by these non-topological potentials which are nonzero within a soliton where $\vec{\mathbf{d}}_0$ is not parallel to $\vec{\ell}$. These potentials arise because of the change in the dipole restoring force as $\vec{\mathbf{d}}_0$ leaves the bottom of the dipole potential well, and because of other anisotropies associated with the orbital state. In fact, the two linear polarization states of the spin wave experience different potentials inside the soliton, which could give rise to phase shifts between them in addition to the Aharonov-Bohm phase.

APPENDIX A

Estimate of Charge Necessary to Stabilize Pair of HQV's.

This appendix contains a derivation of the order-of-magnitude estimate (35) for the level of excitation of the charge rotor mode (and corresponding classical precession frequency) at which its energy becomes comparable to the dipole energy of the soliton connecting a pair of half-quantum vortices. The data and formulas used here can be found in references [10] and [11].

We begin with equation (34), equating the dipole energy with the zero-mode energy:

$$E_D \sim g_D \Delta_A^2 V_{\text{Sol.}} \sim E_{ZM} \sim \gamma^2 \frac{n^2 \hbar^2 \chi_\perp}{V_{\text{Sol}}}. \tag{A1}$$

$\chi_\perp$ is the larger eigenvalue of the magnetic susceptibility tensor. It differs from the susceptibility $\chi_N^0 = \gamma^2 \hbar^2 N(0)$ of a noninteracting degenerate Fermi gas only by a factor of order unity, so we may use this value as an estimate of $\chi_\perp$. In the previous expression, $N(0)$ is the density of states at the Fermi surface, given by $N(0) = m^* k_f / 2\pi^2 \hbar^2$ where $k_f \hbar$ is the Fermi momentum.

We also rewrite the dipole coupling constant in terms of measurable length scales as follows:

$$g_D = \frac{\gamma_0}{\xi_D^2} = \frac{N(0)\xi_0^2}{\xi_D^2}. \tag{A2}$$

γ_0 is a typical coefficient of the gradient energy: in the weak-coupling, or small-interaction limit, the coefficients γ_i in the gradient energy (26) are all equal to γ_0. We have in turn related this coefficient to the coherence length $\xi_0(1 - T/T_C)^{-1/2}$. The two length scales are quoted by [10] as of order $\xi_D \sim 10^{-3} cm$ and $\xi_0 \sim 10^{-6} cm$.

Finally, we use the relation $\Delta_A \sim kT_C(1 - T/T_C)^{1/2}$ for the gap parameter. We can substitute the estimates for $\chi_\perp$, g_D, and Δ_A into (A1). Assuming temperatures in the millikelvin range, molar volumes of a few tens of cm^3, and quasiparticle mass

m^* approximately equal to the atomic weight of helium, we obtain:

$$V_{\rm Sol} \sim \frac{n\hbar^2\xi_D}{\xi_0 m^* k_f k T_C (1-T/T_C)^{1/2}} \sim n \times 10^{-16} cm^3. \tag{A3}$$

We may also express the answer in terms of a classical precession frequency. Expressed in terms of ω, (A1) becomes:

$$\frac{\omega^2 V_{Sol}\chi_\perp}{\gamma^2} \sim g_D \Delta_A^2 V_{Sol}. \tag{A4}$$

Using the same estimates as above, we find:

$$\omega\hbar \sim \frac{\xi_0}{\xi_D}\Delta_A. \tag{A5}$$

This shows that the frequency is of order 10^{-3} times the gap frequency, or about 10 kHz if $(1-T/T_C) \sim 1$. Not surprisingly, this is also of the same order as the cutoff frequency Ω_A for spin waves.

REFERENCES

1. J. March-Russell, J. Preskill, F. Wilczek. Phys. Rev. Lett. **68** (1992), 2567.
2. A. Schwarz, Nuc. Phys. **B208** (1982) 141.
3. M. Alford, K. Benson, S. Coleman, J. March-Russell, F. Wilczek. Phys. Rev. Lett. **64** (1990), 1632. J. Preskill, L. Krauss. Nuc Phys **B 341** (1990), 50.
4. See, for example, I. Chuang, R. Durrer, N. Turok, B. Yurke. Science **251** (1991), 1336.
5. M. Bucher, H.K. Lo, J. Preskill. Nuc. Phys. B 386 (1992), 3.
6. H.K. Lo, J. Preskill, Phys. Rev. D **48** (1993) 4821.
7. M. Alford, K. Benson, S. Coleman,J. March-Russell, F. Wilczek. Nuc. Phys B **349** (1991) 414.
8. A. Everett, Phys. Rev. D **47** (1993), R1227.
9. R. Navin, *Global Analogue of the Aharonov-Bohm Effect*, Ph.D. Thesis (Caltech 1993) and Caltech preprint CALT-68-1896
10. M. M. Salomaa, G. E. Volovik, Rev. Mod. Phys. **59** (1987), 533.
11. D. Vollhardt and P. Wölfle, *The Superfluid Phases of Helium-3* (Taylor and Francis, New York, 1990).
12. A. J. Leggett, Ann. Phys. **85** (1974), 11.
13. M. Cross, private communication.
14. P Wölfle, Physica **90B** (1977), 96. G.E. Volovik, M.V Khazan. Soviet Physics JETP **58** (1983), 551.
15. M.V. Khazan. JETP Lett. **41** (1985), 486. M. M. Salomaa, G. E. Volovik. Phys. Rev. Lett. **56** (1986), 1313.

FIGURE CAPTIONS

1) Definition of angles φ_1, φ_2, and $\Delta\varphi$ in vortex pair geometry.

2) Degenerate configurations of vortex pair. This figure shows two order parameter configurations for a vortex-antivortex pair, related by a global symmetry operation. The order parameter is represented by an undirected line segment. In Fig.2A, the directors all lie within the plane of the page. In Fig.2B, they rotate outward, and only their projection in the plane of the page is shown.

3) Domain wall of dipole energy. The spin axis $\vec{\mathbf{d}}$ is represented by the undirected line segments, while the thick arrows represent $\vec{\ell}$. the region in which $\vec{\ell}$ and $\vec{\mathbf{d}}$ are not parallel has a width of order ξ_D.

4) Parallel transport of orthogonal spin wave modes. The effect of parallel transport about an HQV core on the two degenerate spin-wave modes is shown. $\vec{\mathbf{d}}$ is indicated by the undirected line segments. The amplitude of oscillation of the spin density $\vec{S}$ is shown by the thick arrows. The thin arrows show the corresponding motion of $\vec{\mathbf{d}}$. In mode 1 (upper figure) the spin density amplitude points out of the page and remains the same on transport around the core. For mode 2, (lower figure) the spin density amplitude is within the page and experiences a sign change.

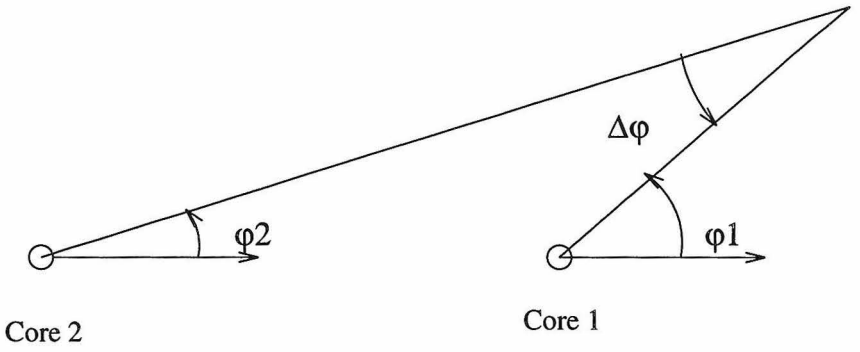

FIGURE 1

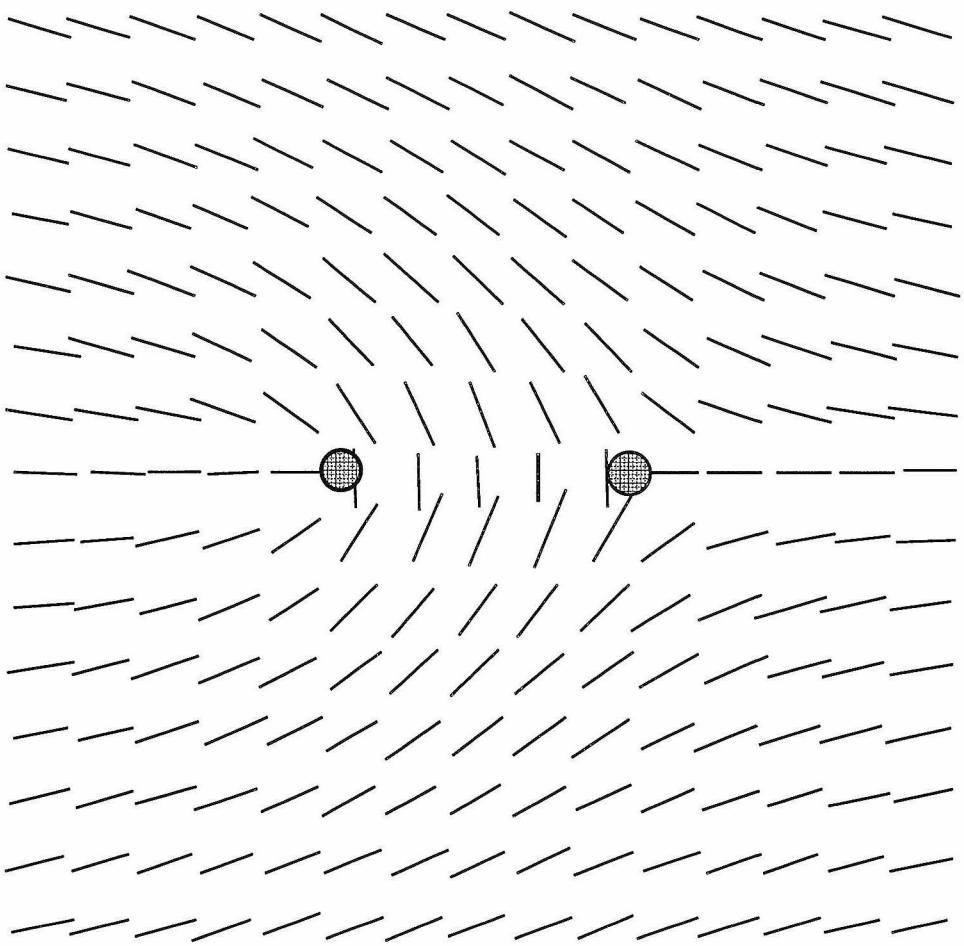

FIGURE 2A

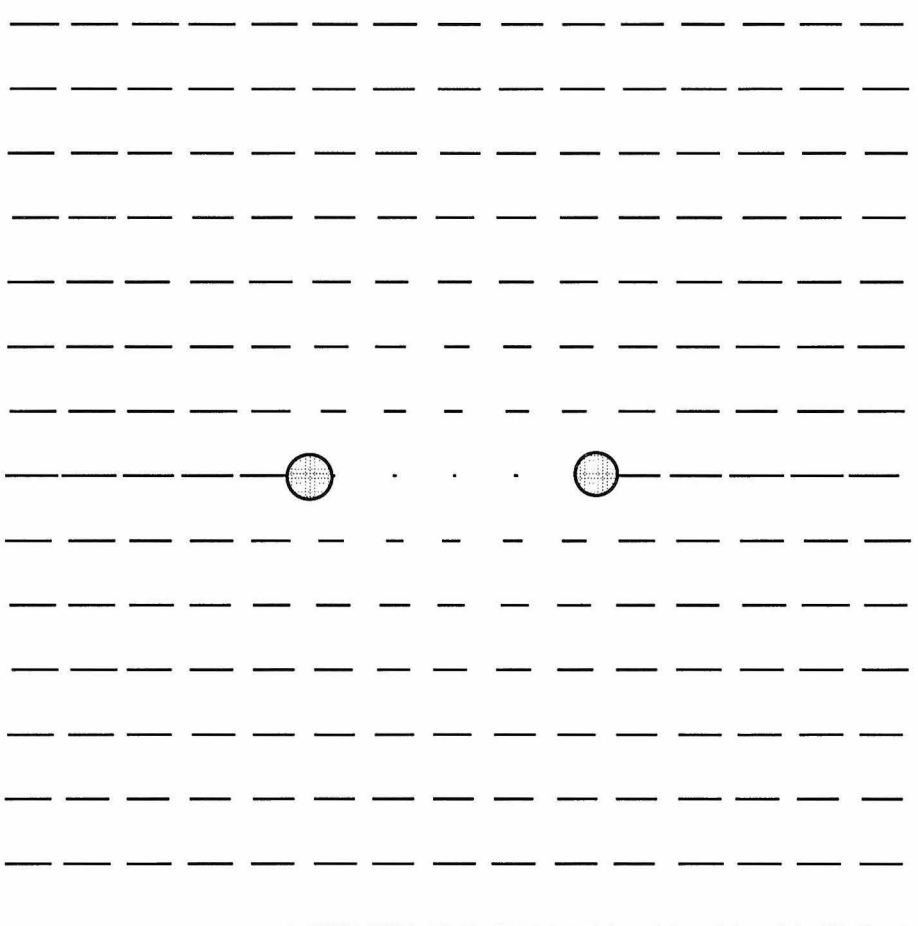

FIGURE 2B

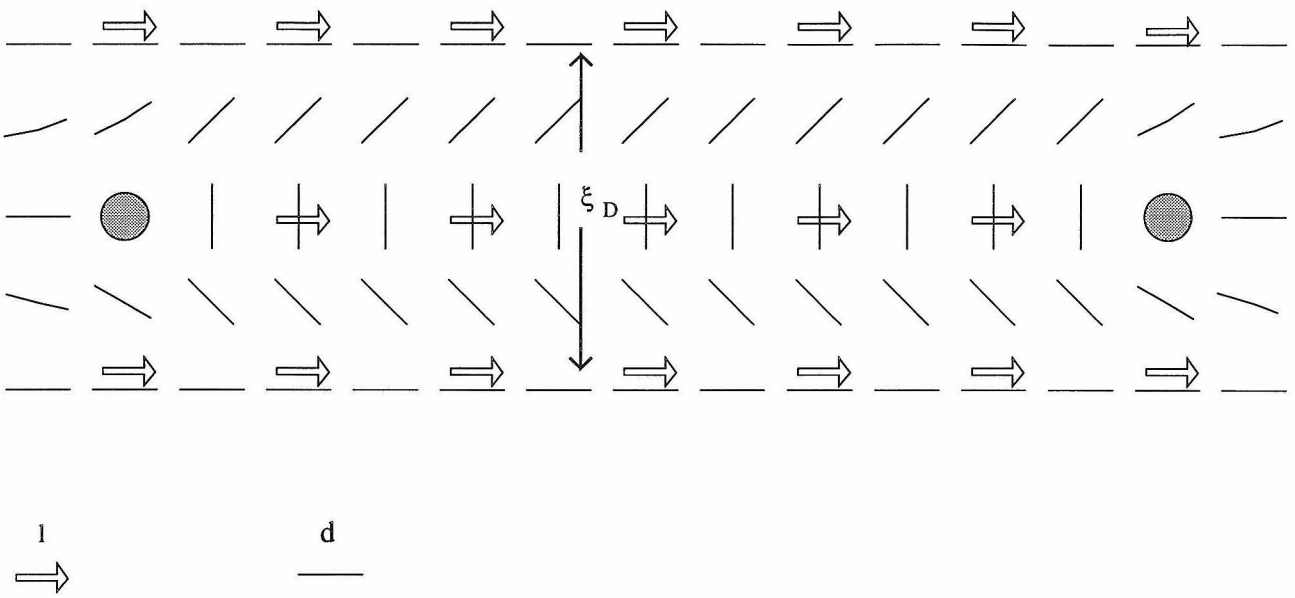

FIGURE 3

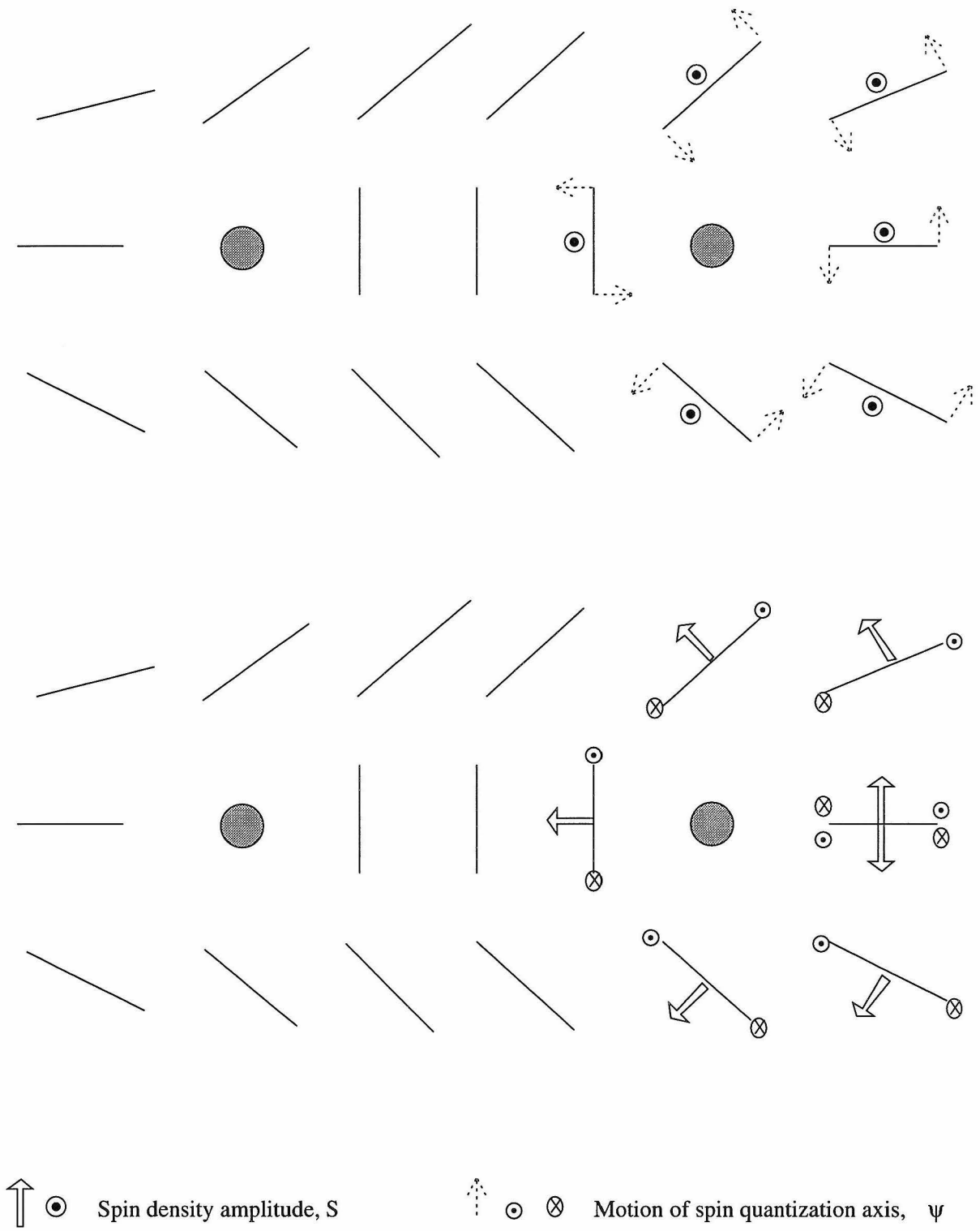
Spin density amplitude, S
Motion of spin quantization axis, ψ

FIGURE 4

Chapter 4

Dynamical Simulation of Non-Abelian Cosmic Strings

A generic feature of many spontaneously broken gauge theories is the existence of topological solitons, including strings or flux tubes. Many grand unified models would predict the formation of such strings, known as cosmic strings, during a cosmological phase transition.[1] The many potential cosmological effects of cosmic strings[2] motivate one to wish to understand the subsequent evolution of such strings. For example, since the gravitational effects of cosmic strings have occasionally been invoked as a possible source of density perturbations leading to galaxy or cluster formation, one is interested in knowing whether the strings are likely to decay very rapidly or persist long enough to seed density perturbations. One is naturally also interested in the probability of observing strings in the present-day universe. On the other hand, one might rule out certain phenomenological models if they seem to predict an abundance of strings inconsistent with present observations, much as the non-observation of monopoles has created difficulties for some models which predict a great abundance of monopoles.

Some theoretical and numerical studies[3] have been devoted to the evolution of networks of Abelian strings such as those corresponding to the Nielsen-Oleson[4] vortex solution of the Abelian Higgs model. It is generally believed that networks of this type are likely to form many closed loops which decay into smaller loops by the mechanism of intercommutation, resulting in a "scaling" distribution of loop sizes such that the number of loops within a cosmological horizon volume of the universe is roughly constant over time. Vachaspati and Vilenkin[5] have performed a numerical simulation of a network of Z_3 strings, which have the novel feature that three strings may intersect in a vertex. Their results suggested that such strings tend to form an infinite network of vertices connected by string segments. The annihilation of these vertices leads to a similar scaling behavior, with the number of vertices and string segments per horizon volume being roughly constant. To my knowledge, however, very little is known about

more complicated models in which the strings carry non-commutative magnetic fluxes and there is more than one type of string. Such strings are known to exhibit a number of exotic types of interactions[6]. Particularly significant is the fact that when two non-Abelian strings cross each other, they cannot generally intercommute, nor can they pass through one another without forming new vertices and becoming joined by a new segment of string. Linked loops of string cannot usually become unlinked, and vice versa. One might expect that this would inhibit the decay of a cosmic network by providing obstruction to the free removal of string segments.

In this chapter, we describe a numerical simulation of a network of S_3 strings. As in the Z_3 case, the strings form 3-string vertices. In the spirit of reference [5] we generate initial conditions from a lattice Monte Carlo simulation and then evolve the network according to highly simplified model of string dynamics which we hope captures the essential features of the system. All string segments are assumed to be straight. The vertices move under the influence of the string tensions acting on them. We will see that a simulation of the non-commutative nature of the strings poses some rather difficult computational problems. Only the method of the simulation is described here; results will be presented elsewhere.[7] Section 1 provides a brief summary of the properties of non-Abelian strings as they apply to this simulation. We demonstrate some of the ambiguities inherent in the description of the state of a network of strings, and the necessity of a (gauge fixing) convention to resolve these ambiguities. Section 2 describes the particular S_3 model which we have chosen to simulate. In sections 3 and 4 we describe the gauge fixing convention implemented by our program, and our method for making any needed comparisons of string fluxes in the simulated network. Section 4 in particular discusses some of the subtleties that arise when periodic boundary conditions are used. Section 5 describes how we generate an initial condition for our simulation using a lattice Monte Carlo method. The transcription of a lattice configuration into a network that is fully specified according to the conventions of our simulation is itself a tricky task. In section 6, we describe the actual procedure for simulating the time-evolution of the initial network, making reference to the conventions described in previous sections. Finally, in section 7, we present some preliminary results from the simulation, which is still in progress.

In this discussion, the strings will be considered as classical objects with well-defined fluxes (after a gauge has been fixed). We will not consider quantum-mechanical effects such as Cheshire charge,[8] even though the possibility exists that Cheshire charge might influence string dynamics.

1 Vortices and strings in a non-Abelian discrete gauge theory

Generically, topological defects of codimension 1 (vortices in two space dimensions, strings in three) occur when a gauge symmetry group G is spontaneously broken to a subgroup H such that there are non-contractible closed loops in the vacuum manifold G/H. This is formally expressed by saying that $\pi_1(G/H)$ is nontrivial, where π_1 stands for the first homotopy group. This does in fact happen when G is simply connected and H is a discrete group. Here, we review very briefly some of the properties of non-Abelian vortices and strings which are important for the current simulation. More details may be found in ref. 6.

The breaking of an underlying G gauge theory to a discrete group H leaves no light propagating gauge fields: At low energies in any simply connected region without defects, the gauge field A_μ^a is pure gauge. However, when string defects are present, the region of true vacuum is not simply connected: it is $\mathcal{R} = \mathcal{M} - \{D\}$, where $\{D\}$ is the union of all defect cores (regions of false vacuum) and $\mathcal{M}$ is the spatial manifold on which the defects exist. Each string gives rise to a class of noncontractible closed paths in $\mathcal{M} - \{D\}$ which encircle the string. The flux enclosed by any closed loop Γ is a group element defined as a path-ordered exponential of the gauge field:

$$\text{flux} = P \exp\left(\oint_\Gamma A \cdot d\ell\right). \tag{1}$$

For any Γ within $\mathcal{R}$ this must be an element of H. This is because the Higgs field is covariantly constant throughout $\mathcal{R}$ and so the transformation that results from parallel transport around a loop must leave the Higgs field invariant.

The flux of a cosmic string is defined by the above exponential along a path which winds around the string. In a non-Abelian theory, this definition of the flux

is not gauge invariant, and may depend on the point at which the path begins and ends. A key observation, however, is that the flux through any loop which does not enclose a string is necessarily trivial, and a corollary is that two closed loops which share the same beginning and ending point x_0, and can be continuously deformed into each other, have the same flux. The relevant structure for the description of the system of defects is the fundamental group or first homotopy group $\pi_1(\mathcal{M} - \{D\}, x_0)$, defined with respect to a basepoint x_0. Each string is associated with a generator of the fundamental group. Once x_0 has been (arbitrarily) chosen, the fluxes of all closed paths (and of all strings) are specified by a homomorphism from $\pi_1(\mathcal{M} - \{D\}, x_0)$ into H. The only remaining gauge freedom is a global one. However, there is a considerable amount of ambiguity in what we mean by "the flux" of one particular string: an arbitrariness in how exactly the set of generators is chosen for the homotopy group. In figure 1, for example, there are two loops, both beginning and ending at x_0, both enclosing the same string without enclosing any others, which are nonetheless representatives of different homotopy classes (and consequently may be associated with different fluxes): Another intervening string prevents one path from being continuosly deformed to the other. The fluxes associated with the two different paths may differ through conjugation by the flux of the other string. In an Abelian theory, conjugation is trivial; not so in a non-Abelian one. It follows that fluxes cannot meaningfully be compared (say, to determine if they are the same) if the paths used to define those fluxes pass on opposite sides of some other string. Comparisons must be made using "nearby" paths.

In the sequel, the establishment of a conventional set of generators for $\pi_1(\mathcal{M} - \{D\}, x_0)$ and determining their associated H elements is often referred to somewhat loosely as "fixing a gauge." As a notational convention, we will usually label the representatives of particular homotopy classes with Greek letters, while using Roman letters for the associated H elements.

The dependence of the definition of a string's flux on other strings between it and the basepoint, as described above, has important consequences for the behavior of a network of non-Abelian strings. One of these is the occurrence of so-called "holonomy interactions" or exotic exchange interactions. These are a consequence

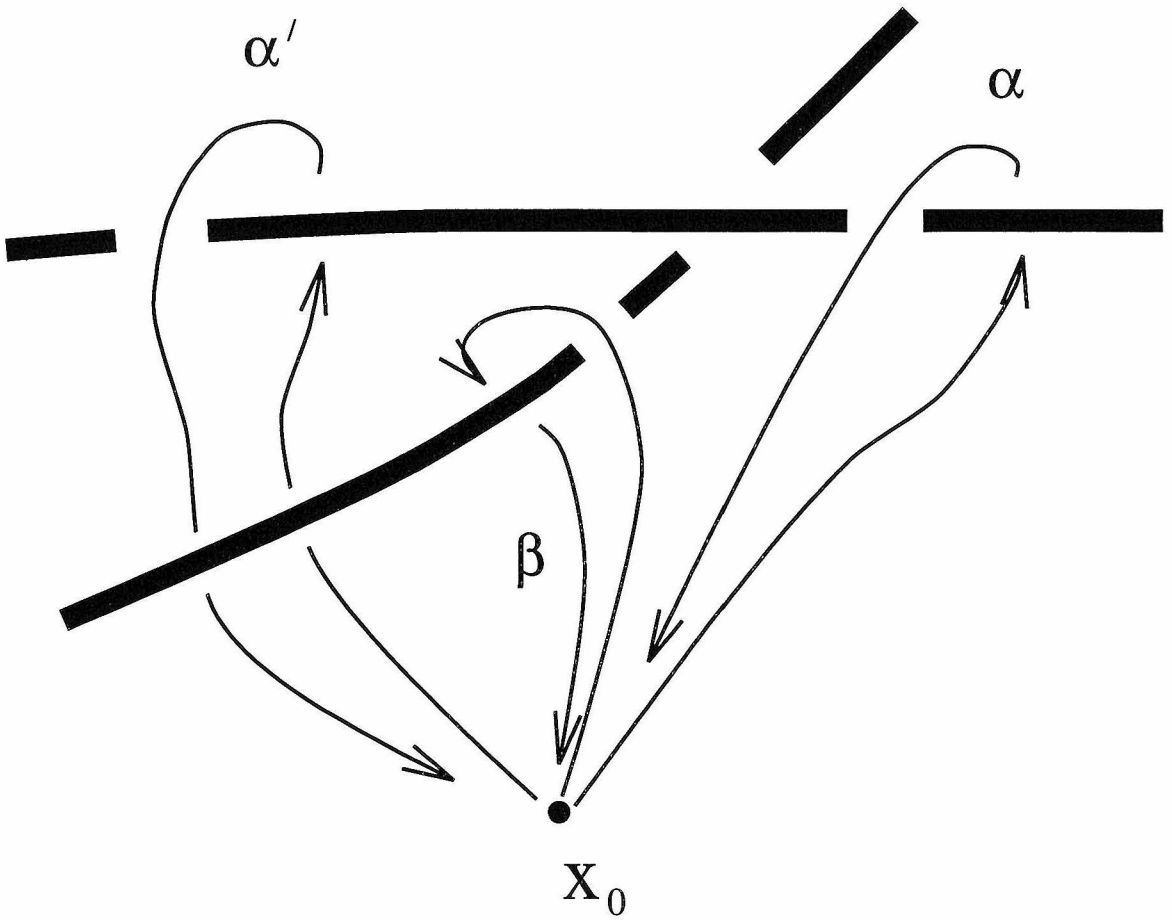

Figure 1: The paths α and α' both enclose the same string and no other strings, but they cannot be continuously deformed into each other without crossing another string. Thus, they represent different elements of the fundamental group $\pi_1(\mathcal{M} - \{D\}, x_0)$, and so the fluxes associated with them may be different. Specifically, the homotopy classes of α and α' are related through conjugation by another generator: $\alpha' \sim \beta\alpha\beta^{-1}$. (We follow the usual convention of composing paths from right to left: $\beta\alpha\beta^{-1}$ means the path formed by traversing first the reverse of β, then α, then β. The relation $\sim$ represents homotopy equivalence.) The associated fluxes are analogously related: a nontrivial relation if the fluxes don't commute.

of the fact that as strings move through space, the paths which are most convenient for describing their fluxes may be required to cross other strings. Strings may thus change their flux quantum numbers simply by changing their positions with respect to other strings. An example is shown in figure 2, where two strings rotate around each other and thus change their fluxes. Since non-Abelian strings with conjugate fluxes may be transformed into one another through holonomy interactions or by gauge transformations, all strings with fluxes in a given conjugacy class must be degenerate with each other in terms of their tensions. Different conjugacy classes of H, however, may be associated with different types of strings.

Another consequence of the non-Abelian interactions is that two strings with noncommuting flux cannot intercommute, nor can they pass through each other unaffected; to do so would violate flux conservation. As illustrated in figure 3, noncommuting strings can only pass through each other if a new string segment is formed, linking the two strings to each other and carrying a flux which is the commutator of the fluxes of the two original strings. We will be especially interested in the consequences of this entanglement process for the evolution of a string network: it might impede the collapse of the network.

2 Our Model: S_3 Strings

We consider here a model with unbroken gauge group $H = S_3$, the permutation group on three objects. The spectrum of this model will include strings whose fluxes are elements of S_3. S_3 has six elements in all. The identity corresponds to the trivial permutation. There are three odd permutations (two-cycles or transpositions) each leaving one of the three elements invariant and interchanging the other two. We may denote these, for convenience, by: $t_1 = \{(123) - > (132)\}, t_2 = \{(123) - > (321)\}, t_3 = \{(123) - > (213)\}$. In this notation, t_i is the two-cycle which leaves the i-th element in the same position. The two non-trivial even permutations are the three-cycles, or cyclic permutations, which we denote here by $s_+ = \{(123) - > (312)\}, s_- = \{(123) - > (231)\}$. In the more conventional cycle notation[9], we have $t_1 = (23), t_2 = (13), t_3 = (12), s_+ = (123), s_- = (132)$.

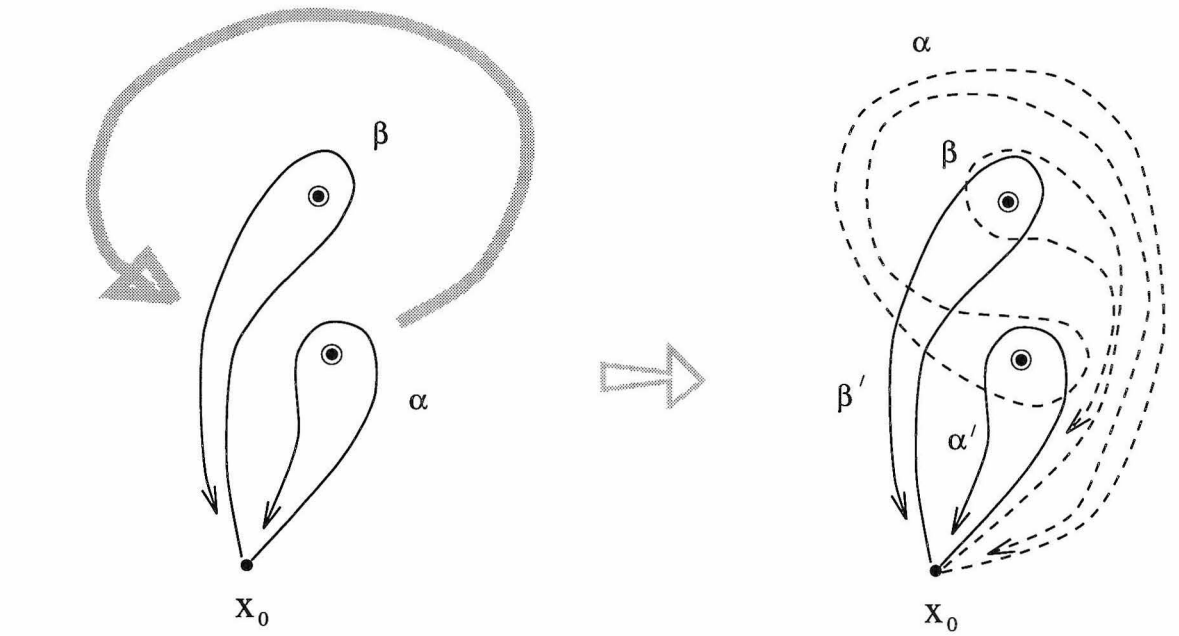

Figure 2: A holonomy interaction: we show here a planar cross-section of a process in which two strings wind around each other. If two strings (or rather their intersections with the plane) are initially in the positions shown in (A), and one of them winds completely around the other, then the path α shown in (A) can be deformed to the dotted path α in (B) without crossing any strings. However, the path shown as α' is the same path *in space* as the old path α, so it makes sense to redefine the flux of the string according to this new path, which is actually homotopically equivalent to $\beta\alpha\beta^{-1}$. Therefore the new flux of one string is conjugated by the flux of the other: if a, b, a', and b' are the fluxes associated with α, β, α' and β' respectively, then $a' = bab^{-1}$. In this figure, the flux of the other string is also affected: $\beta' \sim \alpha'\beta(\alpha')^{-1}$ and hence $b' = a'b(a')^{-1} = (ba)b(ba)^{-1}$. Note that the product of the fluxes is conserved: $b'a' = ba$. This is to be expected as $\beta\alpha$ can be deformed to a loop that completely encircles the pair and need not be affected by their relative motion.

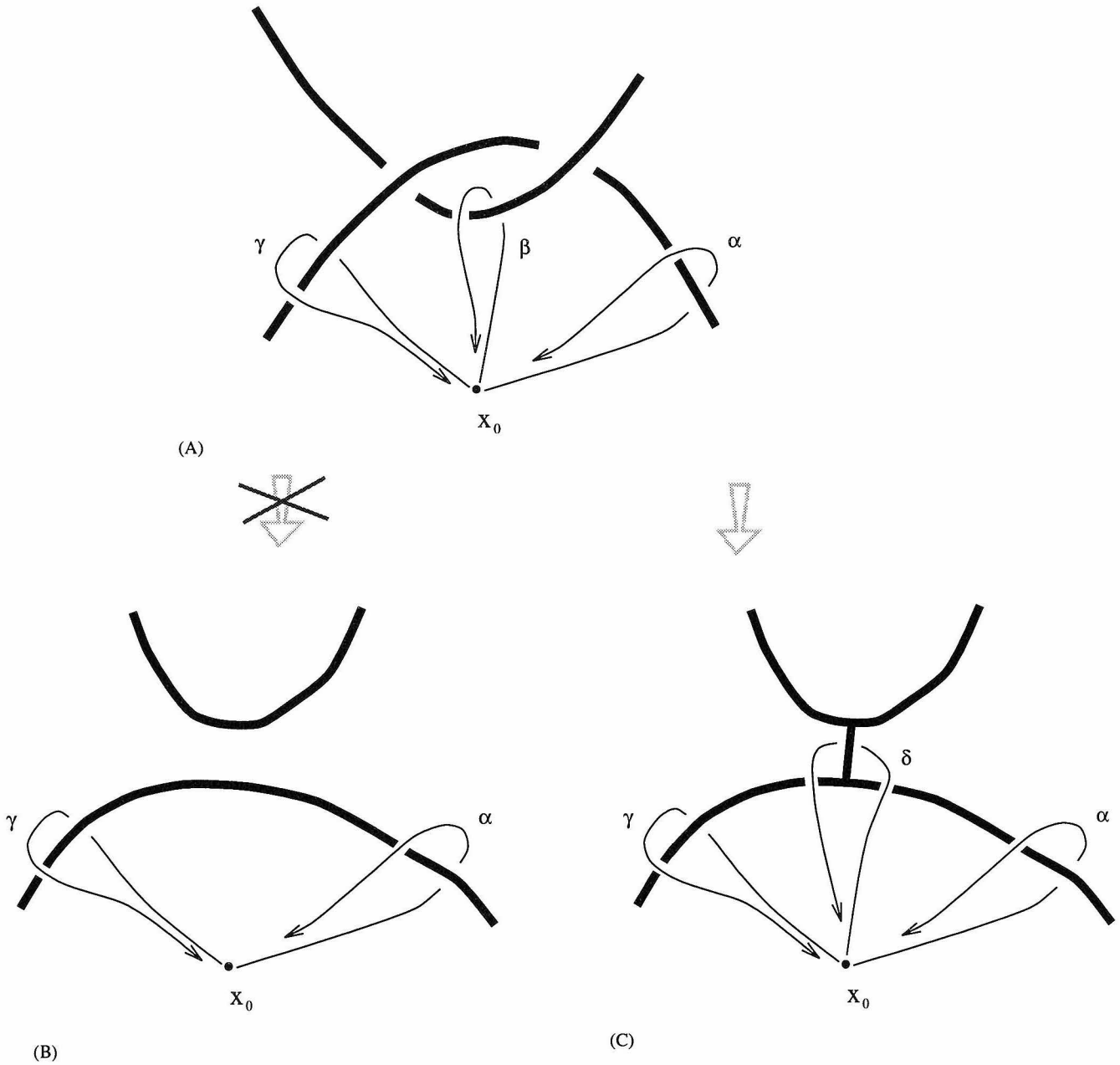

Figure 3: Attempt to pass two strings through each other. In (A) the flux of one string may be defined by either of the paths α or γ, and that of the other string by β. Let the fluxes associated with α, β and γ be a, b, and c respectively. In this case, $c = bab^{-1}$. In general, $c \neq a$. Now, if we attempt to pass the strings through each other, no strings need cross the paths α and γ, so the associated fluxes will not change. But if the strings were to pass through each other freely, as in (B), α and γ would be continuosly deformable into each other. This is impossible if they have different fluxes. In order to conserve flux, the string must branch somewhere and be connected to the other by a new string whose flux as defined by path δ in (C) is $ca^{-1} = bab^{-1}a^{-1}$.

The 2-cycles form one of the two non-trivial conjugacy classes, and the 3-cycles form another. Thus our model supports two types of strings, which we shall refer to as t-strings and s-strings, respectively. The three-cycles generate a Z_3 subgroup, so that any system containing only s-strings will behave identically to the Z_3 string system previously studied in [5]. There can be junctions where three s-strings join. Another type of junction is one where two 2-cycle (or t) strings merge to form a 3-cycle (s) string. Since each two-cycle is equal to its inverse, oppositely oriented t-strings are topologically equivalent. s-strings, on the other hand, possess a natural orientation: The flux through a path encircling it with one orientation is $s+$, while it is $s-$ for the opposite orientation. In subsequent figures, s-strings will often be denoted by oriented lines, with the string carrying flux $s+$ in the direction of the arrow, while t-strings have no arrow. Figure 4 shows the two types of junctions in our model.

The system we propose to simulate consists of s and t strings joined together at two types of vertices (sss and stt) which we shall take to be two types of monopoles. The tensions of all t-strings are the same, as are the tensions of all s-strings. The ratio of these two tensions will presumably depend on the details of the Higgs mechanism which produces the strings, and we will take it to be an adjustable parameter of the model.

In simulating the dynamical evolution, the strings will be approximated as straight segments between junctions. This amounts to averaging over any oscillations of the strings. We will also assume, following ref. 5, that the string junctions undergo damped motion under the influence of string tensions. This assumption may be a crude approximation to the dynamics of any real network. It becomes realistic if the monopoles are imagined as carrying some unconfined magnetic flux. For example, the actual symmetry-breaking pattern may be locally $G- > S_3 \times (SU(3) \times SU(2) \times U(1)_{EM})$, with some discrete factor divided out so that the monopoles at string junctions may carry electromagnetic $U(1)$ charge. Their magnetic charges should then result in radiation damping. Such a pattern has been demonstrated in a model where topological Z_n strings become attached to monopoles which also carry other charges.[10] It is possible in principle for S_3 strings to join at monopoles, although it may require a more complicated model. For example, consider the monopoles that form when

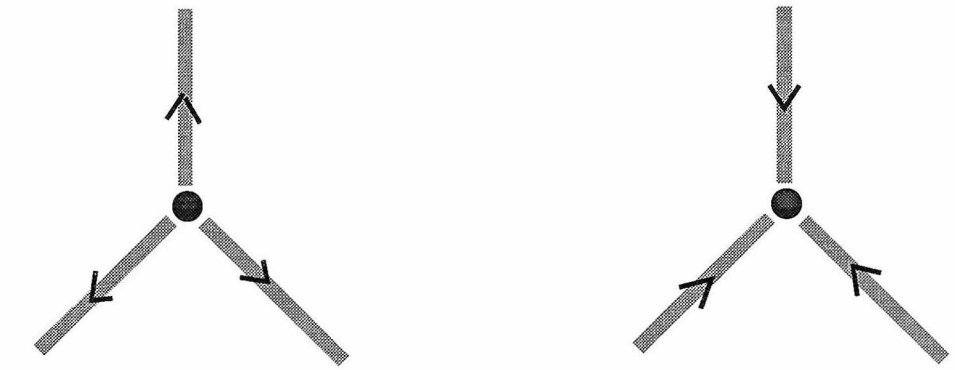

(A)

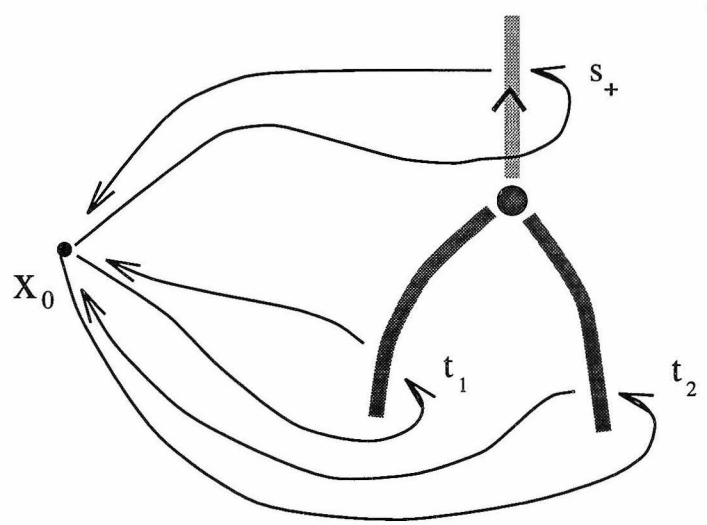

(B)

Figure 4: String junctions in the S_3 model. (A) Two possible *sss* junctions: three strings with the same flux, s_+ or s_-, emanate from the node. (Or two s_+ strings merge into a single s_-, etc.) (B) One of the class of *stt* junctions: Two t-strings merge into an s-string. Fluxes are defined with respect to x_0 by the paths shown. Here, as in many subsequent figures, an s-string is drawn as an oriented line. The string carries flux s_+ in the direction of the arrow: i.e., a counterclockwise path around the arrow encloses flux s_+.

an $SU(5)$ group is broken in the familiar way to $SU(3) \times SU(2) \times U(1)/Z_6$. This transition is known to yield stable monopoles with $SU(3), SU(2)$, and $U(1)$ flux.[11][12] We could imagine a second symmetry-breaking stage in which the $SU(3)/Z_3$ factor is broken down to S_3 in such a way that the resulting srings also carry nontrivial flux in the Z_2 center of $SU(2)$. Whenever three such strings join, the resulting net Z_2 flux can unwind through a monopole, which has both $SU(2)$ and $U(1)$ flux.

The masses and unconfined charges of the two types of monopoles may be model-dependent parameters relevant to the network's evolution.

3 Gauge Fixing Conventions

The present simulation requires that we choose some convention by which to define the fluxes of all strings in the network, and keep track of the evolution of those fluxes as the strings and nodes move.

In our algorithm, the strings and nodes exist inside a rectangular volume with opposite sides identified: a 3-torus. The subtleties associated with the periodic boundary conditions will be discussed later: for now we simply consider a network inside a rectangular volume with boundaries. We choose a cubic volume with one corner at $(0, 0, 0)$ and the far corner at (L, L, L). We choose a basepoint at the center of our simulation volume, $(L/2, L/2, L/2)$. Let each node be associated with a straight line segment (a "tail") along the direction $\vec{BN}$ from the basepoint to the node's location. Then let the flux of each outgoing string be defined with respect to a path which runs outward along this tail to a point which is taken to be vanishingly close to the the node. The path then encircles the string in a counterclockwise direction and returns to the basepoint along the node's tail. This is illustrated in figure 5. This will be our convention for defining the fluxes of the strings which join at a given junction.

As illustrated in figure 6, flux conservation requires that the product of all three fluxes emanating from a node be trivial when the fluxes are multiplied in a clockwise order with respect to the direction $\vec{BN}$. i.e., if the strings in clockwise order are a, b, and c, then

$$cba = e. \tag{2}$$

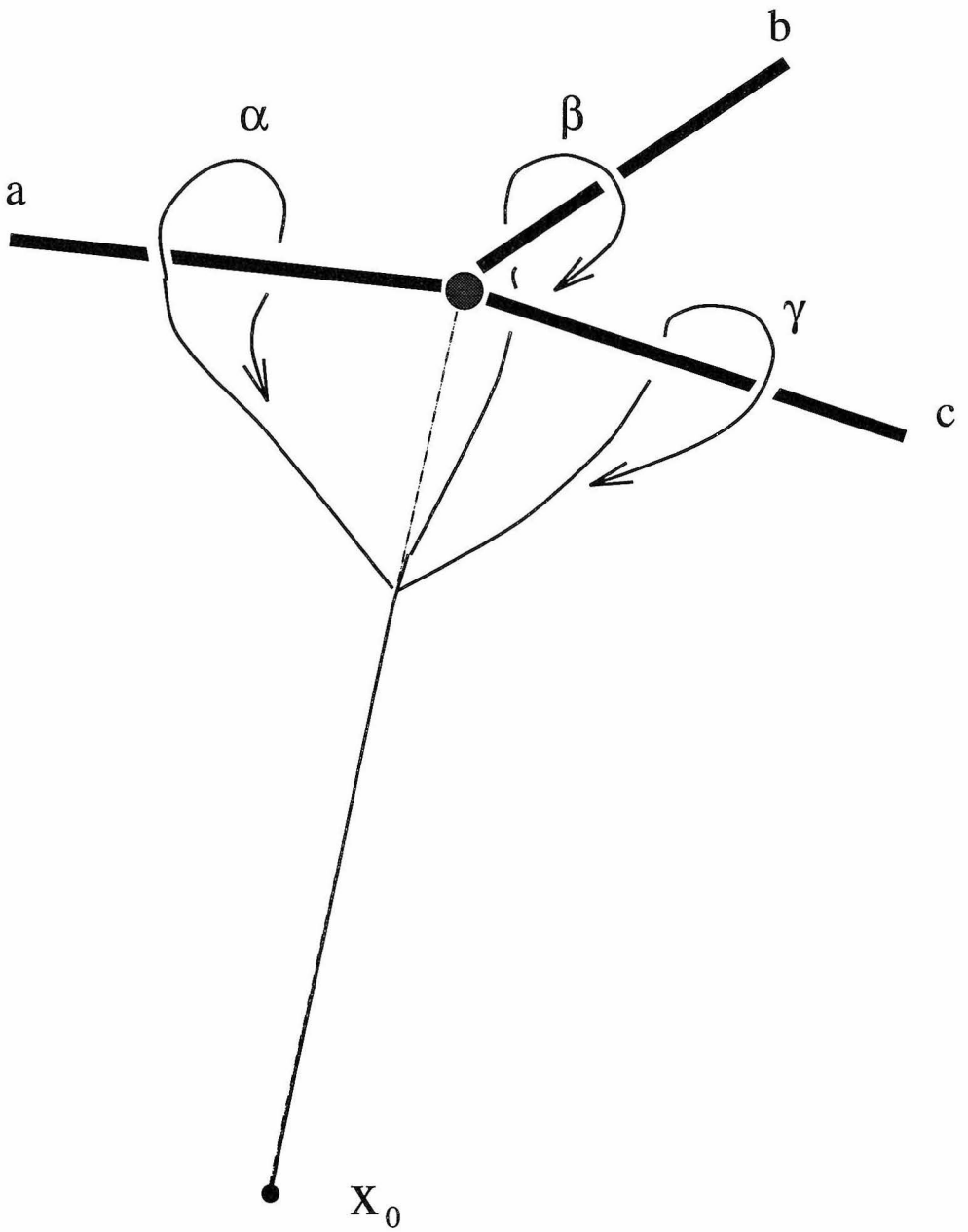

Figure 5: Conventions for measuring the fluxes of the three strings emanating from a node. Each string's flux is defined as the flux through a path which leaves the basepoint x_0 along a straight line toward the node, then encircles the string in a counterclockwise direction as seen from the far end of the string and returns to the basepoint.

In our algorithm, a record is maintained of the geometry of each node: the strings carry labels indicating the appropriate clockwise orientation.

It is possible for a pair of nodes to be connected by more than one string, as shown in figure 7. In this case, the two (or more) segments are treated as collinear, and the order is therefore ill-defined. In such a case we allow the order to be arbitrary, but the fluxes of the two strings must be defined in such a way consistent with that order, such that the product of all three fluxes is as usual trivial. The ordering must also be compatible between the two nodes which the segments join, so that the flux of a given segment is consistent at its two ends. (The consistency of segments from one end to another will be discussed below.)

The collection of standard paths defined above represents a set of generators for $\pi_1(\mathcal{M} - \{D\})$. The flux state of a network of strings is fully specified when we know the fluxes enclosed by all of these standard paths. The condition (2) supplies one set of relations among these generators. For each string segment, there is also a relation involving the fluxes defined at its two endpoints, as discussed below.

"Sliding" flux from the endpoint

By the conventions above, the flux of each string is defined at its two endpoints. But for the purposes of this simulation it will be necessary to make comparisons of the fluxes of strings at arbitrary points along their lengths. For example, if two strings cross each other, it will be necessary to determine whether or not their fluxes commute. A meaningful comparison of the fluxes of nearby string segments can be obtained only if the paths used to define those two fluxes remain close to each other everywhere except in the immediate vicinity of the strings to be compared. In particular, the "tails" of the paths must not pass on opposite sides of any string, because such paths would give different flux measurements for the same string. It is possible to define the flux of a string at an arbitrary point along its length by sliding the standard path to the one which encircles the string at the point we wish to measure, as illustrated in figure 8. If another string with flux b pierces the triangle which is swept out by the sliding path, then the flux at the new position is conjugated by b. If multiple strings occur, then the new flux a' is given by faf^{-1}, where f, the

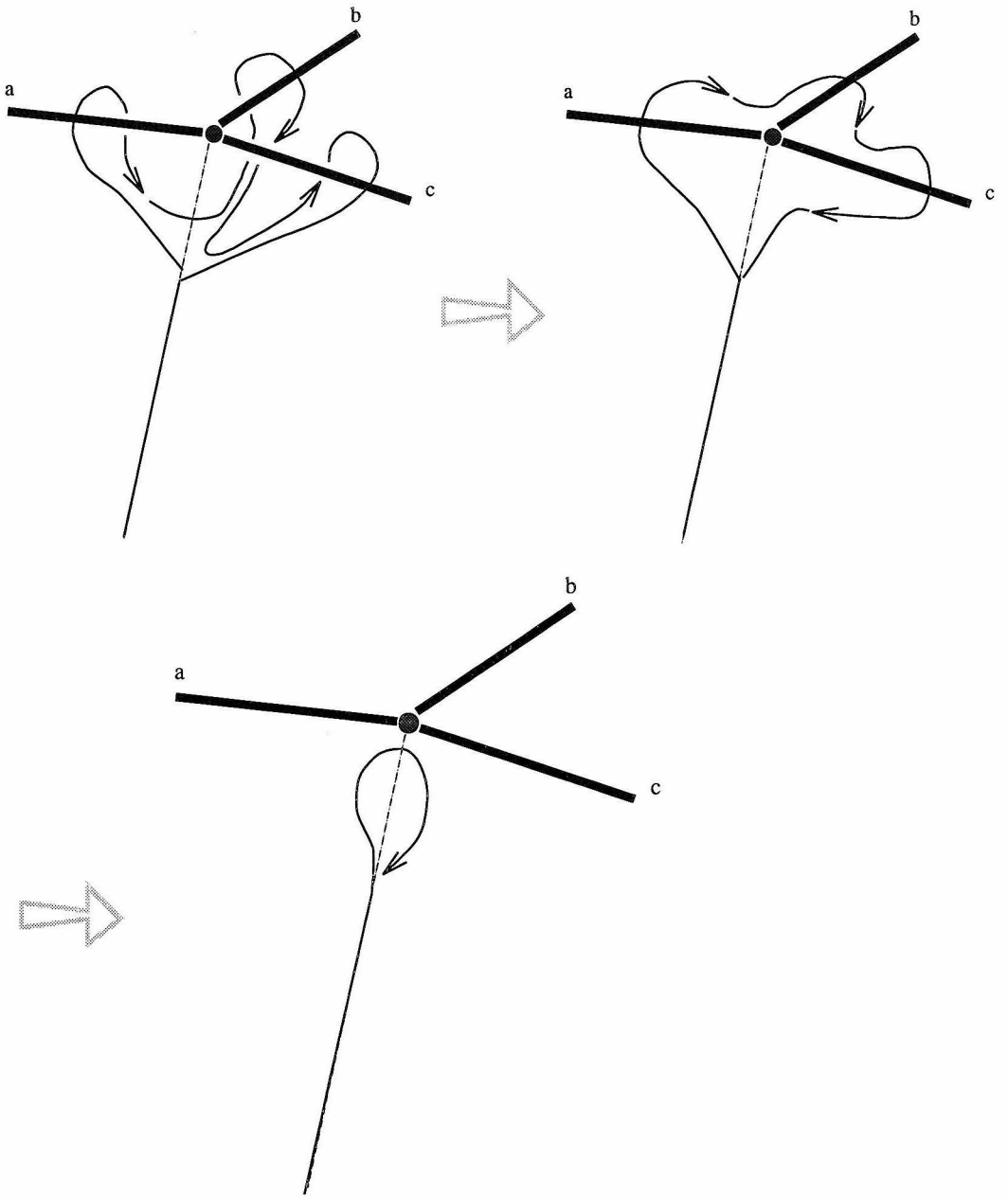

Figure 6: The composition $\gamma\beta\alpha$ of all three paths can be continuously deformed to a point. Therefore *cba*, the product of all three fluxes taken in a clockwise direction as seen from above the node, must be trivial.

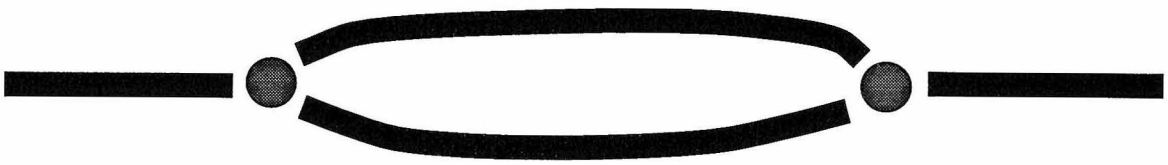

Figure 7: Doubly linked nodes.

total flux inside the triangle, is defined as the product of the fluxes of all enclosed strings, taken in order of increasing angle from the initial ray $\vec{BP}$. The flux of each other string at the point where it pierces the triangle must in turn be defined by a similar sliding procedure from one of its ends. This procedure, applied recursively, can thus define the flux of any string at an arbitrary point P along its length, as measured by a path which follows a straight line from x_0 towards P and encircles the string near P. If one slides the path all the way to the far end of the string, the resulting value of the flux must be consistent with the value measured by the standard path at the other end. This specifies an additional set of relations among the generators of $\pi_1(\mathcal{M} - \{D\})$ and furnishes one way of testing for errors in the simulation.

Holonomy Interactions

As the network evolves dynamically and nodes change their position, it is possible for the fluxes defined by these conventions to change by several different mechanisms. First, as a node moves, its tail may be dragged across another string segment. Conversely, a string segment may be dragged across the node's tail by the motion of other nodes. In both cases, the fluxes of all strings at the node must be conjugated by the flux which is crossed, as shown in figure 9. In addition, the geometry of the strings at a given junction may change, resulting in holonomy interactions among the three strings joined at that node. Such a process is shown in figure 10: the motion of string a causes its standard flux to change, and also changes the clockwise ordering of the strings a, b,and c.

4 Periodic Boundary Conditions

In order to maintain isotropy everywhere in the simulation volume, we use periodic boundary conditions. The cube face $x = 0$ is identified with $x = L$, and similarly for y and z. This identification has two consequences. The first is that there are three additional classes of noncontractible closed loops starting and ending at the basepoint: namely those which wrap around one of the boundaries before returning. It is possible for these loops to be associated with nontrivial flux, and a complete

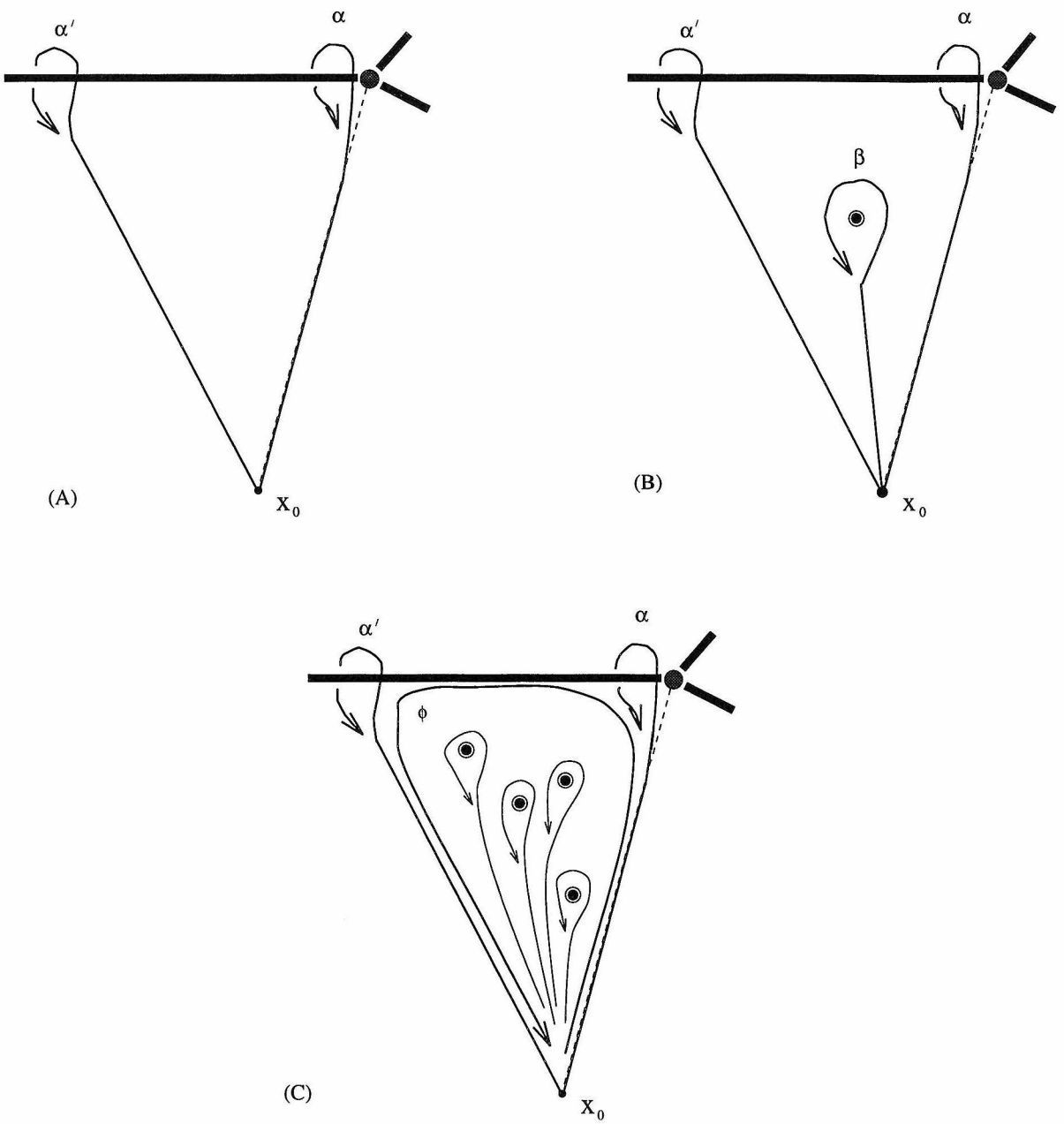

Figure 8: When the flux a of a string has been defined according to a path which encircles it near one end, the flux a' of that string at another point along its length can be defined by "sliding" the standard path α to α' as shown. If no other strings pierce the triangle which is swept out, then this merely represents a continuous deformation of α, and thus $a' = a$ (fig. 8A). However, if the triangle is pierced by string with flux b as measured by path β, then the flux is conjugated by b: $a' = bab^{-1}$ (8B). More generally, if the triangle (or the oriented path ϕ shown in 8C) encloses flux f, then a is conjugated by the total flux f, i.e., $a' = faf^{-1}$. The total flux is given by the product of individual string fluxes, taken in order of increasing angle from the initial tail. (This can be seen by deforming a product of loops to a single loop enclosing all strings.)

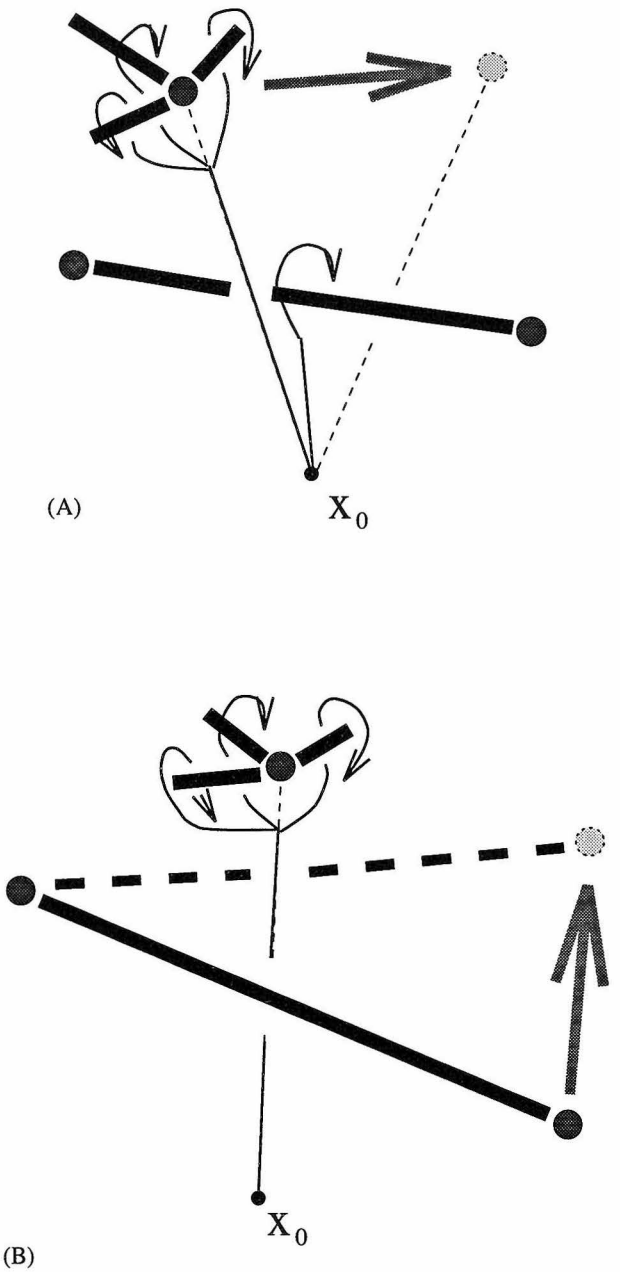

Figure 9: Crossing of a node's tail by a string. This can happen either when the moving node drags its tail across the string (A), or when the string is dragged across the tail due to the motion of another node (B). In both cases, the fluxes of all strings attached to the node whose tail is crossed must be conjugated by the flux of the crossing string.

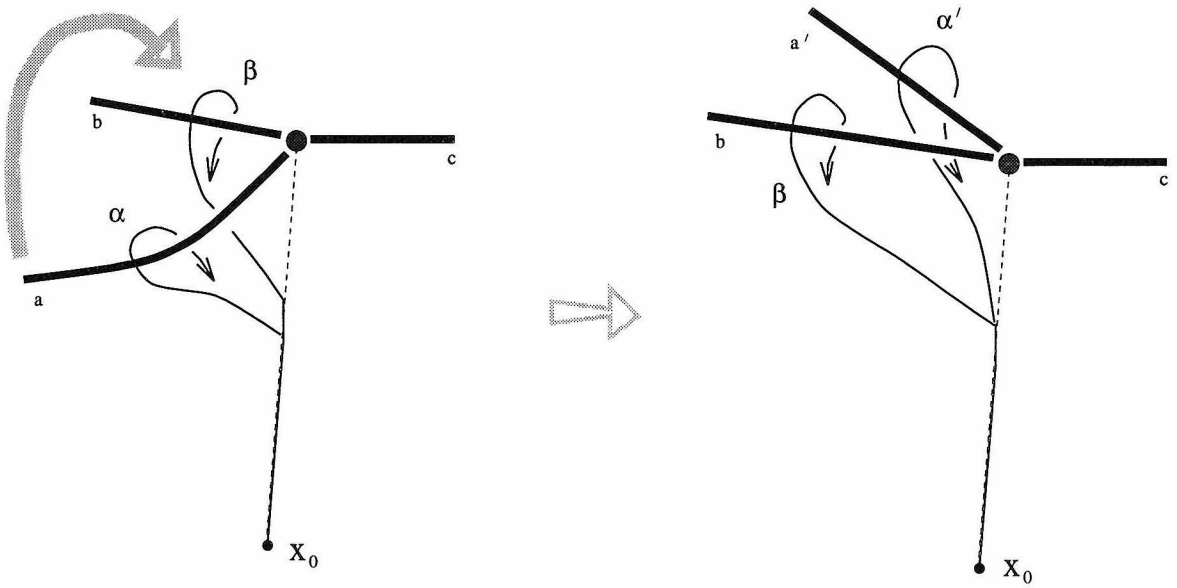

Figure 10: Example of a holonomy interaction between strings attached to the same node. When the string carrying flux a is lifted over the other string carrying flux b, its flux must be redefined as bab^{-1}, and the conventional clockwise order of the three strings changes, with a and b exchanging places. The flux conservation condition is maintained: if $cba = e$ originally, then also $ca'b = e$.

specification of the state of our network requires that we choose representatives of these classes and maintain a record of the associated fluxes. The second consequence is that nodes may move freely across the cube boundaries, and string segments may wrap around from one side of the cube to another.

As representatives of the three "wraparound" classes, we choose straight-line paths which we will refer to as Γ_x, Γ_y, and Γ_z. Γ_x, for instance, leaves the basepoint along the $+\hat{x}$ direction, wraps around the boundary from $x = L$ to $x = 0$, and then returns to the basepoint from the $-\hat{x}$ side.

A record of the fluxes C_x, C_y, and C_z associated with these three paths, combined with the record of all string fluxes as defined earlier, specifies the state of the string network on T_3. In order to complete the description, however, there is one ambigutity to be resolved. The fluxes of strings, as described above are measured along paths which follow a "tail" from the basepoint to the point where the flux is to be measured, then encircle the flux and return to the basepoint. On T_3, however, a segment from x_0 to an arbitrary point x is not unique, as shown in figure 11. The two points may be connected by a line segment which does not wrap around, or by one which does. (In fact, there is an infinite set of possibilities.) We may choose to define all tails in such a way that none of them cross the boundary, but it is still necessary to make flux comparisons across the boundary, and it is necessary to redefine fluxes when a node moves across the boundary. In short, is necessary to relate the alternative definition of a string's flux which are related to one another by wrapping. A prescription for doing so is shown in figure 12: The transformation from one description to the other requires us to know the flux associated with one of the Γ_i.

Much as holonomy interactions may change the measured fluxes of strings, similar effects compel a redefinition of Γ_i when a string segment is dragged across the standard path. As illustrated in figure 13, the new flux value C_i' will be a product of the old value C_i with the flux of the string which crosses it. (The order in which the two are multiplied depends on the handedness of the crossing and on which side of the basepoint it occurs.)

The existence of the three closed paths which wrap around the boundary, and of

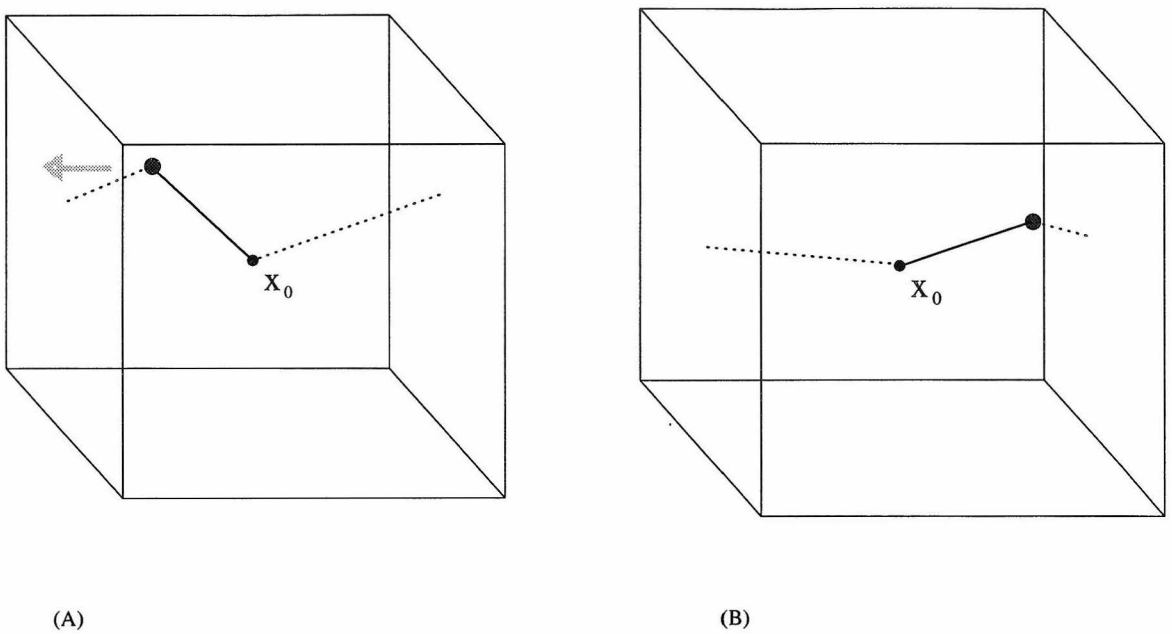

Figure 11: Under periodic boundary conditions, there is more than one straight line segment from the basepoint to a given node. In (A), we show one segment which extends to the left of x_0 and ends at a node (solid line), and another which extends to the right, wraps around the cube boundary, and ends at the same node (dotted line). By convention, we will choose to describe nodes using the shortest possible segment as a "tail" (shown here as the solid line). If the node moves to the left as shown by the arrow, and wraps around the cube boundary to reach the final state shown in (B), then the shortest segment will no longer be the one extending to the left from x_0, but instead it will be the one extending to the right. The new shortest segment is shown as the solid line in (B). Because of this change in the choice of "tail," it is necessary to know how to transform a flux from one description to the other.

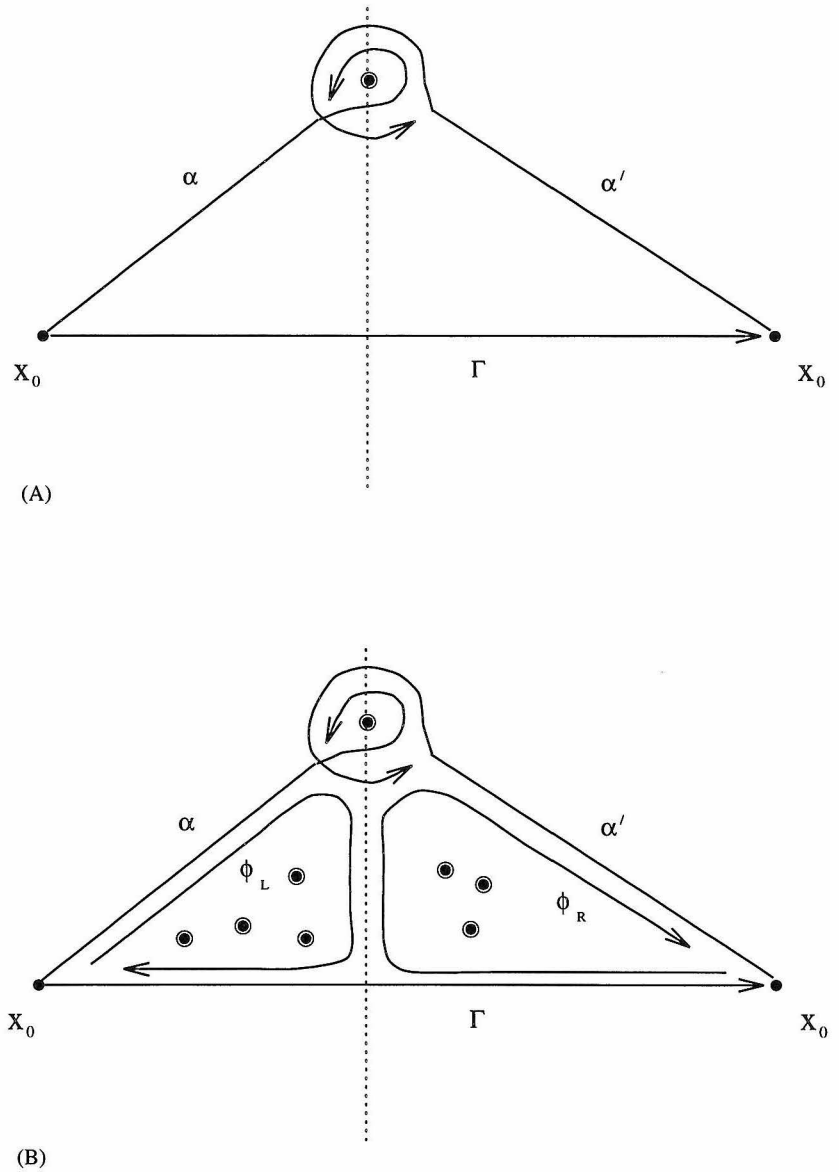

Figure 12: Transformation from one description of a flux to another at the boundary. Here a string is shown intersecting the plane of the page precisely where it intersects the boundary of the cubic simulation volume (dotted line). Under periodic boundary conditions, the two points labeled x_0 are identified. The flux of the string may be described in terms of a path whose tail extends to the right of x_0 (α) or to the left (α'). If no other strings are present, then α is homotopically equivalent to $\Gamma^{-1}\alpha'\Gamma$. In the more general situation shown in (B), $\alpha \sim (\phi_L\Gamma\phi_R)^{-1}\alpha'(\phi_L\Gamma\phi_R)$, and so the two descriptions of the flux are related through conjugation by $f_L C f_R$, where C is the flux associated with the path Γ and f_L and f_R are the overall fluxes enclosed by ϕ_L and ϕ_R, respectively. The latter can be defined in terms of paths lying entirely on one side or the other of the boundary.

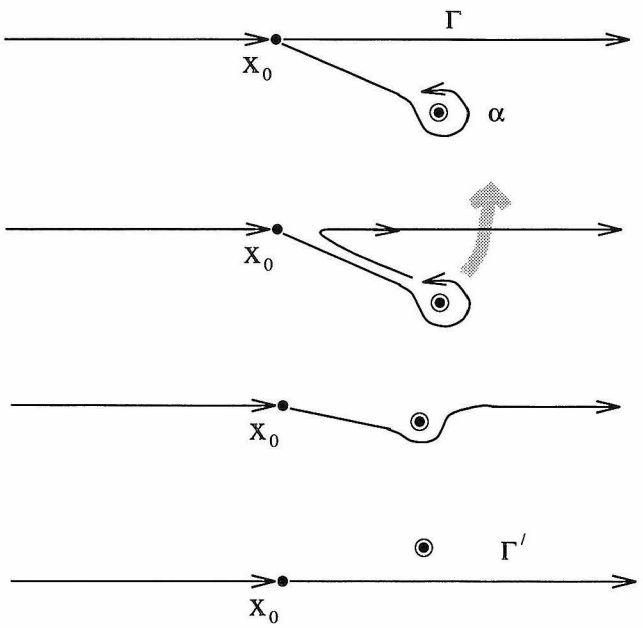

(A)

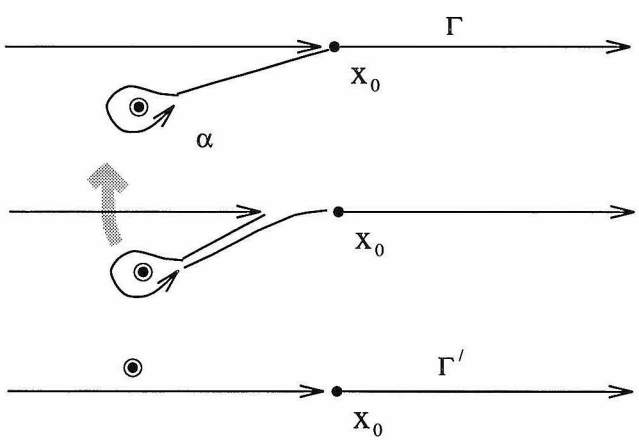

(B)

Figure 13: Interaction between a string and one of the large loops of the 3-torus. As a string with flux a as defined by the path α crosses to the right of x_0 as shown in (A), the path $\alpha\Gamma$, where Γ is a straight-line path which wraps around the 3-torus, can be continuously deformed to the new straight-line path Γ'. Thus the flux C associated with Γ must be multiplied from the right by the string's flux, $C' = Ca$. If the string crosses to the left as in (B), $\alpha\Gamma$ is deformed to Γ' and so the multiplication is from the other side: $C' = aC$.

holonomy interactions between the fluxes of these paths and those of strings, make this system a higher-dimensional analogue of the system of vortices on a Riemann surface which was previously studied by Lee.[13]

5 Initial Conditions

In order to perform our dynamical simulation, we must start with a randomly generated initial configuration. The generation of initial conditions should to some extent be a model of the symmetry-breaking transition which produces the strings. Following the lead of Vachaspati and Vilenkin's Z_3 simulation, we use a lattice to generate an initial string network. The lattice spacing is to be identified in our minds with the correlation length of the Higgs field which acquires a vacuum expectation value in order to break a continuous gauge group to a discrete subgroup H. The Higgs VEV is thus uncorrelated over distances longer than a lattice spacing, and at each site of the lattice, it takes a random value within the vacuum manifold. With a suitable interpolation along the length of each link, any plaquette of the lattice is mapped to some closed loop on the vacuum manifold. If this path is one of the non-contractable loops, then a string must pierce this plaquette. Each link of the plaquette is associated with an element of G which relates the Higgs values at the two ends of the link. The product of these elements must lie within the unbroken group H, and can be taken as the flux of the string which pierces that plaquette. Strings which pierce the faces of a given unit cube must be joined together inside the cube in some appropriate way. If only two faces of the cube are non-trivial, then we interpret this as a single string segment passing through the cube. If three faces are non-trivial, and our model is one in which three-string vertices occur, then we conclude that there is a single vertex inside the cube. Cubes pierced by more than three ends require a more complicated arrangement of nodes and strings inside the cube, and there may be more than one self-consistent way to join the string ends. In the following subsections, we will first describe methods for simulating on a lattice the string-forming phase transition, and then how to translate the results into a string network which can serve as the initial condition for our dynamical evolution algorithm.

Discrete Higgs Simulation

Generating random points on an arbitrary continuous vacuum manifold and then interpolating suitably between them can be a difficult proposition. A useful technique is to approximate the broken group G by a discrete group $\mathcal{G} \subset G$ which contains the unbroken group H as a subgroup.[14,15] Instead of a continuum of values, the Higgs field takes values in a discrete coset space $\mathcal{G}/H$. Then with each link of the lattice there is associated an element of $\mathcal{G}$ which transforms the Higgs field value at one end of the link to the value at the other. The element relating one coset to another is not unique; the possible elements themselves form a coset. The convention in this discrete Higgs method is to choose the "smallest" possible element for each link variable. "Small" is defined with reference to a metric on the continuous group G: if all elements are written in the form $g = \exp(i\alpha T)$ where T is a normalized element of the Lie algebra of G, then the smallest element is the one with the smallest number α. With this prescription the Higgs field is effectively interpolated in the smoothest possible way between lattice points. A suitable gauge transformation can be performed so that all Higgs field values lie in the same coset, and all link variables lie within H, allowing all subsequent computations to be performed in terms of only H link variables. This was the technique used in previous studies of Z_3 networks,[15] and we will use it here, taking $\mathcal{G}$ to be one of the discrete subgroups of $SU(3)$. For example, we may use a 24-element "dihedral-like" subgroup of $SU(3)$ known as $\Delta(24)$.[16] This group is isomorphic to S_4, the permutation group on four elements, and is the smallest discrete subgroup of $SU(3)$ which contains S_3 as a proper subgroup.

An easier way to generate a random network of strings is to use an infinite temperature lattice gauge theory: simply assign a random element of the unbroken group H to each link of the lattice, and evaluate the product of links on the plaquette to find the flux through the plaquette. One thus dispenses with the simulated Higgs field. Either the discrete-Higgs or the lattice-gauge-theory method results in the assignment of S_3 elements to each link of the lattice, and one must only evaluate a plaquette to determine whether it is pierced by a string. These two methods give rise to string distributions which may differ in detail but are qualitatively similar. Experience with the Z_3 model (including my own simulations) shows that the subsequent

evolution of the network is not sensitive to the details of the initial conditions: Z_3 networks generated by the discrete-Higgs and lattice gauge methods begin to behave very similarly after just a few steps of dynamical evolution. We can test whether this is also the case in our S_3 model by comparing the evolution of networks generated by different methods.

Initial location of nodes

The lattice Monte Carlo algorithm, whether it is of the discrete-Higgs or lattice gauge type, generates a set of variables defined on a lattice. From a lattice configuration, one can easily determine which plaquettes are pierced by strings, and it is also easy to determine the conjugacy class of the flux through a particular plaquette. This, however, does not determine the precise location of each string inside the unit cube, or to which other strings a given string is connected. Knowing lattice variables, we know through which cube faces strings emerge, but what happens to these strings inside the cube is completely unspecified. Therefore, the next stage of our Monte Carlo algorithm must specify the actual locations of nodes within each lattice cube, and determine which nodes are connected to each other by straight string segments. Having done this, we will finally be able to define all fluxes according to standard paths with respect to a single basepoint.

In generating a configuration of nodes and strings within a particular unit cube, we use the following criteria: 1) The configuration within a cube should not be more complicated than necessary. 2) Every string which pierces a cube face must end at a node inside that cube. The reasons for this stipulation should become apparent later; one is that it ensures that the flux of the string will be well-defined at some point inside the cube (since our conventions define string fluxes near their ends). 3) Nodes inside a cube are placed approximately (not necessarily exactly) at the center of the cube. This is purely for the sake of simplicity. 4) Nodes inside the same cube should be separated from one another by some non-zero distance. In order to define the conventional clockwise order of strings at each node, it is necessary that all strings have nonzero length. It is for this reason that not all nodes are placed *exactly* at the center of the cube.

Anywhere from two to six string ends, or none at all, may emerge from a given unit cube. A cube with three ends emerging is simple: we simply place a single vertex at the center of the cube. If exactly two plaquettes of a cube are nontrivial, we could interpret this as a single string entering the cube through one face and exiting through the other. In compliance with criterion (2) above, our algorithm interrupts such a segment with a doubly linked pair of nodes. This ensures, as previously mentioned, that the flux of the string will be well-defined at a point inside the cube (a necessity when we perform the gauge fixing in order to define all fluxes with respect to the same basepoint.) It also allows for the possibility that the string bends inside the cube. A cube with string ends emerging from two adjacent faces implies that the string bends as it passes through the cube. Since our simulation only allows for straight string segments between nodes, a bent string can only be implemented by introducing a doubly linked pair of nodes. In the later dynamical evolution of the network, these nodes may annihilate, allowing the string to straighten. In the process of straightening, the string may be obstructed by other non-commuting strings, and so it is important that the straightening not be allowed to happen until all string fluxes are suitably well-defined to allow the necessary comparison. In order to separate the two nodes by a finite distance (see point (4) above), each one is displaced slightly away from the center and toward the cube face through which its string emerges. Examples are shown in figure 14.

Cubes with four or more emerging strings are more complicated. In general, there may be more than one consistent way of connecting the ends inside the cube. In our algorithm, we attempt to choose more or less at random from among the set of possibilities. A helpful observation is the following: If two plaquettes are nontrivial, but the product of links along a path which circumnavigates both is trivial, then it is possible to connect the two associated string ends through a string segment which has no linking with any of the other strings in the cube. (See figure 15.) Let us call this a "free segment." Our procedures for dealing with cubes of four, five ,or six emerging strings consist, roughly speaking, of searching in random order for a pair of faces allowing such a free segment. If one is found, then it is formed in the same manner as for a cube with two ends, i.e., by inserting a doubly linked pair of nodes. In the case

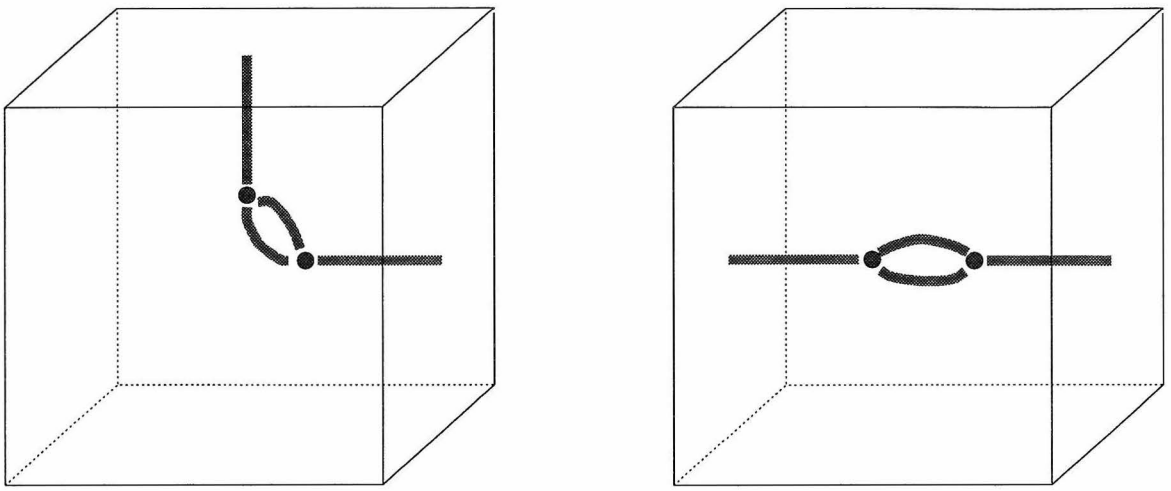

Figure 14: When strings pass through exactly two ends of a lattice cube, this represents a segment, either straight or bent, passing through the cube. Our Monte Carlo algorithm represents this as a doubly linked pair of nodes.

of four or five ends, the connection of the remaining ends is determined as soon as one free segment has been established. In the 4-end case , the two remaining ends join in an another free segment; in case of five, the three remaining ends meet at a node. In the case of a cube with six outgoing strings, if a free segment is produced from two of the ends, then a similar search for a consistent configuration can be performed on the remaining four ends. For a cube with five outgoing ends, another possibility, aside from one free segment and one node, is a 3-node configuration of the type shown in figure 16, in which one of the nodes is attached to just one outgoing string, and the others are each attached to two outgoing strings.

The procedure of our Monte Carlo algorithm for establishing the nodes inside a cube with five ends is to search through a list of possible patterns involving either one free segment or none, starting at a random place in the list and checking them for consistency by evaluating appropriate products of links around pairs of cube faces. When a pattern is found which is consistent, the nodes are established in that pattern.

For a 6-string cube with some t-strings, the procedure is as follows: Pick, at random, two adjacent faces of the cube, and determine whether or not those two faces can be connected by a free segment. If so, connect them; otherwise, they are assumed to join at a node which has an additional connection to another node inside the same cube. Then pick randomly a pair of adjacent faces from among the remaining four and apply a similar procedure. The possible results of this procedure are that zero, one, or three pairs of adjacent faces are joined by free segments. If only one pair is connected by a free segment, then the other four strings are connected in pairs to nodes which are then connected to each other (figure 17B). If no free segments are found, then there are three nodes, each attached to two of the outgoing segments, and we connect these by additional string segments to a fourth node located at the center of the cube (figure 17C).

In order to ensure a nonvanishing distance between nodes, we displace each node by a small distance (such as .05 of the lattice spacing) from the cube center in the direction of each external string attached to it. For example, if a node is connected to strings which exit the cube in the $\hat{x}$ and $\hat{z}$ directions, the node is displaced in the $\hat{x}+\hat{y}$

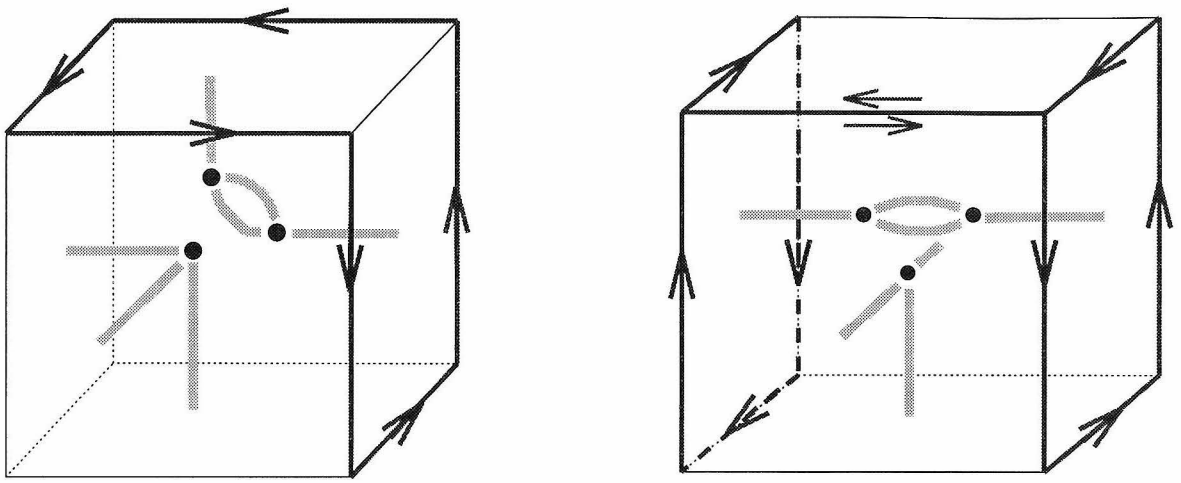

(A) (B)

Figure 15: (A) If a string segment (or a string segment interrupted by a doubly linked pair of nodes) passes into a cube through one face and out through an adjacent one, with no linkage to any other strings in the cube as shown here, then the highlighted path along the edges of both faces can be continuously shrunk to a point without crossing any strings; hence the corresponding product of links must be trivial. Conversely, if the product is not trivial, then the connection of those two string ends by a free segment is not consistent. An analogous criterion applies in (B).

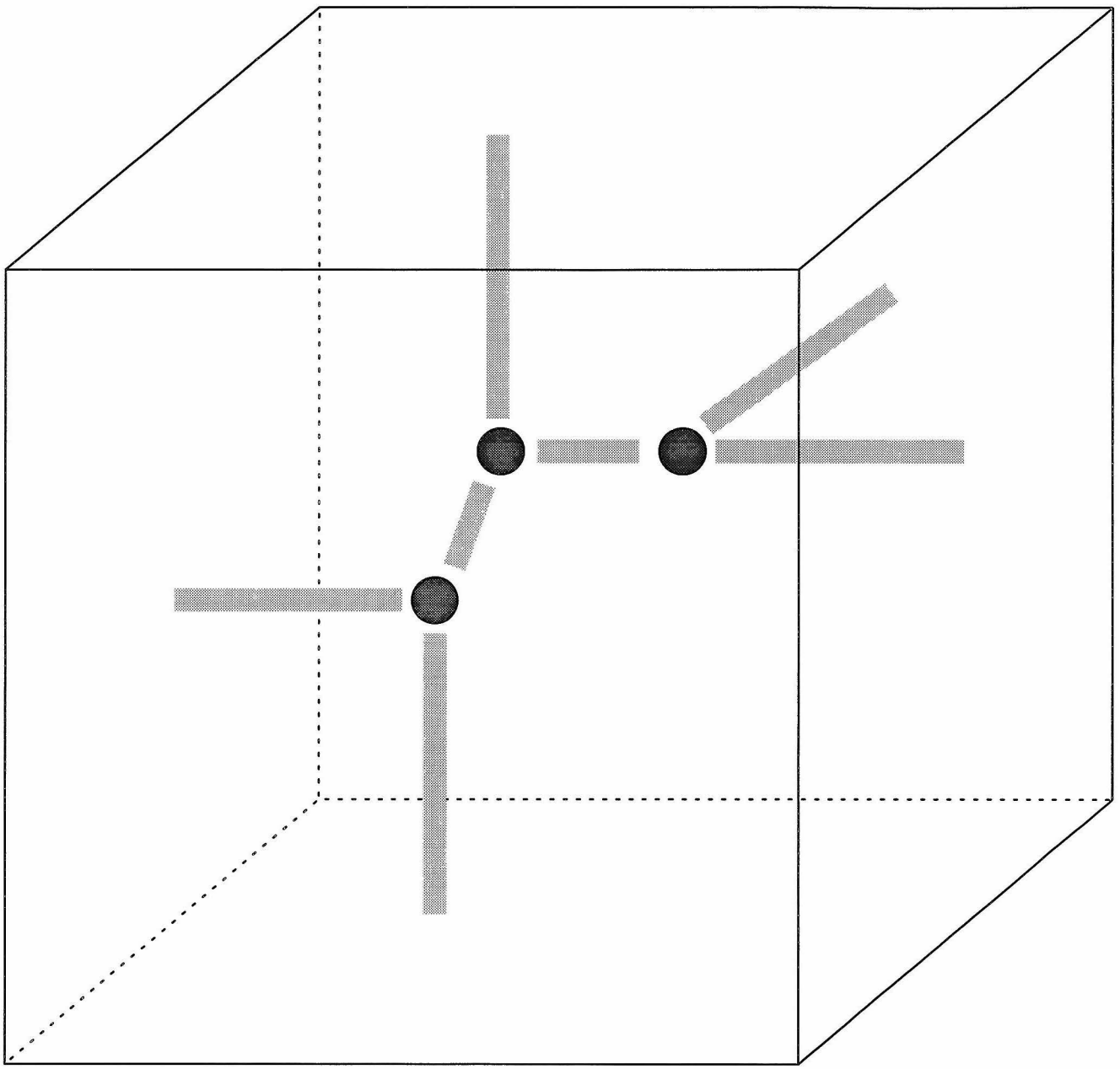

Figure 16: Example of a cube with five outgoing strings but no free segments.

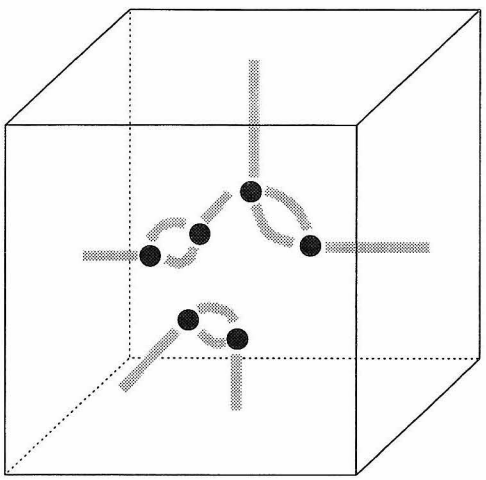

(A)

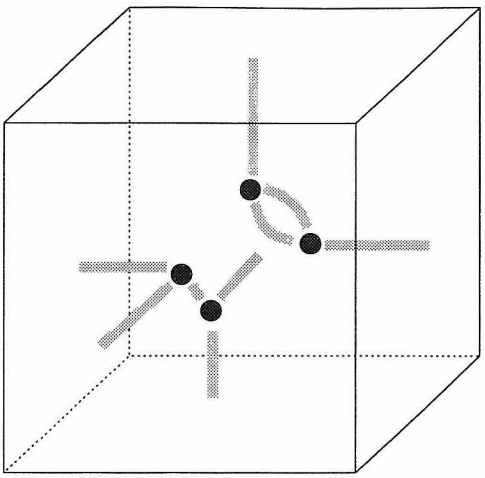

(B)

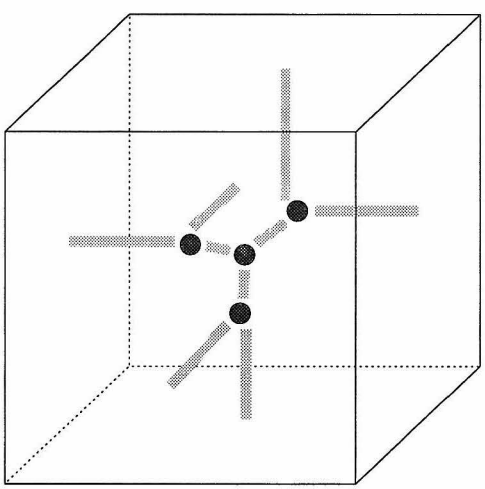

(C)

Figure 17: Configurations for a cube with all six faces pierced by strings: (A) Three free segments. (B) One free segment. (C) No free segments.

direction. Finally, a small random perturbation is added to the position of the node. This last step is purely a precaution against problems which could arise in defining the fluxes if many nodes were precisely aligned along some ray from the basepoint.

It is hoped that the above procedure generates an adequately representative initial configuration of strings and nodes. Experience with the Z_3 model indicates that the precise details of the initial conditions are not crucial.

Gauge-fixing of the initial network

When the location of all nodes has been established, along with their connections to each other, the gauge fixing which establishes definitions of all of the fluxes must still be performed. The problem is that initially, fluxes are defined only on paths consisting of lattice links. The establishment of canonical flux definitions according to the prescription of the previous section requires that lattice paths be deformed into paths involving only straight-line tails from the basepoint and short loops encircling the strings near their ends. We proceed in two steps. First, we perform a gauge fixing within each individual unit cube, choosing one corner of the cube as a local basepoint and defining a tail from this basepoint to each of the nodes within that cube. Then these standard paths are attached to an external tail to form a path beginning and ending at the global basepoint. Initially, this external tail consists of lattice links, but it can in turn be deformed to a straight line path.

The first step, local gauge-fixing on a lattice cube, is illustrated in figure 18. Each string end emerging from a cube is treated individually. We first compute, by multiplying link variables, the flux through a lattice path which encircles the string in question. If the string passes through one of the three cube faces which include the corner we have chosen as local basepoint, then this path is simply a plaquette; otherwise the path runs along an edge to the face which is pierced by string f, then around that face and back along the same edge, as shown in figure 18A. By construction, only one string may emerge through any given face. Therefore, the lattice path can be shrunk to the one shown in figure 18B without crossing any other strings, and thus this path must have the same flux. The flux is now defined along a path consisting of a tail and a small loop enclosing only the string, near the point

where it pierces the cube face. We then wish to straighten the tail as in figure 18C, and finally slide the path so that it encircles the string near its end (figure 18D) as do the standard paths of figure 5. In some cases these last two steps can occur without any other string segments being crossed, and so the flux as defined in figure 18D is the same as that of the original lattice path in 18A. In other cases, however, the tail may cross another string as it is being deformed (figure 19). Then the flux of the first string must be conjugated by the flux of the other. Hence, the flux of the first string cannot be defined until that of the other string has already been defined. When computing the fluxes of the strings emerging from a given cube, we first deal with those ends which do not depend on other strings, and then compute others. As long as every string passing through a cube ends at a node inside the cube, it will not be necessary at this stage to refer to any nodes outside of the cube.

In order to complete the definition of flux, we attach the path from the cube corner to the node to a tail which runs from the global base point to the cube corner. This tail is initially defined as lattice path of the type shown in figure 20, consisting of three straight segments along each of which only one coordinate changes. If the product of links along this tail is t, and the "local" flux of a path within the cube starting and ending at the corner is a, then the new flux of the string is $t^{-1}at$. The tail is then deformed to a single straight line by several steps, as shown. At each stage of the straightening, other strings may be crossed within other cubes. The flux measurement is conjugated by the appropriate fluxes. Finally, we arrive at a flux defined along a path which proceeds along a straight line to the corner of the unit cube in question and then from there to a node, where it encircles string a. As a final step, we straighten this path to a single line segment (figure 21), obtaining a definition of the string's flux according to the conventions of section 2. Since this definition depends on the values of string fluxes in other cubes, the unit cubes of our lattice must be handled carefully in order. The flux definition procedure must be applied first to those cubes closest to the basepoint, and then, layer by layer, to the cubes farther away.

After the fluxes of all strings emerging from the cube have been defined, those which link one node to another *inside* the same cube may be fixed by means of the flux

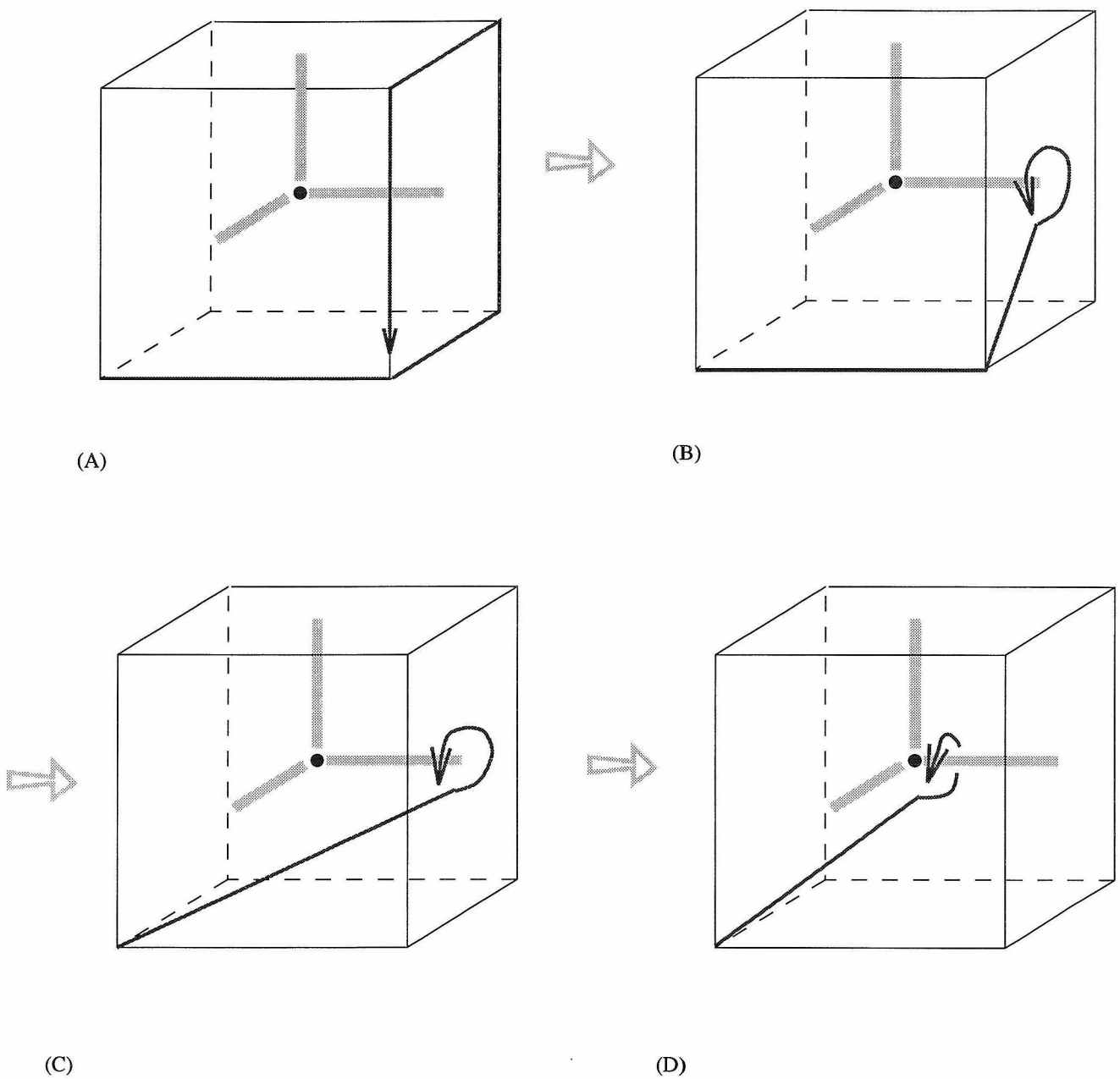

Figure 18: "Local" gauge-fixing on a unit cube of the lattice. The flux of a string piercing the cube face is defined first along a path consisting of lattice links. The path is then deformed to a path which runs along a straight tail to the node inside the cube, and encircles the string near its end. If this deformation can be done without crossing any other strings, then the flux defined by the final path shown in 18D is the same as that defined by the lattice path in 18A.

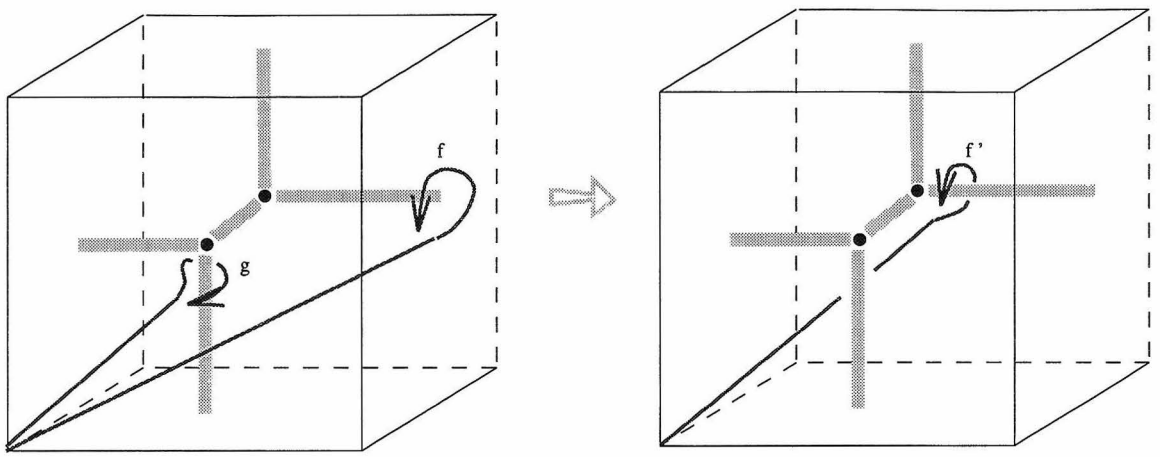

(A) (B)

Figure 19: Example of an obstruction to the last stage of the deformation shown in figure 18: A string has flux f as defined by the path in 19A (which corresponds to 18C), but in the final stage of deformation, the tail crosses another string whose flux is g. The flux f must be conjugated: in this case $f' = g^{-1}fg$.

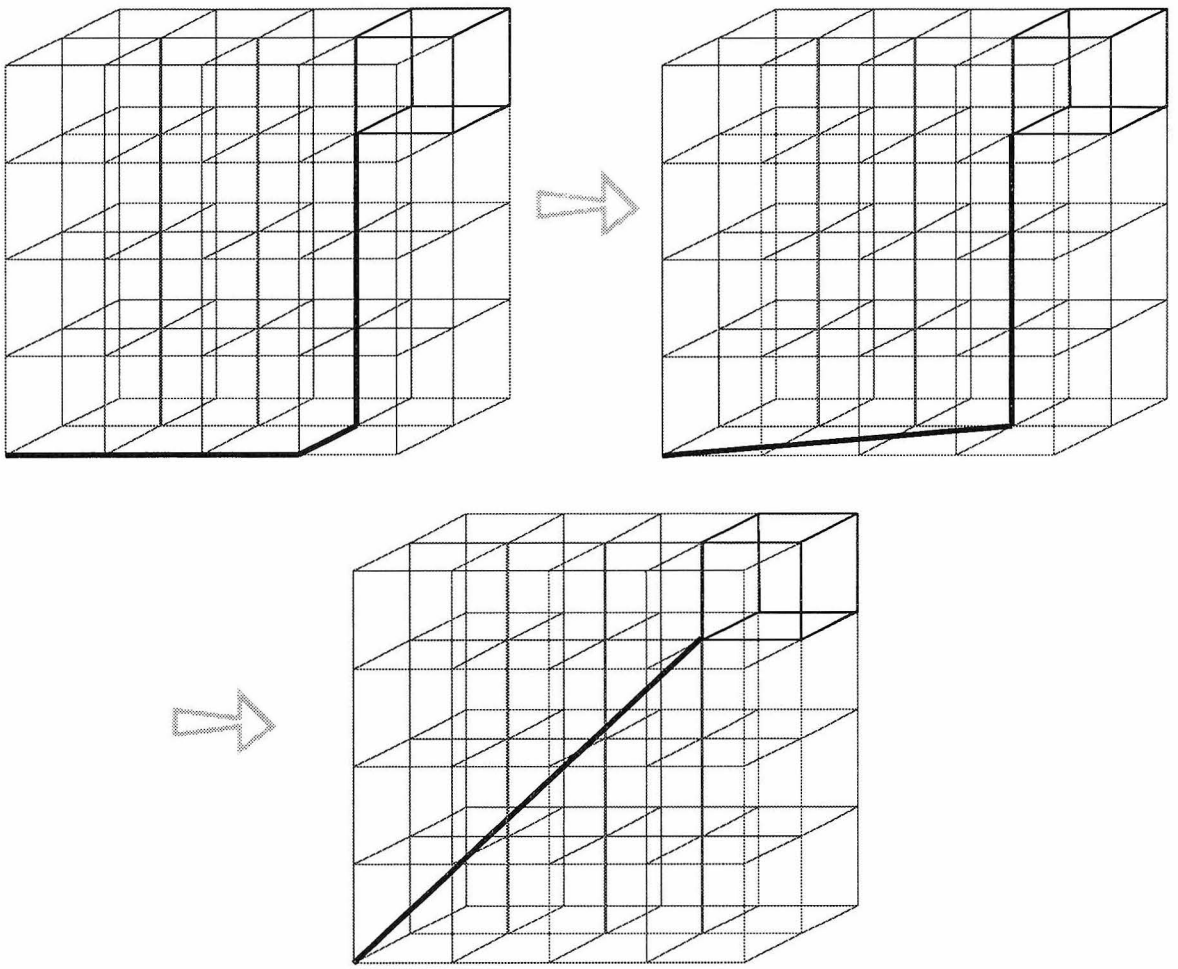

Figure 20: Defining a tail from the basepoint to the corner of a lattice cube. Initially, the tail is defined as a product of lattice links. This tail is then deformed to a single straight segment. If other strings are crossed during this deformation, then the flux is adjusted appropriately. This procedure requires that the fluxes of strings in intervening cubes have been defined already.

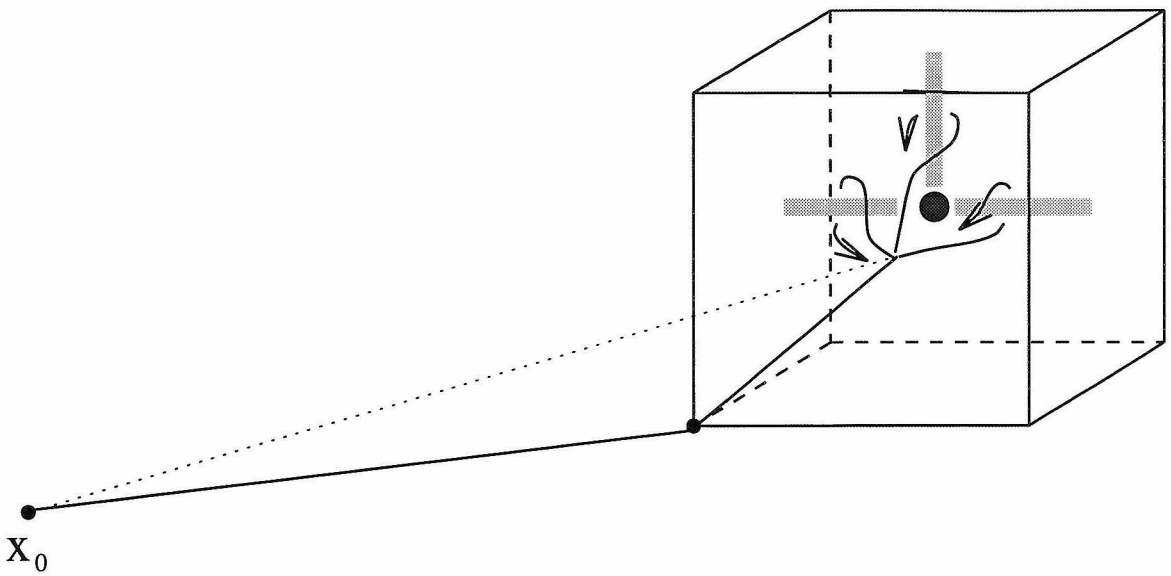

Figure 21: When the procedure of figure 20 has been applied, the tail from x_0 to a given node consists of one straight segment to the corner of a unit cube, and another to the node itself. The final stage is to remove the last kink, straightening this tail to the one shown here as a dotted line. Then all fluxes of strings joining at the node are well-defined according to the conventions used in the dynamical simulation.

conservation condition: the product of all strings joining at a node (taken in clockwise order as defined in the previous section) must be the identity. With all string fluxes thus defined, and the fluxes of the wrap-around paths Γ_i computed by multiplying lattice links, we then have a fully specified initial condition for the evolution of the network.

6 Dynamical Evolution

After the establishment of initial conditions, we may proceed with the dynamical evolution of the network. The system we are modelling, as in ref. 5, is one of monopoles (vertices) connected by cosmic strings, which we are modelling as straight line segments. The monopoles, as stated earlier, are assumed to undergo damped motion under the influence of string tensions. Our simulation proceeds as follows: During each time step, each node is moved by a displacement proportional to the vector sum of all tensions acting on it. This type of evolution corresponds to damped motion: Force $\propto$ Velocity. The constant of proportionality is a parameter which may be absorbed into the size of the time step. However, the ratio of damping constants for the two types of nodes may be a separately adjustable parameter. The ratio of tensions of the two different types of strings (s- and t-type) is also separately adjustable. The nodes are moved one at a time during each time step. During the motion of a given node, all effects of this motion on the flux definitions throughout the space are monitored. (For example, the necessary adjustments are made if one of the moving node's strings crosses the tail of another.)

In addition to this simple motion of the node, the following other types of events may occur.

i) Intercommutation. If in the process of moving a node from its initial to final position, one of its string segments intersects some other segment, then the fluxes of those two segments are compared at the point where the crossing occurs. If these two fluxes commute, then the the two segments may either pass through each other unaltered, or intercommute. The probabilities of these two outcomes may be taken as an adjustable parameter of the simulation. It is widely believed that intercommu-

tation is generically the more common outcome whenever two cosmic strings cross. Thus it seems most natural to let the probability of intercommutation be 1, or close to 1. Intercommutation may occur in two possible situations: either both strings are 3-cycle strings, or both are 2-cycles. In the latter case, the fluxes of the two strings must in fact be equal. In an intercommutation, the string ends are rearranged in such a way as to conserve flux. In the case of two s-strings, there is always only one way to rearrange the ends, as shown in figure 22a. A string end carrying flux s_+ to the point of intersection may not be joined to one carrying the inverse flux s_-. When two t-strings intercommute, however, there are two possible rearrangements of the ends, owing to the fact that a 2-cycle is equal to its own inverse and 2-cycle or t-strings consequently have no preferred orientation* (fig. 22b.) In the absence of a reason to prefer one of these rearrangements over the other, the choice must be made randomly. After intercommutation, the newly joined segments straighten immediately. Of course, all necessary adjustments are made if they should cross any tails during the process of straightening. It may also happen that as the rejoined segments straighten, they intersect other segments, which may lead to further intercommutations. Segments straighten as much as they are able to before encountering obstructions.

ii) Non-commutative intersection (or linking). If two non-commuting strings intersect, then it is assumed that they form a new pair of nodes and thus become linked by a new segment, as shown in figure 23. The flux of the intervening string segment is uniquely determined by the requirement of flux conservation. (The intervening flux must always be a 3-cycle, as the commutator subgroup of S_3 is Z_3.)

The actual implementation of this linking process in the simulation is slightly tricky. Defining the flux measurements of the two new nodes requires a reference to previously existing nodes. But linking events occur when one node is moving, dragging

---

* Strictly speaking, we can only say that there is no *topological* reason for a t-string to have a preferred orientation. It is possible that the field equations could have two distinct solutions, corresponding to differently oriented strings, which are topologically equivalent but can be deformed into one another only by surmounting a finite energy barrier. A situation of this sort occurs in the global vortices of nematic liquid crystals. This was pointed out to me by J. Preskill.

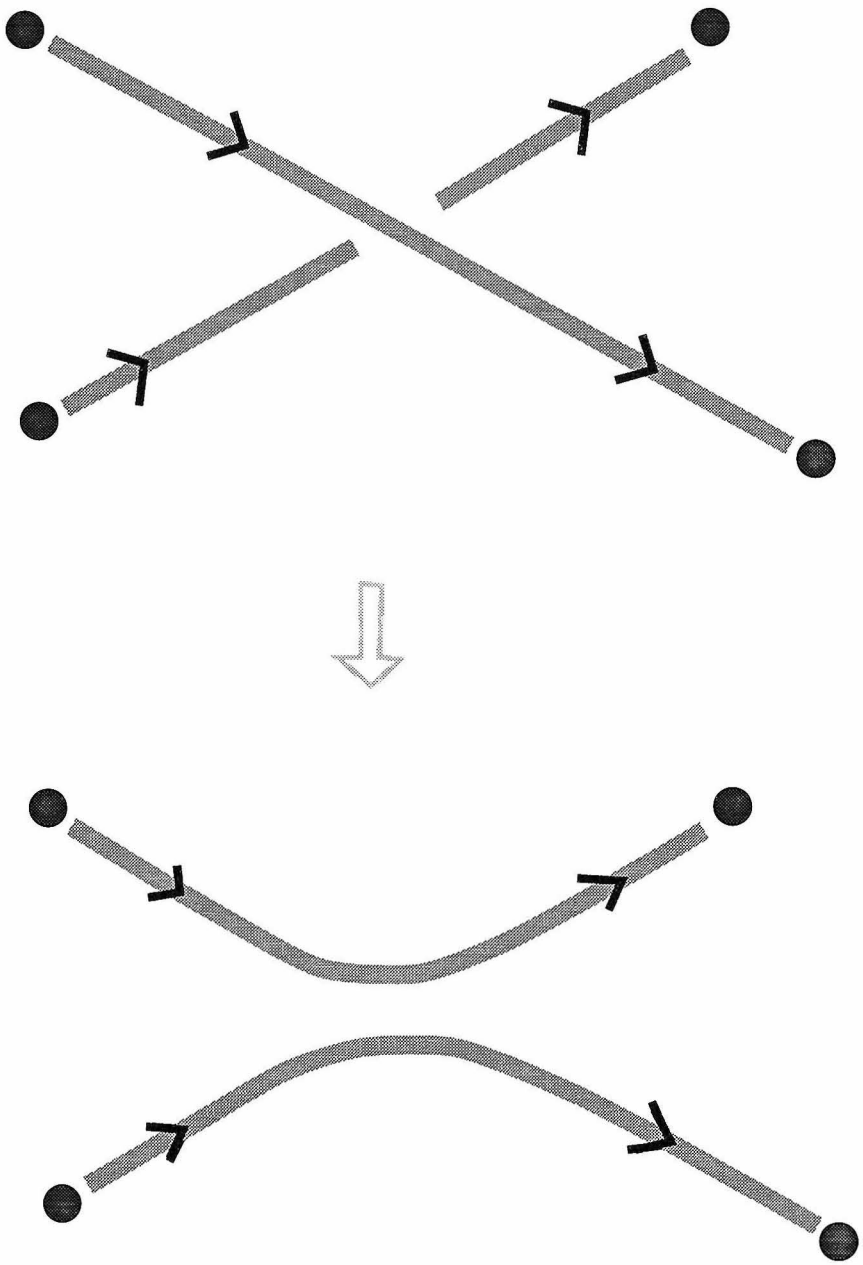

Figure 22A: When two three-cycle or s-strings intercommute, there is a unique rearrangement which is compatible with the orientations of the strings.

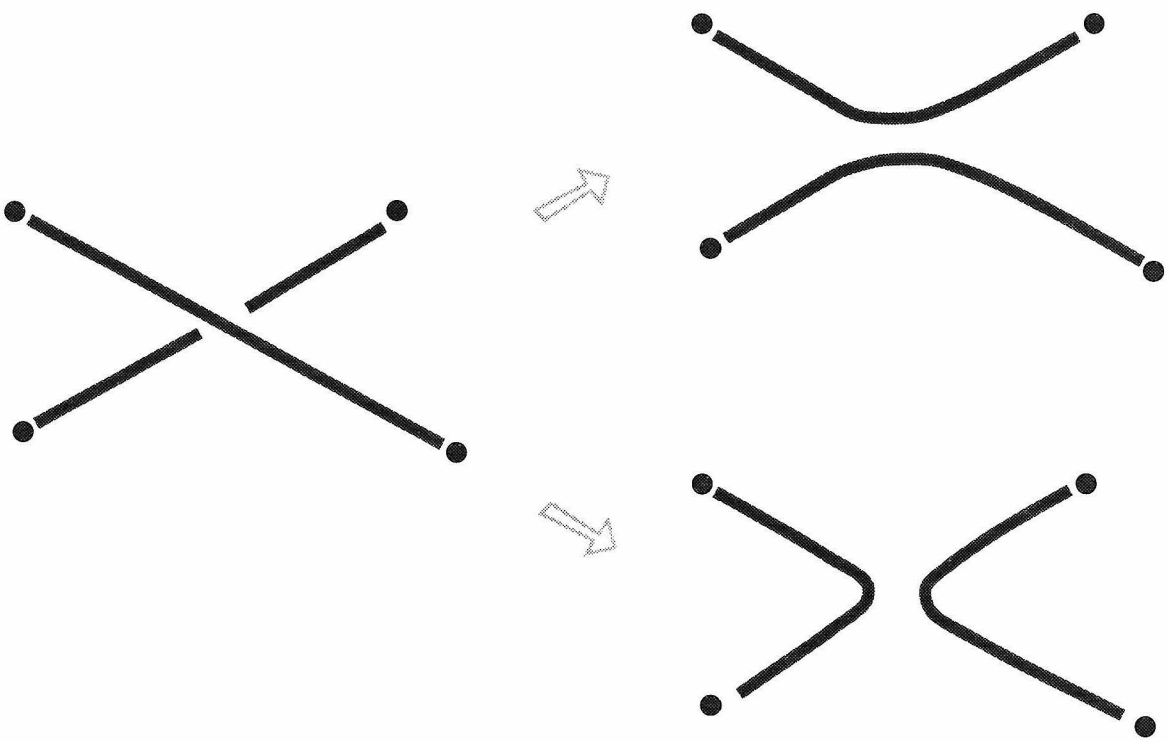

Figure 22B: Since t-strings (2-cycle strings) have no orientation, an intercommutation can result in either of two possible rejoinings of the ends.

an attached string segment to cross another. One must be careful that this motion not cause holonomy-type interactions with the newly created nodes before the new nodes are properly specified in terms of their associated fluxes. Our strategy is to create and fully specify the new nodes first, before the previously existing node is moved at all. This requires that the linking of strings actually be accomplished before the existing node has moved. A prescription for doing this is shown in figure 24. Related issues arise to some extent in implementing an intercommutation event: intercommutations occur when one node is moved, dragging along a string segment which intersects another as it is being dragged. Tail crossings and other holonomy interactions occur both as a result of the node's motion and as a result of the rearrangement of string ends during the intercommutaion, the non-commutativity of fluxes requires careful attention to the order in which these interactions are handled. As in linking events, the present simulation follows a strategy of making all rearrangemements of string ends before any existing nodes are actually moved.

The linking process creates new nodes and new strings, and therefore it might be expected to impede the collapse of the network.

iii) Annihilation. When two nodes approach each other closer than a distance r_{min} which is a parameter of the simulation, they are allowed to annihilate. The segment(s) which join the two nodes is eliminated, and the other segments emanating from the two annihilating nodes are joined to each other and straightened (or straightened until an obstruction is encountered). Two nodes are able to annihilate only if there is a consistent way to rearrange the free string ends (i.e., each string is able to find a partner with the same flux). Annihilation is always possible if the two nodes are doubly linked as shown in figure 25. It is also always possible if both junctions are of the sss type, even if they are only singly linked. In this case, there are two possible rearrangements of the free string ends (figure 26). One of these two must be chosen at random. When two stt-type junctions approach each other, there may exist at most one consistent rearrangement of the free ends allowing the two nodes to annihilate. Annihilation requires that *each* of the two segments on one side be matched with one on the other side carrying the *same flux*. Figure 27 shows an example of a pair of nodes which cannot annihilate because there is no consistent

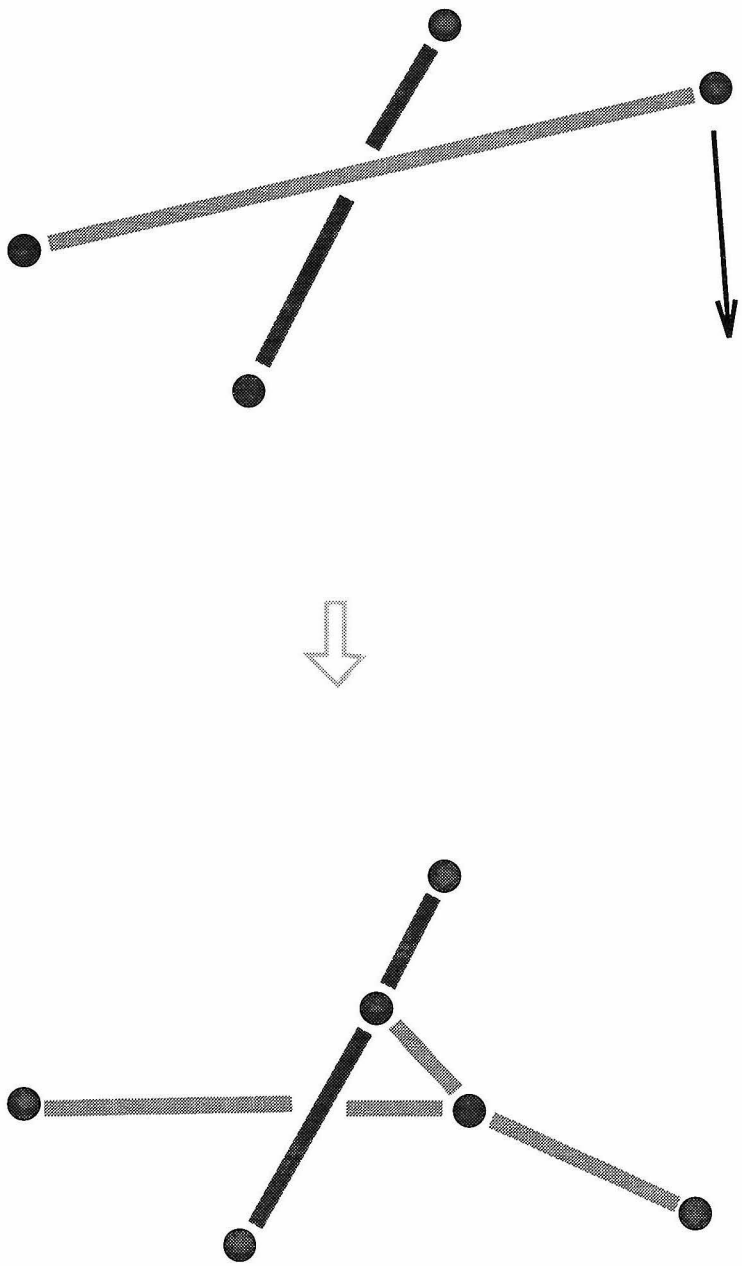

Figure 23: The intersection of two strings whose fluxes do not commute causes them to become linked by a new segment.

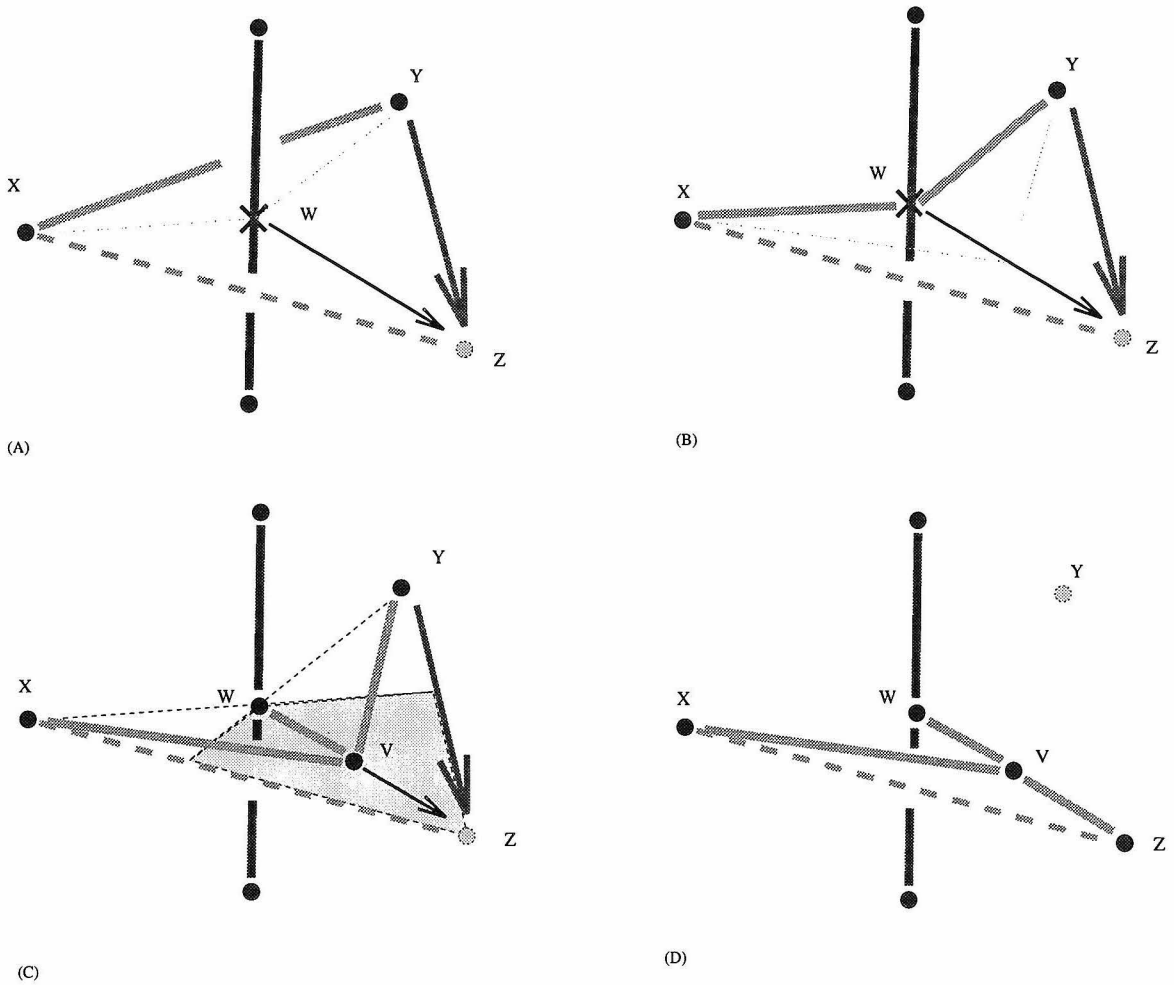

Figure 24: Actual implementation of the "linking" or "non-commutative intersection" process shown in Fig. 23. (A) If the node at point Y were to move to Z while dragging with it the string segment XY, the string would intersect another one (with non-commuting flux) at the point labelled W and marked with a cross. We create the new nodes first before moving the existing node. (B) First, the two nodes are both created at the intersection point W, and the moving segment is deformed to two segments joined at W, making all necessary adjustments for the crossing of other nodes' tails, etc. (C) In order to define the conventional clockwise order of the two new nodes, they must be separated. We do this by moving one of them to a new point V. V must be chosen so that the path consisting of XV and VY actually does lie on the opposite side of the other string as compared with XY; i.e., so that the linking of strings has occurred even though the node at Y has not moved yet. Assuming V is coplanar with X,Y and Z, this means it must lie in the shaded region. This can be ensured by placing V somewhere along the segment WZ, and we may arbitrarily choose to put it at the midpoint of that segment. The fluxes of the new nodes at W and V are then fixed by requiring consistency with the string segments to which they are attached and with the single-node consistency relation (2). (D) Finally, the node may move from Y to its destination Z.

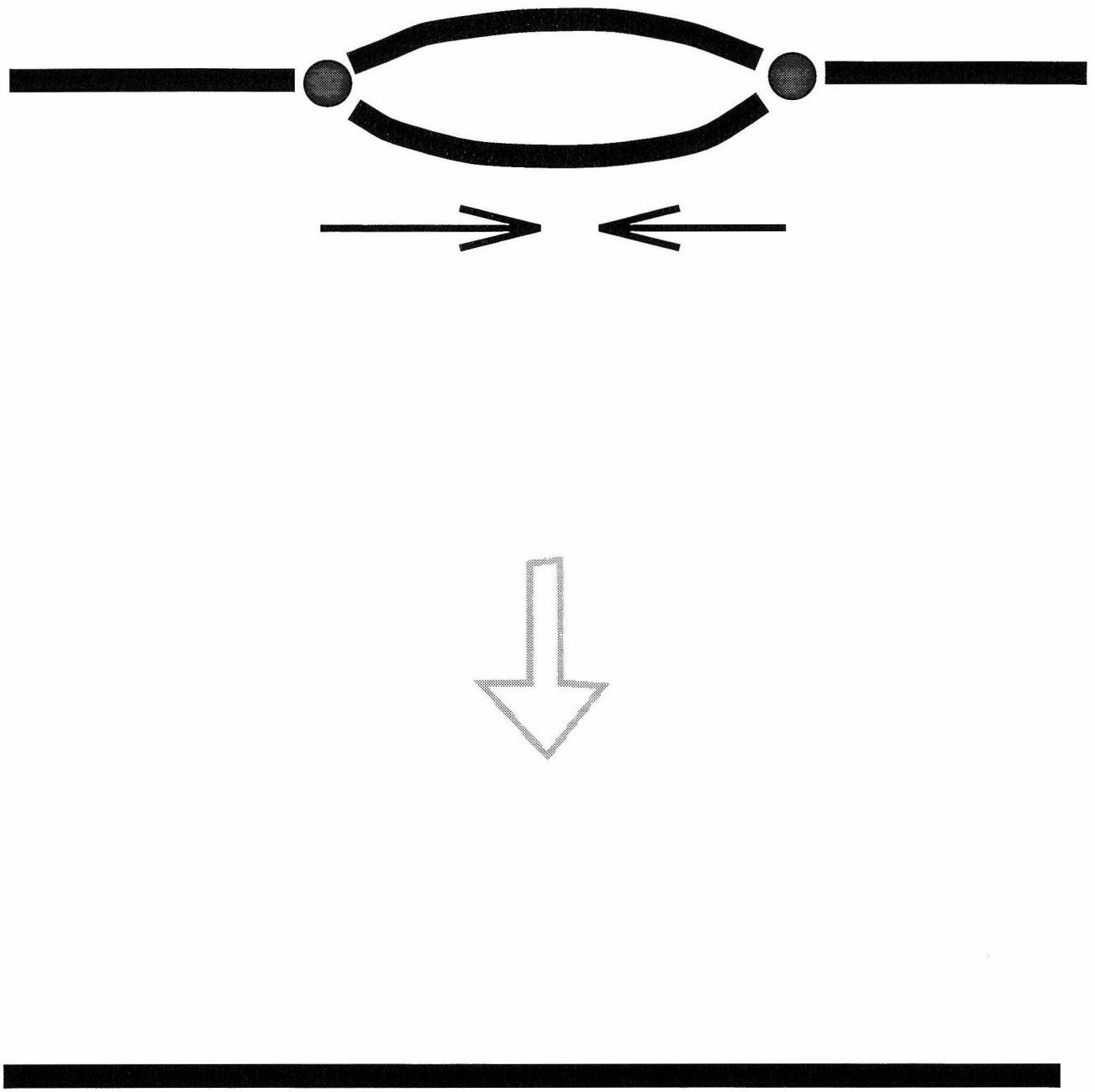

Figure 25: A pair of nodes linked by two strings may annihilate, leaving a single string.

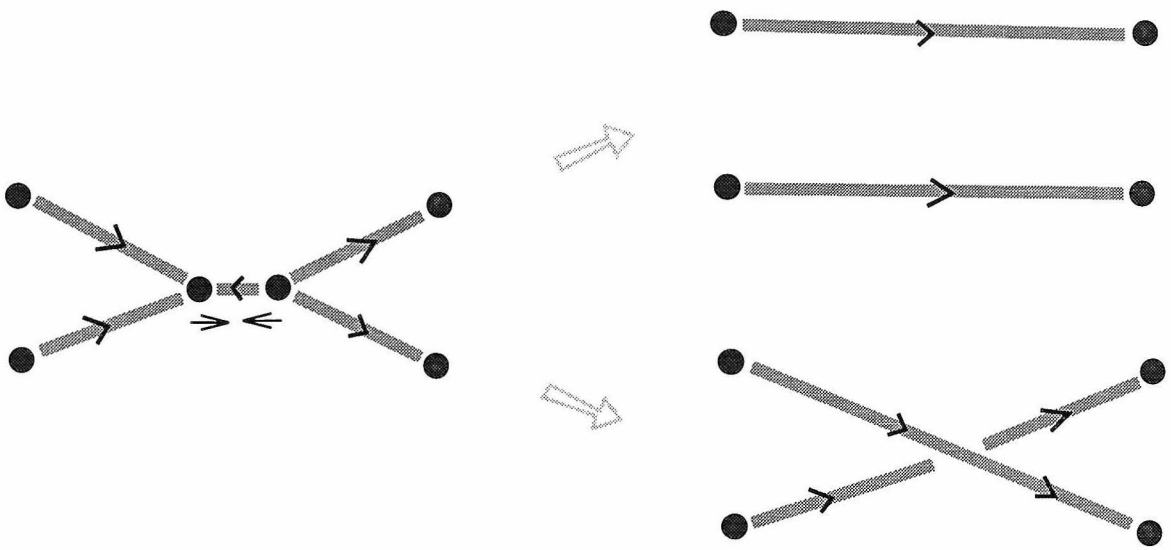

Figure 26: Annihilation of two *sss* nodes joined by a single string. There are two possible ways to reconnect the strings consistent with their orientation.

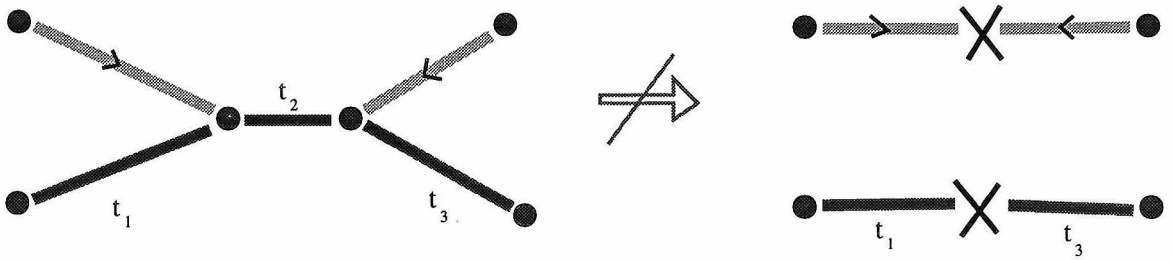

Figure 27: The two nodes shown here cannot annihilate, because there is no consistent way to reconnect the string ends.

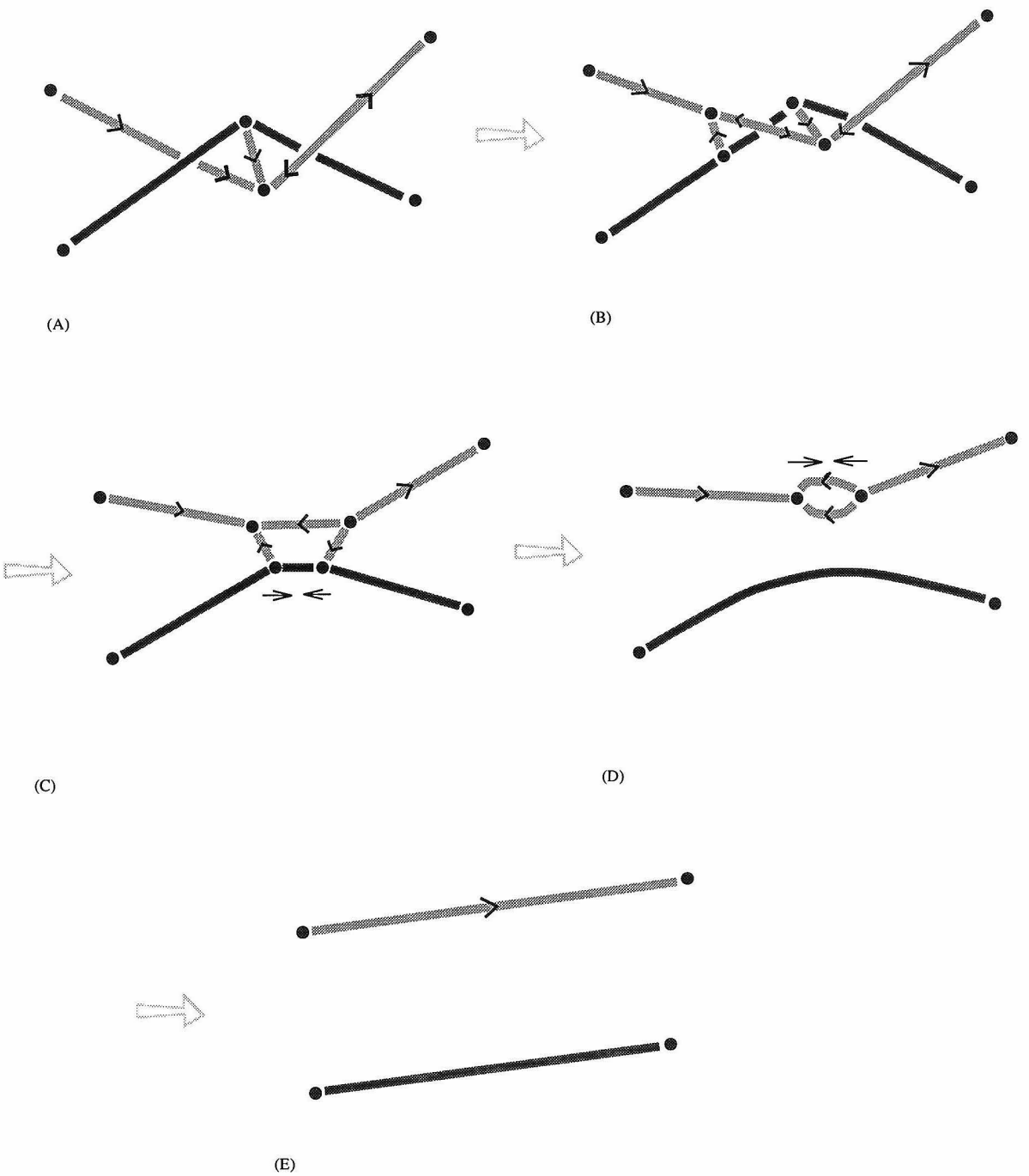

Figure 28: Unlinking of two strings– the inverse of the process shown in figure 23– can occur in several steps if the string tensions pull in the right direction to unlink the strings. A linking followed by two annihilations has the net result of removing the short intervening segment and unlinking the two longer strings. In this figure, the basepoint is assumed to lie behind the page, so that the definition of an s-string's flux changes when it passes in front of any t-string.

rejoining of the string ends. If two junctions approach each other but are unable to annihilate, then they continue to move normally, going wherever they are pulled by string tensions. They might either remain nearby or be pulled apart once again. If two stt-type nodes do annihilate, it is easily seen that there can never be more than one consistent rearrangement of string ends. If two of the outgoing ends are s strings and two are t strings, then there cannot be more than one rearrangement because each string can only be joined with one in the same conjugacy class. If all outgoing strings are of t type, then all four cannot have the same flux– if they did, then the total flux of any pair would be trivial and they would not be connected by a segment. Nor may any three have the same flux. It follows that, at best, each string end may reconnect with a unique partner. Annihilation of nodes is, of course, the principal mechanism by which the network dissipates its energy in our model.

We might imagine another type of annihilation process which is the inverse process to the non-commuting intersection. If string tensions were pulling in appropriate directions, then two nodes might annihilate, leaving two strings free which were previously connected by another string. Because of, among other things, the difficulty of constructing an algorithm to determine when this may occur, we do not include such events explicitly in the simulation. The unlinking of two strings can occur, however, through a multi-step process involving several string intersection and annihilation events (figure 28). We expect that such a process probably *will* occur whenever the geometry is appropriate for the unlinking of two strings, so that it is not necessary to perform the unlinking "by hand" in a single step within the simulation.

Finally, let us note a problem that may occur if the length an individual string segment becomes comparable to half the width of the simulation volume. A segment of string is defined by its two endpoints, which are the locations of two nodes. As in the case of the tail from each node to the base point, there is in principle an ambiguity associated with winding around the the periodic conditions (see figure 11 and the accompanying discussion). As long as nodes are close together, there is no difficulty in always defining a string as lying along the shortest possible segment connecting two nodes. However, if two nodes connected by a string move far enough apart, it is possible that this definition will change suddenly, just as the motion of

a node across the boundary can cause the tail to be redefined as in figure 11. If a string were allowed to change its winding in this manner, flux conservation might be violated. We can prevent this from happening by adding a new doubly linked pair in the middle of the long segment before it changes its winding.

7 Some Preliminary Results

The algorithm we have just described has been implemented with a 14,000-line C program which is beginning to produce results. It has been run sucessfully on a 4^3 simulation volume (in units of the initial lattice spacing). The program has been prone to occasional violations of flux conservation, and these errors have only recently been sufficiently brought under control so that the program can be run reliably on larger volumes. Much larger volumes may eventually require additional computing resources.

In this section we present briefly some of the data that have been obtained so far. More thorough analysis will be postponed until more results are available.

The Z_3 Network

Since S_3 contains Z_3 as a subgroup, our program can easily be used to simulate a Z_3 network by generating only s-strings in the initial conditions. This was done at an early stage in the development of the simulation code, and the results for the Z_3 network agree well with those obtained by Vachaspati and Vilenkin. Figure 29 shows the total string length and total number of nodes as a function of time for a typical run on a 30^3 simulation volume. The initial conditions were generated with a Z_3 lattice gauge method, rather than the discrete Higgs method of [5]. The difference in initial conditions has no noticeable effect after the first few time steps. Every node was moved in each time step according to $\Delta\mathbf{x} = \Delta t \sum_r \mathbf{t}_r$, where Δt is the time step (.05 in this case) and $\mathbf{t}_r$ is the unit vector along the direction of the r-th string connected to the node. The time variable plotted on the x-axis in the figure is $i\Delta t$, where i is the number of elapsed time steps. (This will be our convention for all remaining plots.) All distances and lengths are measured in units of the original lattice spacing. Following [5], we transform the data in a way that displays more

clearly the "scaling" behavior of the network. The inverse cube root of the number of nodes per unit length is a quantity with the dimensions of length and represents a typical distance between nodes. (Let us call it $D(n)$.) From figure 30, we can see that this length scale grows linearly with time. The slope of approximately 0.3 is close to that observed in reference [5]. Note that the energy stored in the strings (which is proprotional to the total length) also follows a scaling law. The total length of string is given by the total number of segments multiplied by their average length:

$$L_{total} = nl_{Av}. \tag{3}$$

In a scaling evolution characterized by a single length scale D, n is proportional to the inverse cube of the scale, while the average segment length is proportional to the scale, so $L_{total} \propto D^{-2}$. In the second plot of figure 30, the the inverse square root of the string length per unit volume (let us call this $D(l)$) is plotted as a function of time. We see that $D(l)$ also grows linearly with time and is approximately equal to $D(n)$.

Initial Conditions from the Lattice Monte Carlo

In the simulation of the S_3 system, two different Monte Carlo methods were used to generate initial conditions: the lattice-gauge method and the discrete Higgs method using the $\Delta(24)$ subgroup of $SU(3)$. Both of these methods generate infinite networks of strings (finite networks or loops are almost never observed.) In this respect, the two methods are similar, but they differ in statistical details. In the table below, we summarize some statistical features of the initial conditions generated by the different methods. For comparison, we also include the corresponding information for the Z_3 system (including both a Z_3 lattice-gauge method and the tetrahedral discrete-Higgs simulation of [15]. The Z_3 discrete-Higgs numbers are from Reference [15], and the numbers in the other three columns are averages over three runs of each Monte Carlo algorithm on a 10^3 lattice.[17] For each method, the fractions of plaquettes pierced by strings of each conjugacy class is reported. (In the Z_3 case, of course, there is only one class.) Note that in the lattice gauge method, each group element is weighted equally; therefore 2/3 of all plaquettes are pierced by strings in the Z_3 lattice gauge

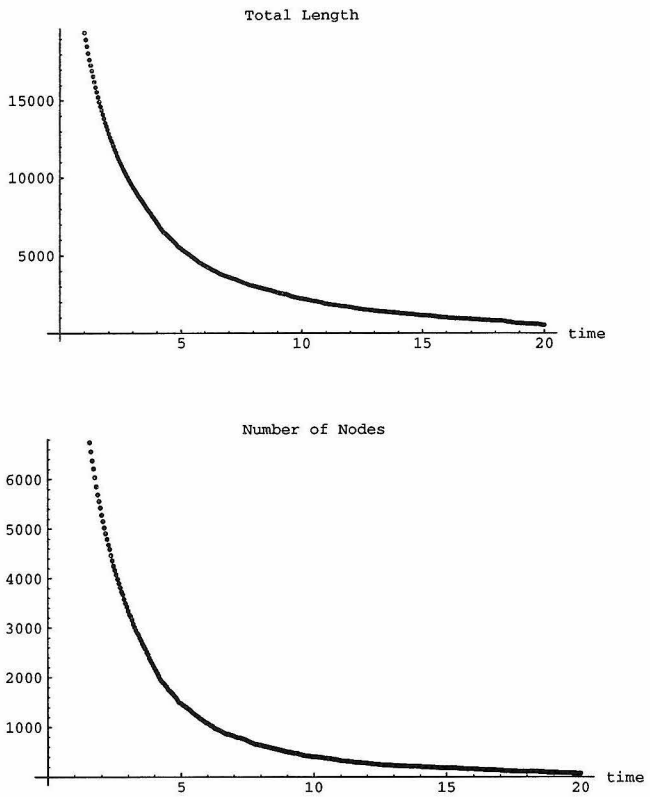

Figure 29: Number of nodes and total string length as a function of time for Z_3 strings on a 30^3 volume.

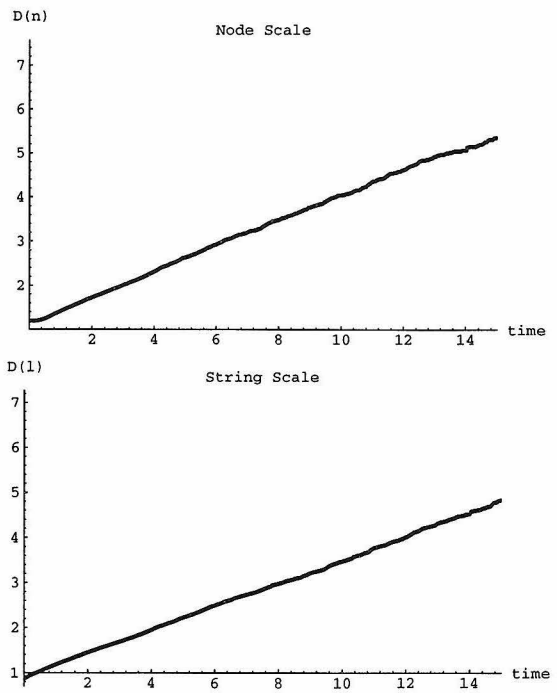

Figure 30: Scaling behavior of Z_3 strings on a 30^3 volume. The typical distance between nodes, $D(n)$, grows linearly with time, and so does the inverse square root of the string energy density, $D(l)$.

case, and 5/6 for S_3. Below this are the fractions of cubic lattice cells with 0,2,3,4,5 and 6 of their faces pierced by strings. It is evident that for both Z_3 and S_3 systems, the lattice gauge method produces a denser network: more cube faces are pierced by strings and more cells have high numbers of strings emerging through their faces.

Method	Z_3 L.G.	Z_3 Higgs	S_3 L.G.	S_3 Higgs
Faces with				
s string	0.67	0.52	0.33	0.14
t string	–	–	0.50	0.37
Cubes with				
0 ends	0.01	0.04	0.00	0.06
2 ends	0.12	0.34	0.01	0.32
3 ends	0.17	0.20	0.05	0.21
4 ends	0.38	0.32	0.21	0.31
5 ends	0.24	0.09	0.20	0.02
6 ends	0.09	0.02	0.55	0.08

Table 1: Statistics of Initial Conditions

Evolution of S_3 Networks

We now display the results of several early runs of the S_3 dynamical simulation on a 4^3 volume. The displacement of each node during each time step is given in this case by $\Delta \mathbf{x} = \Delta t \sum_r T_r \mathbf{t}_r$, where T_r is the magnitude of the tension of the appropriate type of string. Runs were conducted using three different pairs of values of the tensions T_s, and T_t of the two classes of strings (s and t), in order to probe the cases $T_s > T_t$, $T_s = T_t$ and $T_s < T_t$. Figures 31 - 36 include plots generated by six different runs (labelled as runs 1-6). The first two have tensions $T_s = 1$, $T_t = 0.5$, runs 3 and 4 use $T_s = T_t = 1$, and the last two runs are for $T_s = 0.5$, $T_t = 1$. Each of these three sets of parameters was used for two runs; one using lattice gauge and another using discrete Higgs initial conditions. In each case, the "string scales" $D(l)$ were computed separately for the two different types of strings and plotted on the same axes as functions of time. The total number of nodes is also plotted as a function

of time in each case. The "node scale" D(n) is not shown because its graph did not appear to be very enlightening in any of these cases; it was too bumpy to show clearly either linear scaling or its absence. Finally, for comparison, corresponding plots are shown in figure 37 for a typical run of the Z_3 simulation on the same volume (4^3).

A few comments are in order concerning these plots. One is that, to a first approximation, the shapes of the curves are not strongly dependent on the initial conditions used, but their intercepts are certainly different when starting from different conditions. Another is that the behavior of the system shows signs of being quite a bit more complicated than the Z_3 network.

The case with large s string tension is particularly interesting: The energy density in t strings shows no sign of decreasing with time, but rather appears to become frozen, even though the s strings are shrinking in the manner typical of a scaling solution. ($D(l_s)$ grows linearly with time.) Especially in run 1, the annihilation of nodes from the network all but ceases after a brief relaxation. Nodes frequently approach each other closely, but are unable to annihilate in a flux-conserving manner. In this case the system appears to be approaching a near-equilbrium state consisting of t strings tied to each other by very short segments of s string. A snapshot of such a state is shown in figure 38.

A contrasting picture is seen in the opposite limit where the t string tension is larger than the s tension. An example of a late-time configuration in this case is shown in figure 39. It appears in this case that the t strings do not become tangled to the same degree. The formation of new s strings is comparatively cheap in this case, and so it is apparently possible for strings to pass through each other and continue moving while stretching an s string between them. The network in figure 39 has the appearance of a few relatively long, straight t strings joined to each other by a web of s strings.

It is apparent from these preliminary results that the system of S^3 strings can exhibit a range of interesting behaviors not seen in Abelian strings. The evolution does not, in general, seem to be a self-similar one characterized by only a single typical length. In some regions of parameter space, the energy density of the network

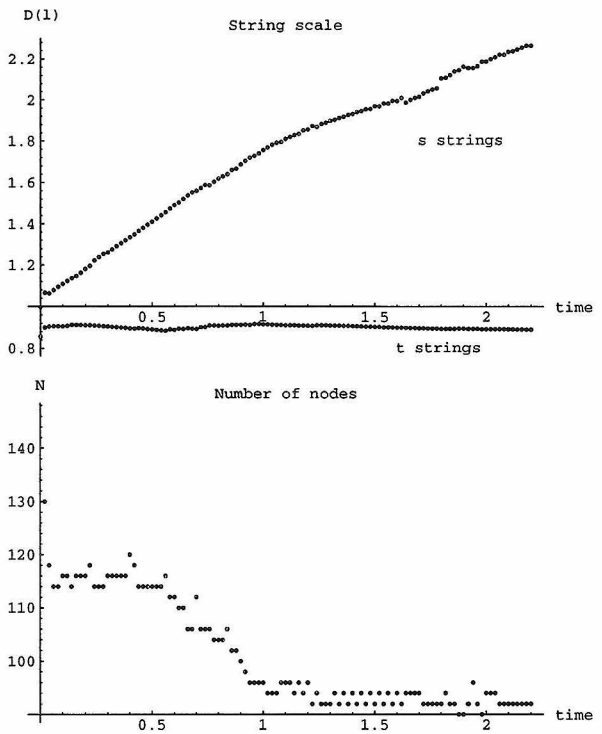

Figure 31: Plots for run 1: $T_s = 1$, $T_t = 0.5$ with lattice gauge initial conditions.

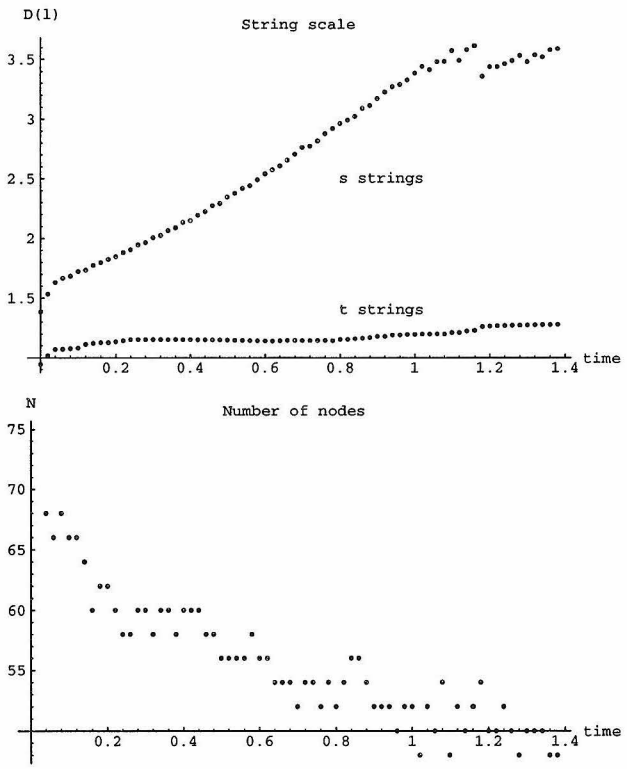

Figure 32: Plots for run 2: $T_s = 1$, $T_t = 0.5$ with discrete Higgs initial conditions.

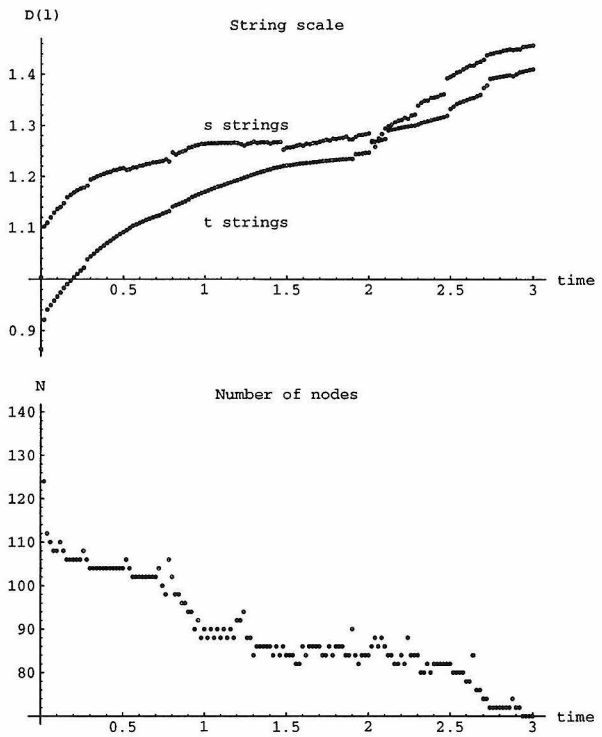

Figure 33: Run 3: $T_s = 1$, $T_t = 1$ with lattice gauge initial conditions.

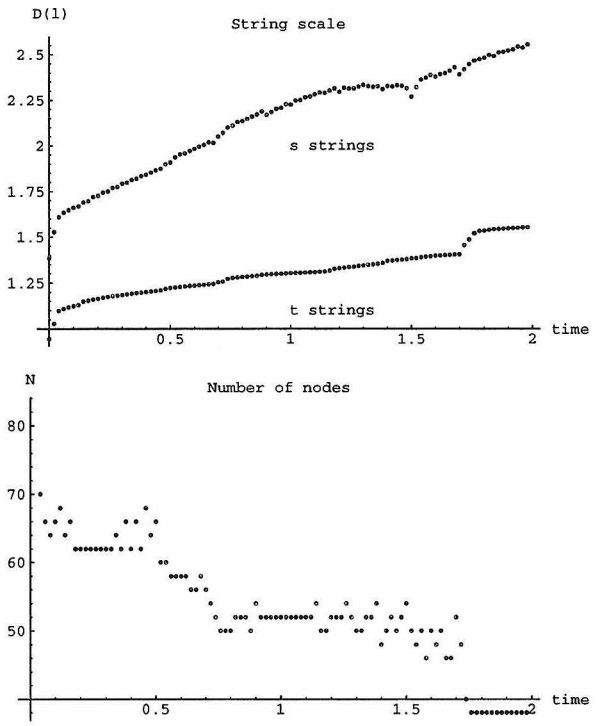

Figure 34: Run 4: $T_s = 1$, $T_t = 1$ with discrete Higgs initial conditions.

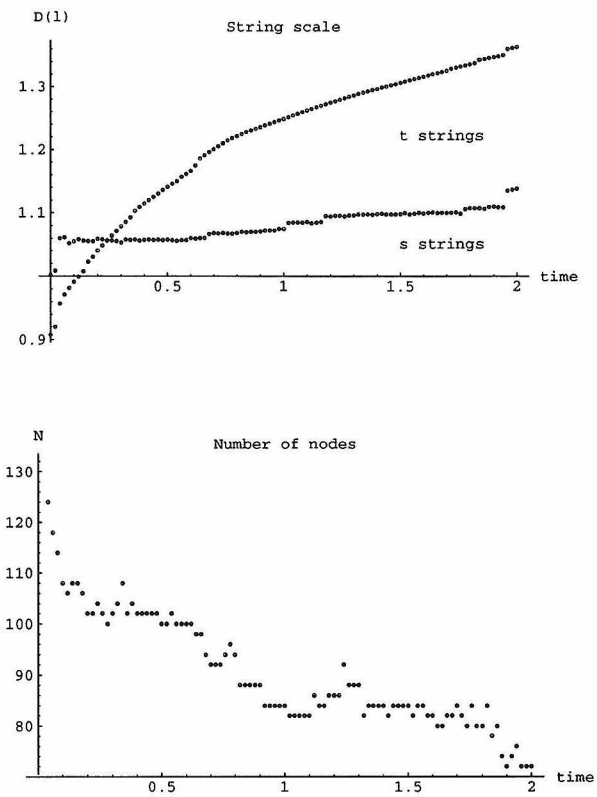

Figure 35: Run 5: $T_s = 0.5$, $T_t = 1$ with lattice gauge initial conditions.

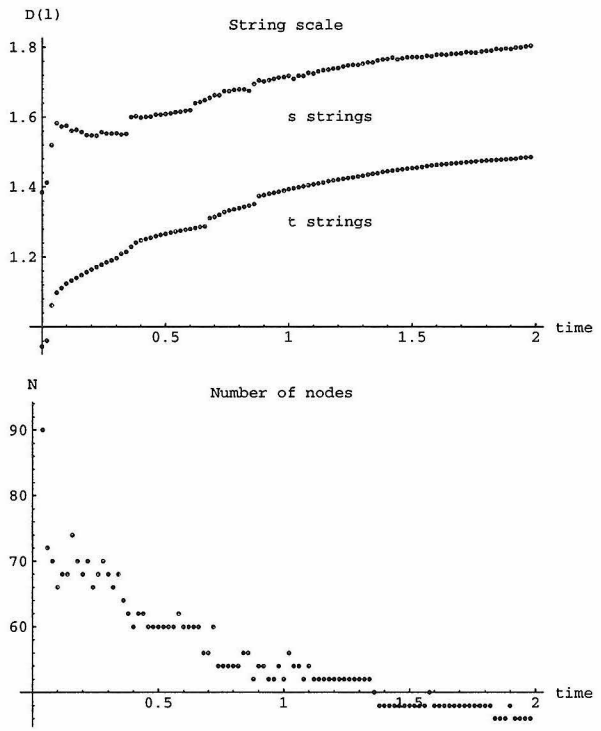

Figure 36: Run 6: $T_s = 0.5$, $T_t = 1$ with discrete Higgs initial conditions.

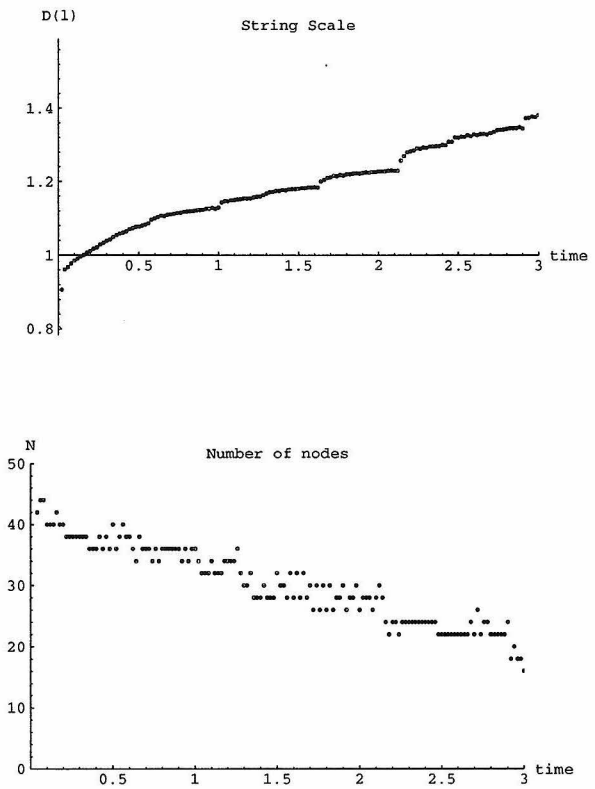

Figure 37: A run of the Z_3 simulation on a 4^3 volume, included for comparison with the S_3 data.

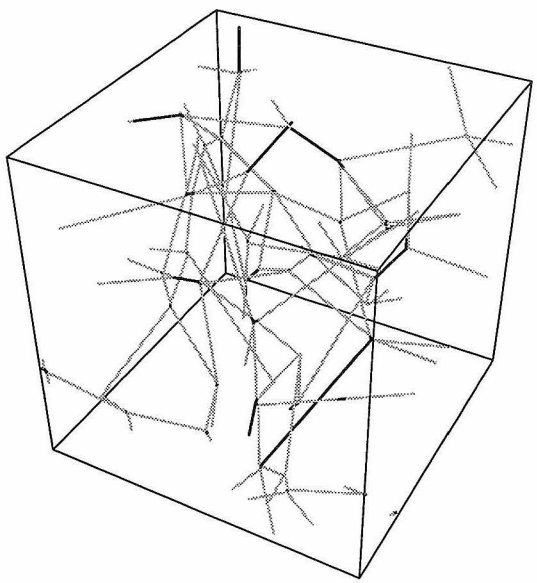

Figure 38: Configuration of the S_3 string network at a late time for the case where $T_s = 1$ and $T_t = 0.5$. The dark-colored segments are s strings, and the light-colored segments are t strings. The configuration, resulting from the evolution of a lattice-gauge Monte Carlo initial network, which was reached after time $t = 3.0$ and remained nearly static except for a slow shrinking of the remaining long s segments. It is dominated by a tangle of t strings tied together by short s segments.

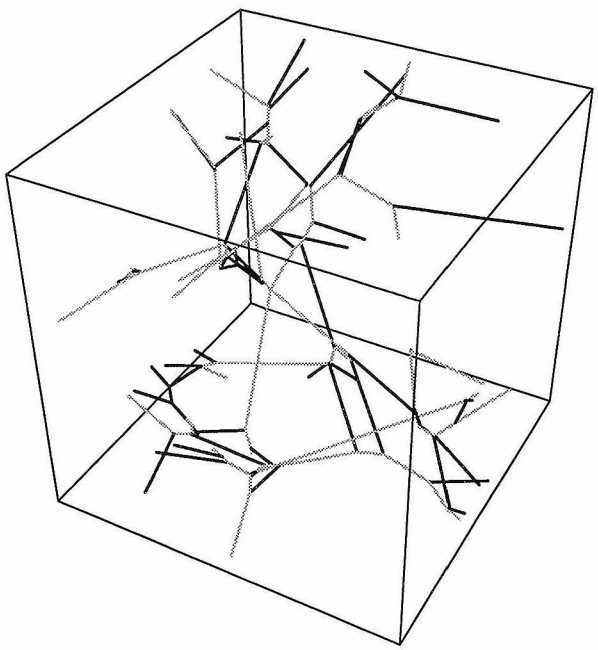

Figure 39: Configuration of the network after evolving with $T_s = 0.5$ and $T_t = 1$. This was obtained at evolution time $t = 3.0$ during the evolution of a discrete-Higgs initial network on a volume of size 6^3. The configuration appears to contain a few comparatively long, straight t strings between which are stretched webs of s strings.

shows a tendency to become static rather than scaling away as time progresses. More conclusive statements await the results of simulations on larger volumes.

REFERENCES

1. T.W.B. Kibble, Phys. Rep. **67**, 183 (1980).
2. See, for example: A. Vilenkin, Phys. Rep. **121**, 263 (1985).
3. T. Vachaspati and A. Vilenkin, Phys. Rev. **D 30**, 2036 (1984) and references therein.
4. H.B. Nielsen and P. Oleson, Nucl. Phys. **B 61**, 45 (1973).
5. T. Vachaspati and A. Vilenkin, Phys. Rev. **D 35**, 1131 (1986).
6. See, for example, M. Alford, K-M Lee, J. March-Russell and J. Preskill, Nuc. Phys. **B 384**, 251 (1992) and references therein.
7. P. McGraw, in preparation.
8. M. Alford, *et al.*, Phys Rev. Lett. **64**, 1632 (1990); **65**, 668 (E); Nuc. Phys. **B 349**, 414 (1991).
9. I.N. Herstein, Abstract Algebra. (Macmillan, New York 1986).
10. M. Hindmarsh and T.W.B. Kibble, Phys. Rev. **D 55**, 2398 (1985).
11. M.Daniel, G.Lazarides, and Q. Shafi, Nuc. Phys. **B 170**, 156 (1979).
12. J. Preskill, Ann. Rev. Nucl. Part. Sci., **34**, 461 (1984).
13. K.M. Lee, Phys. Rev. **D 49**, 2030 (1994).
14. T. Vachaspati and A. Vilenkin, Phys. Rev. D 30, 2036 (1984). T.W.B. Kibble, Phys. Lett. B 166, 311 (1986).
15. M. Aryal, A.E. Everett, A. Vilenkin and T. Vachaspati, Phys. Rev. D 34, 434 (1986).
16. W.M. Fairbairn,T. Fulton, and W. H. Klink, J.Math.Phys. **5**, 1038 (1964).

17. Concerning the Z_3 lattice gauge algorithm, see also L. Nayvelt and J.E. Woods, "Initial Configuration and Evolution of Z_3 Cosmic Strings," unpublished report (Caltech, 1988).

Concluding Remarks

The goal of this thesis was to shed light on a few questions concerning the dynamics and phenomenological relevance of systems exhibiting non-Abelian topological interactions. Many other questions in this category are likely to continue to provide fruitful subjects for research, and some of the subjects described in the preceding chapters are ripe for further study.

The $U(2)$ anyon model seems to call for more work that goes beyond the zeroth order mean field approximation near the fermionic limit. The many-body physics of "nonabelions" (objects obeying non-Abelian braid statistics) is intrinsically intriguing whether or not an obvious manifestation can be found in nature. Kent Bradford is currently conducting numerical studies of the many-body quantum mechanics of S_3 vortices;[1] hopefully this will also lead to a more general understanding of non-Abelian statistics.

Work on the cosmic string simulation of Chapter 4 is still in progress. The early results are tantalizing, especially in the cases where the t-string energy appears to become static. This work might potentially lend credence to the scenario of a string-dominated universe[2] resulting from a persistent non-Abelian string network. There has been some recent new interest in such models as a resolution of the cosmological age puzzle.[3]

REFERENCES

1. K. Bradford, work in progress.

2. A. Vilenkin, Phys. Rev. Lett. **53**, 1016 (1984).

3. W. L. Pen, private communication with J. Preskill.